Protein engineering for polyethylene terephthalate degradation

Von der Fakultät für Mathematik, Informatik und Naturwissenschaften
der RWTH Aachen University zur Erlangung des akademischen Grades
einer Doktorin der Naturwissenschaften genehmigte Dissertation

vorgelegt von

Master of Science (M. Sc.)
Biologie

Nina Lülsdorf

aus Troisdorf

Berichter: Universitätsprofessor Dr. rer nat. Ulrich Schwaneberg

Universitätsprofessor Dr. rer nat. Lothar Elling

Tag der mündlichen Prüfung: 26. Januar 2016

Table of content

I. Acknowledgements

This work was financed by the innovation initiative industrial biotechnology of the German Federal Ministry of Education and Research (BMBF): “Functionalization of Polymers” [FKZ: 031A227F].

First of all I want to thank Prof. Dr. Ulrich Schwaneberg for giving me the opportunity to work on my PhD-thesis in his research group. I want to thank him for the challenging project, his support and time for discussions over the past three years, which significantly influenced my personal development. I also would like to thank Prof. Dr. Lothar Elling for being second referee and PhD defence committee member.

I want to thank both of my supervisors Dr. Ronny Martinez and Dr. Ljubica Vojcic for all the support, fruitful discussions and motivation. Thank you Ronny, for the great time I could spend with you, I enjoyed the discussions, kicker and beach volleyball with you. I learned a lot from you and it was a pleasure to work with you, even after you left you were still supporting me. Special thanks to Ljubica as my new supervisor, for supporting me with manuscript and thesis writing.

Dr. Anna Joelle Ruff and Ursula Holter are acknowledged for always having time for discussions and their invaluable support in molecular biology. Dr. Marco Bocola is acknowledged for support in computational analysis and fruitful discussions. Special thank goes to Christian Pitzler, who always had great ideas resulting in successful joint projects. I thank my students Anastasiia Bazhenova, Sandra Knopp, Daniel Sexauer and Lukas Weiler for their great help in the progress of my work.

I want to thank my cooking group fellows Julia Kinzel, Christian Pitzler, Dr. Erik Arango, Dr. Christian Lehmann, Dr. Marcus Arlt and Anne Wallraf for the relaxing lunch breaks with a lot of new taste experiences.

I also would like to thank the whole Schwaneberg group and all members of the HTS subgroup for the help, support and friendly working atmosphere.

Special thanks go to my closest coworkers Julia Kinzel and Dr. Marcus Arlt. I really enjoyed a lot the time in the office, during coffee breaks or long evenings with you.

My brother Stefan is acknowledged for supporting me in generating chemical structures and answering all my chemical questions. The most special thanks go to my parents who always supported me during my studies and in my whole life. With all their patient love they made it possible that I could complete this work. Last but not least I thank Chris for his endless love and love support in all situations, without him I couldn’t have managed the last months.

II. Abbreviations

Δ	Deletion
4AAP	4-aminoantipyrine
AA	Amino acid
AcN	Acetonitrile
Amp	Ampicillin
BCA	Bicinchoninic acid
B. licheniformis	*Bacillus licheniformis*
B. subtilis	*Bacillus subtilis*
CD	Circular dichroism
Da	Dalton
DMSO	Dimethyl sulfoxide
DNA	Deoxyribonucleic acid
DSC	Differential scanning calorimetry
E. coli	*Escherichia coli*
Em	Emission
epPCR	Error-prone PCR
et al.	*et alii*
EV	Empty vector
Ex	Excitation
GOx	Glucose oxidase
h	hour
HRP	Horse radish peroxidase
HTS	High throughput screening
IPTG	isopropyl ß-D-1-thiogalactopyranoside
J	Joule
LB	Luria Broth
MTP	Microtiter plate
OD	Optical Density
PCR	Polymerase chain reaction
PET	Polyethylene terephthalate
PET-dimer	Bis(*p*-methylbenzoic acid)-ethylene glycol ester
PET-trimer	Bis(benzoyloxy-ethyl)-terephthalate
*p*NBEBL	*p*-nitrobenzyl esterase *B. licheniformis*
RFU	Relative fluorescence units
SDM	Site-directed mutagenesis
SDS	Sodium dodecyl sulfate
SeSaM	Sequence saturation mutagenesis
SSM	Site-saturation mutagenesis
v/v	Volume/volume
WT	Wildtype
w/v	Weigth/volume
YASARA	Yet Another Scientific Artificial Reality Application

III. Abstract

Plastics play an important part in nowadays life since it became the material of choice used in countless application (*e.g.* packaging, automobiles or furniture). Among all plastics, polyethylene terephthalate (PET) is globally one of the most abundant and in 2014 approximately 40 million tons of PET were used for the production of plastic bottles, synthetic fibers, and foils. In order to meet requirements of modern life style, most of the commonly sport clothing are made of highly hydrophobic PET polymer making the clothes waterproofed and antimicrobial if linked to silver. Washing of synthetic clothes causes microplastic PET accumulation into freshwater systems through household sewage discharge. Additionally, low PET biodegradability causes its accumulation in terrestrial and aqueous environment in form of either by products during PET production or accumulated PET after final usage.

Chemical or mechanical PET degradation is usually performed under harsh conditions (high acidic, high basic, high pressure) in a time consuming manner resulting in incomplete PET degradation. Alternatively, enzyme-based PET degradation showed to have an application potential to completely degrade PET into monomers and offers environmentally friendly method for removal of accumulated plastic particles. Up to date no successful enzyme-based PET degradation was achieved since principle and underlying molecular basis of hydrolysis of PET is still not elucidated. In previous studies it was shown that potential enzymes with an ability to catalyse PET degradation are hydrolases (*i.e.* esterases and cutinases) with still weak activities towards PET. In order to be applied in biodegradation processes (*e.g.* waste water treatment, laundry detergents) the enzyme candidates need to be further optimized regarding its specific activity towards PET, and resistance towards high temperatures.

The enzyme optimization was since 1970s done using directed evolution and rational design. A main bottleneck of every directed evolution experiment is the design of a screening system which mimics application conditions as close as possible. In order to evolve hydrolases having high specific activity towards PET the complex aromatic model substrate, phenol benzoate was used to develop and optimize microtiter plate (MTP)-based screening system. The screening system is based on indirect monitoring of esterolytic activity through detection of phenols with 1,5-dimethyl-1-4-(4-oxo-cyclohexa-2,5-dienylidenamino)-2-phenyl-1,2-dihydropyrazol-3-one. The product formation is followed continuously as an increase of absorbance at 509 nm. Validation of novel screening system was done by screening error-prone PCR (epPCR) esterase mutant library for improved esterase activity at elevated temperature. The identified esterase variant T3 (Ser378Pro) showed a 4.7-fold improved residual activity after thermal treatment.

MTP screening formats offer screening throughput of 10^4-10^5 variants which is insufficient to cover sequence space in generated gene diversity library (10^8-10^9). In order to increase screening throughput and increase coverage of sequence space a novel ultra-high throughput screening system was optimized as a part of a universal screening toolbox for hydrolases. The screening is based on coupled enzyme reaction using glucose derivatives as

substrates which upon hydrolysis forms a fluorescent hydrogel layer on the surface of the *E. coli* cells. Applying a developed screening platform on epPCR esterase library resulted in a variant E1 (Glu256Gly, Gly401Val) with a 7.1-fold higher k_{cat} and 2-fold reduced K_M.

Additionally, in order to generate first hypothesis on PET degradation mechanism, an in-depth analysis of esterase lid like loop (18 amino acids) in close proximity of the active site was done. Shortening and complete deletion of the esterase loop was performed and its influence on PET degradation activity was followed. The activity decrease correlates with the decrease in loop length and revealed in an inactive esterase variant in case the complete lid like loop was deleted. This confirmed that the lid like loop has a key importance for the esterase activity.

Part I: General Introduction

1. Directed evolution and protein engineering

Enzymes are proteins which can catalyse many biochemical reactions in living cells ensuring their survival. The isolated enzymes from natural habitats are efficiently operating under defined conditions such as temperature, pH, defined salt concentration and in aqueous environment[1]. In order to be employed in various industrial applications enzymes needs to fulfil industrial demands such as high substrate concentrations, highly acidic or basic pH, high temperatures, and high organic solvent concentrations. Therefore, there is a constant need to tailor and optimize natural biocatalysts. Up to now, many success stories were generated on modifying enzymes to match requirements of industrial application. The successful implementation of enzymes in the industry was shown for the *Candida antarctica* lipase B which replaced the conventional chemical processing of oleo chemical esters. The benefit of the enzymatic-based production was the reduced energy use, due to increased enzymatic specificity in the catalysis yielding in a product purity of 96.4 %[2].

A common way to tailor enzymes is protein engineering to improve enzyme stability, activity and thus general adaptation to industrial conditions. Common strategies for protein engineering are directed evolution and rational design[3-4]. Both methods were developed to tackle the limitations of natural enzymes by tailoring their properties to the needs of a particular application or working conditions and simultaneously identify and investigate structure-function relationships[5].

Rational design is based on methods like computational chemistry, molecular modelling or X-ray crystallography to get a fundamental knowledge about the structure-function relation as well as the catalytic mechanism. Based on this knowledge a prediction of possible amino acid exchanges is performed in order to optimize the enzyme performance. Site-directed mutagenesis (SDM) and site-saturation mutagenesis (SSM) are used to generate the proposed substitutions in enzymes. It was shown for a glucose 1-dehydrogenase that by introducing disulfide bonds the thermal stability was increased and the half-life was improved compared to wildtype (1868-fold)[6]. Nevertheless the final improvement of the modified enzyme variant is not predictable even though all available methods are used for analysis[7].

In contrast to rational design directed evolution does not require knowledge about the structure-function relation of a protein[8-9]. Figure 1 shows the three major steps applied in a directed evolution experiment. In the first step "*Gene diversity generation*" the gene of interest encoding for the protein of interest is randomly mutated[10]. In the next step "*Screening for improved variants*" mutant libraries are expressed and screened in conditions directly comparable with the final application. Finally, improved variants are identified and "*Isolation of gene encoding for improved protein variant*" takes place in order to analyse the

sequence. This workflow is repeated through iterative cycles until the protein with the desired improvements is identified.

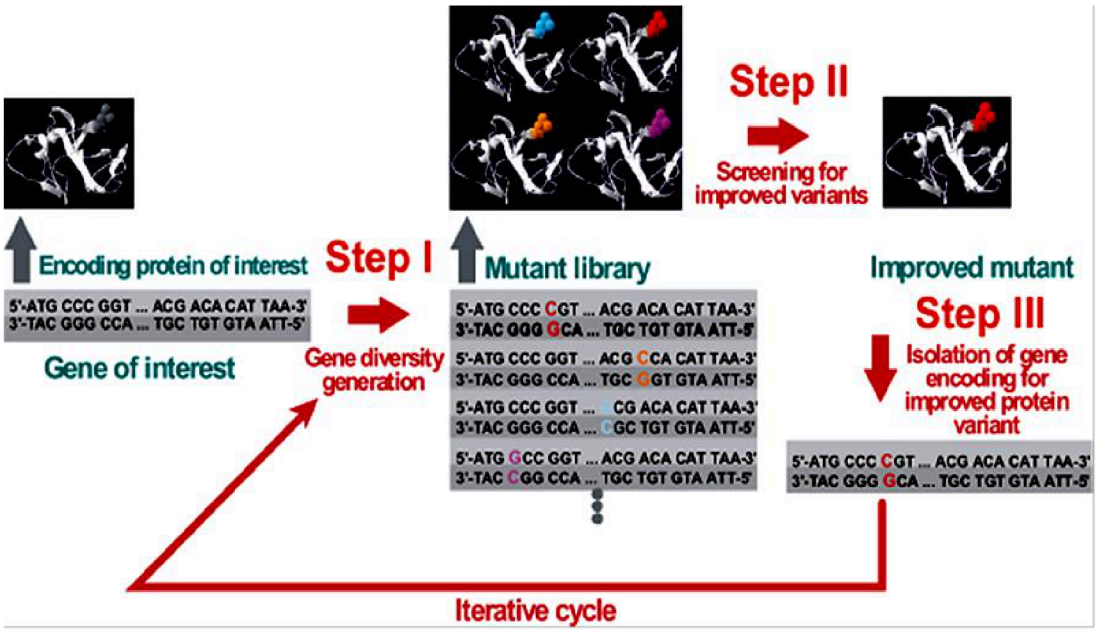

Figure 1 Schematic overview of a directed evolution experiment. **Step I:** Gene diversity generation, **Step II:** Screening for improved variants, **Step III:** Isolation of gene encoding for the improved protein variant, these steps can be repeated in iterative cycles[11].

The number of iterative cycles depends on the starting activity of the protein, resistance of its gene to mutations and the level of improvement to be achieved. The main challenges to perform a successful directed evolution experiment are the generation of a library with unbiased diversity and developing a screening/selection system that mimics as close as possible the desired working conditions in order to apply a correct selection pressure[12].

Diversity generation methods are crucial for the success of a directed evolution experiment. The classical example of diversity generation method used in directed evolution is *error-prone polymerase chain reaction* (epPCR). In most PCR reactions, *Thermus aquaticus* (Taq) *DNA* polymerase is used to amplify DNA[13]. Taq DNA polymerase has a missing 3'-5' proofreading exonuclease activity which leads to errors in the amplified DNA sequence[14]. Eckert and Kunkel observed in a standard PCR with Taq DNA polymerase an error frequency from $2*10^{-4}$ to $1*10^{-5}$ meaning one mutation per 50000 to 100000 nucleotides[15]. In addition, there are many different factors influencing the error frequency (mutations per nucleotide per cycle) such as applying high concentrations of $MnCl_2$ or $MgCl_2$, unbalanced dNTPs ratio, usage of nucleotide analogs, or addition of propanol/acids[16-20]. The main limitation of the epPCR method is a fairly uncontrollable mutation frequency and a biased mutational spectrum, 40.9 % of all substitutions are from A→T, T→A[21]. Since epPCR has so many limitations, the novel gene diversity method sequence saturation mutagenesis (SeSaM) was developed and widely used as a method of choice for diversity generation[22]. The advantage of SeSaM is the truly unbiased randomization of the target sequence at every single nucleotide position[22]. Thereby SeSaM overcomes the limitation of biased polymerases for transition (A↔G, T↔C) over

transversion (A/G→C/T, C/T→A/G). SeSaM is divided into four steps: (1) generation of DNA fragments with different lengths, (2) elongation with universal bases using terminal transferase, (3) amplification of the full length of the fragment and (4) exchange of the universal base[22]. Wong *et al.* described the optimal techniques to generate a diverse mutant library as followed: 1. unbiased mutational spectrum, 2. controllable mutation frequency, 3. consecutive nucleotide substitutions or codon-based substitutions, 4. enable subset mutagenesis, 5. independent of gene length, 6. technically simple and reproducible and 7. economical[23]. SDM and SSM are the methods of choice used as focused approaches within a directed evolution experiment. A pair of mutagenesis primers can be designed for the introduction of mutations at specific position in the gene sequence[24]. These changes can either be point mutations, insertion and/or deletion. It is a very fast, simple and straight forward method because the whole plasmid is amplified in a single PCR and no additional steps, such as purification, and cloning, are necessary. The disadvantage of SSM and SDM is that multiple or simultaneously mutagenesis is not possible. The developed method OmniChange allows the saturation of five independent codons simultaneously. Thereby, OmniChange is fragment size and sequence independent and final gene hybridisation is working without any additional PCR amplification or use of restriction enzymes[25].

A crucial step after gene diversity generation within a directed evolution campaign is the screening. Thereby the optimal screening system needs to mimic the final enzyme application conditions as close as possible and increases the possibility to identify improved variants regarding *e.g.* higher stability at defined pH or temperature, higher activity or higher affinity for the specific substrate. Leemhuis *et al*. described several different screening methods: agar plate screening, microtiter plate (MTP) screening, pico and femto-liter reactors: cells in droplets, cells as micro-reactors, cell surface display and *in vitro* selection and screening (Table 1)[26]. During agar plate screening the colonies are incubated with the substrate enabling detection of active enzyme via a visual signal like halo-formation or colour development[27]. The most common screening method is still MTP screening. The advantage is that 96 to 384 clones can be screened simultaneously, and furthermore several analytical tools can be used (such as colorimetric and fluorometric-based screening systems). The disadvantage of this screening strategy is the limitation in throughput of 10^4 variants per round, which is classified as a medium throughput system. Therefore, flow cytometer-based systems are used to overcome the above mentioned screening limitations by enabling a screening of up to 10^7 events per hour[28]. Flow cytometry screening systems can be performed *in vivo* using bacterial cells for expression (*E. coli* or *Bacillus*) and/or displaying the enzyme on the surface of the cell via anchoring motifs. Another method for flow cytometry screening system is *in vitro* using *e.g.* water-in oil-in water double emulsion compartmentalization of DNA encoding for an enzyme and *in vitro*-transcription-translation mixture[29-31]. The main challenge of flow cytometry screening systems are selection of suitable fluorogenic substrate which doesn't diffuse out of the cells or double emulsion compartment[32]. An overview of the screening methods employed in directed evolution campaigns is given in Table 1.

Table 1 Overview of screening and selection methods, their library size, advantage and disadvantage [26].

Strategy	Library size	Advantage	Disadvantage
Selection	$\sim 10^9$	Yields desirable variants	Only possible if activity gives growth advantage
Agar plate screen	$\sim 10^5$	Simple to operate	Limited dynamic range
Microtiter plate screen	$\sim 10^4$	All analytical methods possible, excellent dynamic range	Relatively low screening capacity
Cell-in-droplet screen	$\sim 10^9$	Large libraries	Fluorescence detection and DNA modifying enzymes
Cell as microreactor	$\sim 10^9$	Large libraries	Fluorescence detection
Cell surface display	$\sim 10^9$	Large libraries	Fluorescence detection
In vitro compartmentalization	$\sim 10^{10}$	No cloning steps, large libraries	Fluorescence detection and DNA modifying enzymes

2. Esterases

Hydrolases are a class of enzymes which catalyse the cleavage of chemical bonds using water as a nucleophile. Hydrolases include *e.g.* esterases, lipases, proteases, phosphatases, and nucleases. Esterases and lipases are very similar in their catalytic function both cleaving esters bonds (EC 3.1) and releasing *e.g.* fatty acids (Figure 2). In particular, esterases act on water-soluble carboxyl ester molecules which are composed of short-chain triglycerides[33-34].

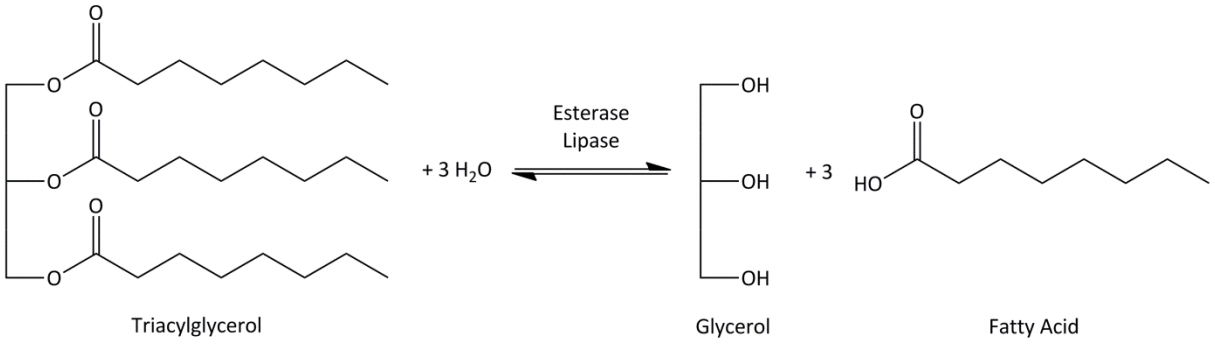

Figure 2 Hydrolysis of triacylglycerol catalysed by esterase or lipase. Modified from[35].

Ollis *et al.* showed that most hydrolytic enzymes have one element in common, the α/β hydrolase fold[36]. The α/β-hydrolase fold comprise eight β-strands and six α-helices (Figure 3). Most of the esterase and lipase have in a catalytic triad three amino acids Ser-Asp-His surrounded by the consensus sequence Gly-X-Ser-X-Gly[33]. Serine as a nucleophile is located between the β-5-strand and the α-C-helix, aspartic or glutamic acid is placed between β-7-strand and α-D-helix, whereas histidine is located after the β-8-strand (Figure 3).

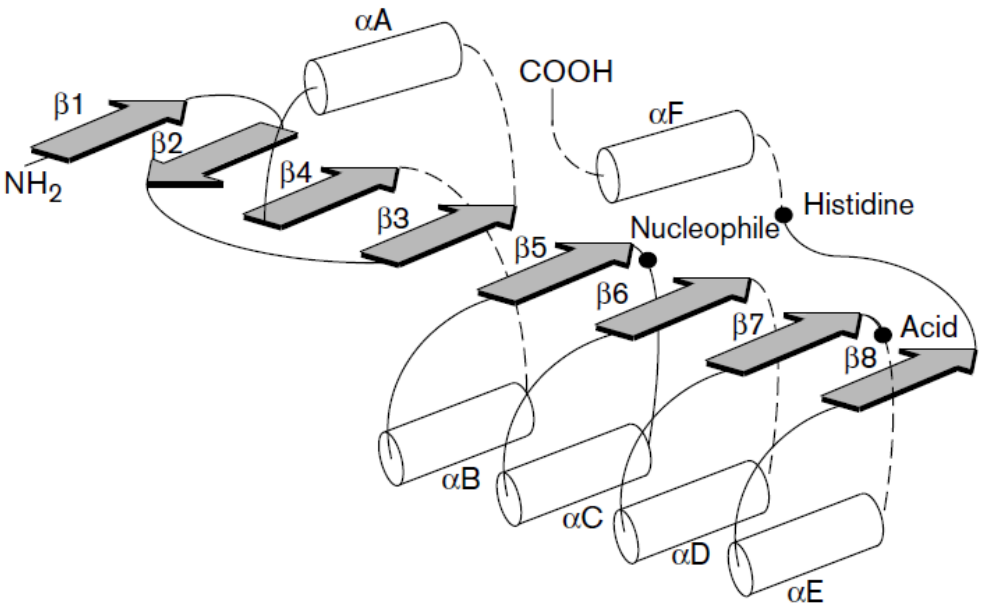

Figure 3 Schematic overview of the α/β hydrolase conformation. The arrows symbolise the β-strands, the cylinders show the α-helices, the three points are the catalytic amino acids (Ser, His and Asp), and the dotted line shows difference to the other hydrolases[36-37].

Structural similarity of serine protease and other hydrolases (*i.e.* catalytic triad, α/β-hydrolase fold) indicates that all serine hydrolases share the same reaction mechanisms[38]. The reaction mechanism is divided into two phases: acylation and deacylation. At the beginning of the acylation the hydroxyl group of the serine starts a nucleophilic attack on the carbon of the substrate (Figure 4A)[39]. The reaction proceeds via a negative charged carbonyl-oxygen (Figure 4B). The outcoming tetrahedral intermediate, which is stabilized in the oxyanion hole release an alcohol resulting in an acyl-enzyme intermediate (Figure 4C). The oxyanion hole is composed of two amino groups of the peptide chain (Gly193, Ser195)[40]. During the de-acylation the oxyanion hole stabilizes a tetrahedral intermediate which is formed by an attack of deprotonated water (Figure 4D). The catalytic mechanism ends by the release of the acid and the regeneration of the catalytic triad by rearrangement of electrons and proton of the histidine (Figure 4E)[40-41].

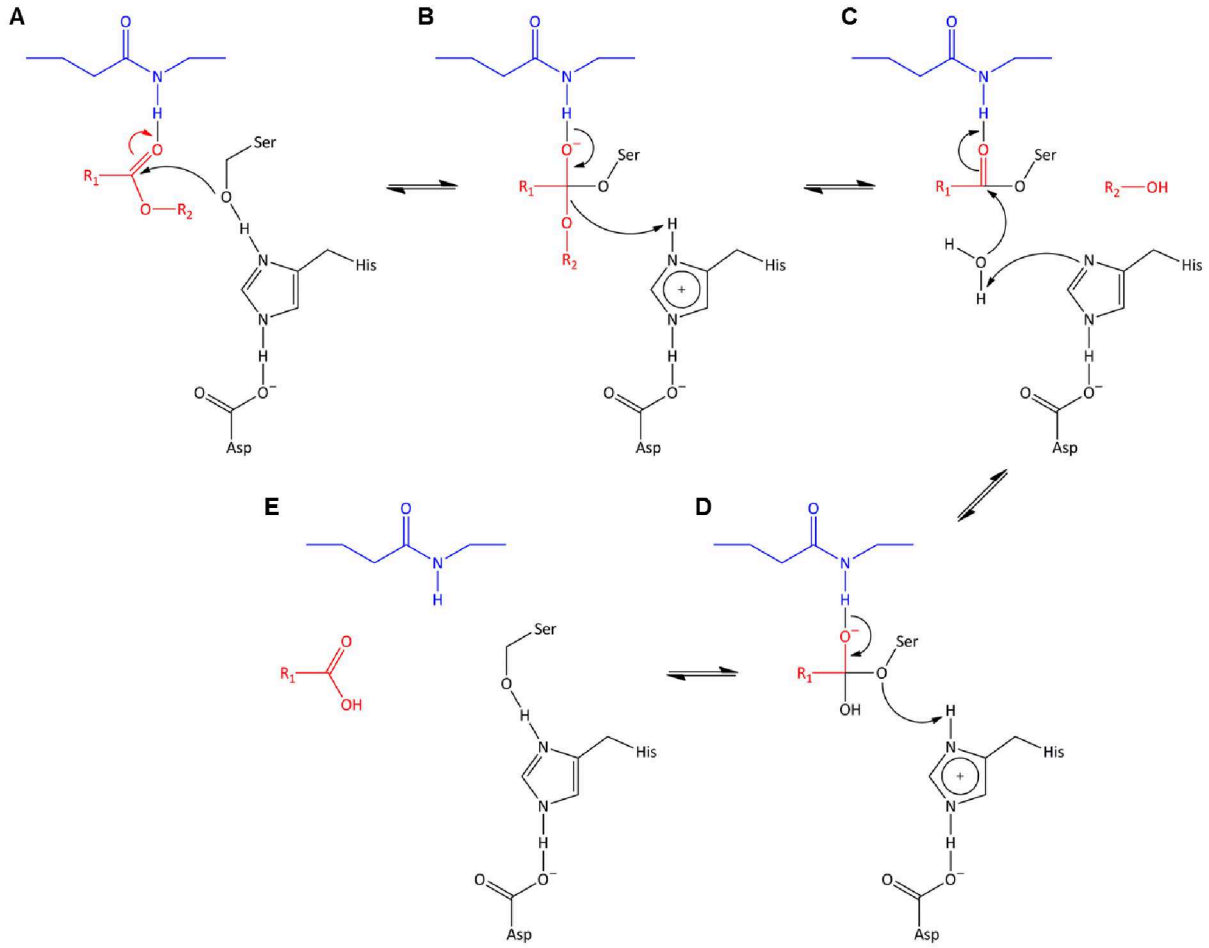

Figure 4 Mechanism of acylation and deacylation of the hydrolysis. Reaction is catalysed by esterases or lipases. **A:** nucleophilic attack, **B:** tetrahedral intermediate with oxyanion hole, **C:** acyl-enzyme intermediate and release of alcohol, **D:** tetrahedral intermediate with oxyanion hole, **E:** release of acid and regenerated catalytic triad. The substrate, released alcohol and acid are shown in red, the oxyanion hole in blue and the catalytic triad is shown in black, modified from[39].

Esterases can be found in many microorganisms (*e.g. Pseudomonas aeruginosa*, *Salmonella typhimurium*) as well as in nearly all plants and animals (*e.g.* pig, *Anthurium polyneuron*)[34, 42]. Esterases are an interesting enzyme class in the field of biotechnology due to the absence of cofactors for the catalytic reaction and their stability in organic solvents (*e.g.* DMF 15 %)[43]. Furthermore, esterases also have a wide temperature profile *e.g.* the carboxyl esterase NP from 35°C to 55°C[34, 44]. A wide range of different microorganisms has been screened (*e.g.* metagenome libraries) in order to identify new esterases for industrial applications[45]. Thereby, new esterases were identified and afterwards implemented in different production processes. The esterase from *Pseudomonas sp.* is used in the production process of ibuprofen, because the enzyme hydrolyses the reaction in a stereo-specific manner with more than 99 % efficiency[46]. Another esterase from *Ophistoma piceae* is implemented in the paper manufacturing application because of the efficient hydrolysis of triglycerides and sterol esters[47]. In the bio-fuel industry feruloyl esterases play key physiological role due to their possibility to degrade the complex structure of plant cell walls, which is involved in the crosslinking of hemicellulose and lignin[48-49]. Additionally, esterases isolated from *Bacillus sp.* are preferred enzymes for laundry detergents due to their ability to hydrolyse polyethylene

terephthalate (PET) substrate which are commonly used in the textile industry for the production of novel sport textiles[50]. Overall it is shown that esterases are widely applicable in different production processes and will be more and more used in the chemical industry.

3. Polyethylene terephthalate

Polyethylene terephthalate (PET) is one of the plastics which production and use recently expanded in European market. In the year 2011 6.5 % of the overall used plastics was PET, beside the other five groups: polypropylene (PP), polyethylene – low density (PE-LD), polyethylene – high density (PE-HD), polyvinyl chloride (PVC), polystyrene (PS), and polyurethane (PUR) (Figure 5)[51].

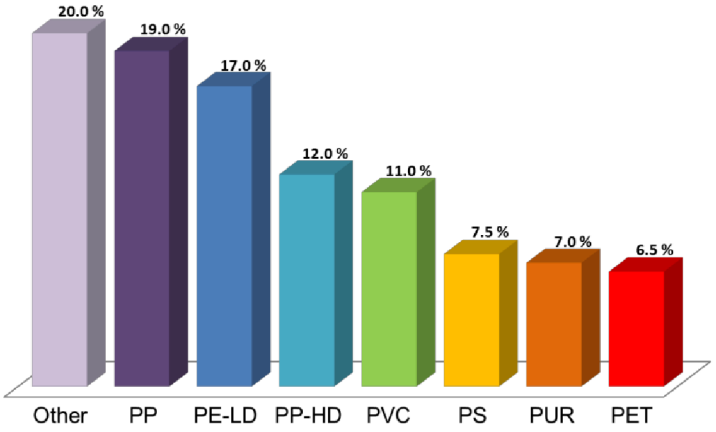

Figure 5 European plastic demand of different plastics types in the year 2011 (polypropylene (PP), polyethylene – low density (PE-LD), polyethylene – high density (PE-HD), polyvinyl chloride (PVC), polystyrene (PS), polyurethane (PUR), polyethylene terephthalate (PET)), modified from[51].

PET is a thermoplastic polymer belonging to the family of polyesters. PET monomers can be produced by (1) reaction of dimethyl terephthalate with ethylene glycol in a transesterification reaction with methanol as byproduct or (2) esterification of terephthalic acid and ethylene glycol with water as byproduct[52]. A polycondensation reaction takes place to build up the aromatic linear PET polyester (Figure 6) with no crosslinks[53].

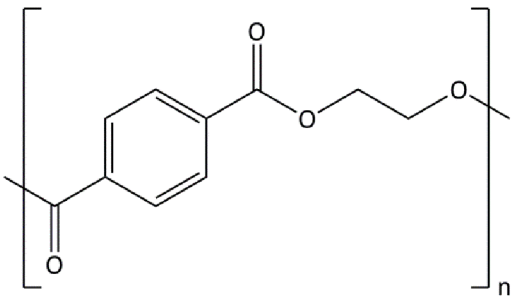

Figure 6 Structure of polyethylene terephthalate (PET) with n number of repeating units.

Dependent on final application (beverage containers, textiles and food packaging) produced PET can be semi-rigid to rigid or flexible, with a high tear strength and light resistance and can be used as a moisture barrier[54-55]. Additionally, PET exhibits high mechanical strength, low permeability to gases and a chemical resistance making PET-fibers very interesting for

the textile industry[54]. In the textile industry PET-fibers were used for the production of novel sport textiles, because they improve the wetting properties and furthermore the strength retention of polyester fabrics. Interestingly, an anti-pilling effect of hydrolases (cutinase; esterase; and lipase) is reported for PET-fibers which makes esterases also very attractive for the laundry industry[56]. The esterases can be implemented in novel detergents for sport textiles (based on PET-fibers) to minimize the pilling effect.

The worldwide annual production of plastic bottles, synthetic fibers, and foils accounts for 40 million tons of PET (http://www.verpackungsbarometer.de/fuer-verbraucher /materialkunde2/vom-erdoel-zur-pet-flasche, accessed 24.10.2015)[57]. PET shows a high resistance towards humidity or microbial attacks and do not rot in the environment which makes its degradation challenging[53]. The low biodegradability of PET causes waste accumulation in either terrestrial or aqueous environment after washing of synthetic clothes and release of microparticels in sewage water[58]. Due to the high global PET production, PET degradation and recycling are important topics for achieving a sustainable bioeconomy[59].

Mechanical degradation through disintegration, granulation and recycling of PET can only be applied partially to remove PET waste and do not result in high value degradation products due to missing high quality standards[60]. Until now, the most common way is the chemical PET degradation: (1) methanolysis, (2) glycolysis, (3) hydrolysis, (4) ammonolysis, (5) aminolysis and (6) other processes[60]. A advancement would be to design plastic which can undergo a controllable biological degradation[61]. Since 1970 the research is done to find enzymes which are able to catalyze the biological PET degradation. In 1977 Tokiwa and Suzuki showed that extracellular lipases attack ester bonds in polyester and are promising candidates for the degradation of PET[62]. The potential of an esterase to degrade PET polymer was firstly reported by Ribitsch *et al.* in 2011[59]. Until now PET degradation is reported for hydrolases like esterases, lipases and cutinases[63]. The essential step performed by the enzymes is the hydrolysis of the ester or amide bonds in the polymers[53]. The problematic of the current enzymatic degradation is the elevated temperature. The optimal enzyme reaction temperature for the degradation of PET is around ~40°C. However at this temperature, PET substrate is crystal and rigid. Therefore, a hydrolysis of the PET is not possible, due to the low accessibility of the substrate for the enzyme. By increasing the temperature above 60°C the flexibility of PET side chain can be increased and allows a better substrate fitting in the active site of the hydrolases[64]. Nevertheless, the required temperature for the PET degradation (above 60°C) has a negative effect on the enzyme activity, since most of the enzymes are inactive at temperatures higher than 60°C.

4. Objectives

The project “Functionalization of Polymers” (FKZ: 031A227F), founded by the innovation initiative industrial biotechnology of the German Federal Ministry of Education and Research (BMBF), aims to optimize enzymes to efficiently modify natural or synthetically polymers for a sustainable usage in the industry. The main objective in the frame of “Functionalization of Polymers” project is the enzyme-based functionalization of synthetic PET polymers in order to improve its degradation, and to tailor enzymes to efficiently perform in laundry detergent application such as improving appearance, as well as the life time of the fibres.

The goal of this thesis was to generate improved esterase variants which can fulfil industrial requirements like PET degradation. For an economically reasonable application the esterase needs a significant higher activity towards PET degradation. In order to achieve a higher specific activity a protein engineering campaign had to be performed. A screening system needed to be developed which has a low standard deviation and a substrate that mimics the PET structure. First insights into principles and underlying molecular basis had to be elucidated by investigating structure function relationships.

The main objectives were divided into three parts (Part II, Part III Part IV). The aim of the Part II was the optimization of the esterase towards increased activity and degradation of PET by means of directed evolution using an esterase isolated from *B. licheniformis*. The second objective presented in Part III of this work was the optimization and validation of an ultra-high throughput screening platform in order to overcoming the limitations in throughput obtained by a MTP-based screening system. In the Part IV, in-depth analysis of esterase structure especially on lid like loop as key feature for substrate acceptance is presented in order to generate first hypothesis on PET degradation activity.

Part II: Development of a continuous MTP screening system for esterases based on conversion of aromatic model substrates resembling complex PET structure

Parts of this chapter were published by the author in the journal of Applied Microbiology and Biotechnology. Reproduced with kind permission from Springer Science and Business Media.

"Lülsdorf N., Vojcic L., Hellmuth H., Weber T. T., Mußmann N., Martinez R. and Schwaneberg U. (2015) *A first continuous 4-aminoantipyrine (4-AAP)-based screening system for directed esterase evolution*. Appl. Microbiol. Biotechnol. 99(12), 5237-5246"

Goals and main results

The aim of this work was to develop a screening system which overcomes the limitation of available screening systems based on *p*-nitrophenyl- (*e.g. p*-nitrophenyl acetate) or umbelliferyl-esters and broadens substrate scope towards more complex aromatic substrates. The novel screening system based on the substrate phenol benzoate was established and optimized for medium throughput screening in MTP for increased thermal resistance, with a standard deviation less than 5 %. The screening system was validated by screening of *p*NBEBL (*p*-nitrobenzyl esterase *B. licheniformis*) mutant library and identification of variant T3 Ser378Pro with 4.7-fold improved residual activity after thermal treatment.

1. Introduction

Identification of improved enzyme variants in directed evolution campaigns requires a robust and reliable screening system[65-66]. In directed esterase evolution indicator agar plates supplemented with tributyrin[34] are commonly used to qualitatively screen up ~10^5 variants[26]. Medium or high throughput screening systems are based on chromogenic or fluorogenic phenols, like acetates or butyrates of nitrophenol or 4-methylumbelliferone, resofurin or fluorescein[67-68]. The most prominent assay relies on monitoring esterolytic activity based on *p*-nitrophenyl-esters as substrates. The release of the product *p*-nitrophenolate can spectrophotometrically be monitored at 410 nm[69]. The main disadvantage of *p*-nitrophenyl-based screening systems is the pH sensitivity[70-71]. At a pH higher than 8.0 a spontaneous hydrolysis of the aliphatic esters in aqueous solutions takes place resulting in a high background signal[67, 72-73]. Nevertheless, mainly *p*-nitrophenyl-based screening systems were applied in directed esterase evolution campaigns. Moore *et al.* used *p*-nitrobenzyl ester as substrate to increase the activity of *p*-nitrobenzyl esterase 16-fold compared to WT[43]. The thermal stability of a *B. subtilis p*-nitrobenzyl esterase was improved after six rounds of random mutagenesis. The identified variant showed an improved

thermostability with more than 14°C increase in T_M[44]. In addition, four rounds of random mutagenesis and two subsequent rounds of recombination were needed to generate a *p*-nitrobenzyl esterase variant with a 150-fold improvement in presence of 15 % dimethylformamide[74]. A report about a *p*-nitrobenzyl esterase highlighted the identification of a variant with 100-fold increased activity in aqueous-organic solvents. The isolated variant was generated by epPCR and gene shuffling library and screened with the *p*-nitrobenzyl-ester of the antibiotic loracarbef[75]. In addition to the colorimetric-based screening systems pH-stat and fluorometric assays were applied for the characterization and identification of improved esterase variants. An overview of esterase activity detection methods is provided in Table 2.

Table 2 Overview of available screening formats, substrates and methods employed for esterase activity determination[76].

Method	Substrate	Reference
Agar plate	*p*-nitrophenyl acetate (C2)	69
	Tributyrin	77-79
Colorimetric (cuvette, microtiter plate)	*p*-nitrophenyl acetate (C2)	69, 79-86
	p-nitrophenyl propionate (C3)	80, 82
	p-nitrophenyl butyrate (C4)	79-80, 82, 86-88
	p-nitrophenyl valerate (C5)	78
	p-nitrophenyl caproate (C6)	78, 80, 82, 86, 89
	p-nitrophenyl caprylate (C8)	80, 82, 87, 89
	p-nitrophenyl caprate (C10)	78, 80, 82, 86, 89
	p-nitrophenyl laurate (C12)	80, 82, 86, 89
	p-nitrophenyl myristate (C14)	89
	p-nitrophenyl palmitate (C16)	78, 89
	p-nitrophenyl stearate	89
	Triacetin	79, 86
	Tributyrin	86
	Tricaproin	86
Flow cytometry	5,6 carboxy fluorescein diacetate	90
	Fluoresein diacetate	90
Fluorometric (cuvette, microtiter plate)	4-methylumbelliferyl acetate	91-92
	4-methylumbelliferyl butyrate	91-92
	Diehtyl 4-methylumbeliferyl phosphate	85
	p-nitrophenyl palmitate (C16)	92
Titration (pH-stat method)	Diethyl *p*-nitrophenyl phosphate	81
	Triacetin	89
	Tributyrin	89
	Tricaprin	89
	Tricaproin	89
	Tricaprylin	89
	Triolein	89
	Tripropionin	89

Hydrolases *e.g.* cutinases, esterases, and lipases showed an anti-pilling effect for PET-fibers and additionally improving the wetting properties and thereby strength retention of polyester fabrics, which gave a first hint for a possible PET degradation application[56]. Ribitsch *et al.* reported in 2011 the degradation of PET polymer by esterases[59]. They used HPLC analysis to detect the degradation of PET and of the model substrate bis-(benzoyloxyethyl)-terephthalate by identifying the released monomers. For a directed evolution campaign the HPLC method is not useful, because the number of analysis is limited and therefore a mutant library (with ≥2000 clones) cannot be successfully screened. Another possible PET degradation detection method is halo formation through agar plates, where PET or bis-(benzoyloxyethyl)-terephthalate is solubilized. Applying this method only allows a qualitative evaluation. The challenge in detecting PET degradation activity is to generate a reliable MTP-based screening system although PET is poorly soluble *e.g.* in σ-cresol. Overcoming this problem a model substrate mimicking PET had to be employed. As PET has an aromatic structure the similar substrate phenyl benzoate was selected which resembles the aromatic structures of PET and additionally has the same orientation of the ester bond.

In this part of the thesis a directed esterase evolution towards hydrolysis of aromatic esters was reported applying a continuous high throughput screening system in 96-well MTP format. The screening system was validated in a directed evolution campaign employing a random *p*NBEBL mutagenesis library in a single round of direction evolution.

2. Material and methods

2.1. Material

Chemicals were of analytical-reagent grade or higher quality and purchased from Invitrogen (Darmstadt, Germany), Carl Roth GmbH (Karlsruhe, Germany), Sigma-Aldrich (Hamburg, Germany) and AppliChem (Darmstadt, Germany). All enzymes were purchased from New England Biolabs GmbH (Frankfurt, Germany). Thermal cycler (Mastercycler proS; Eppendorf, Hamburg, Germany) and thin-wall PCR tubes (Multi-ultra tubes; 0.2 ml; Carl Roth GmbH, Karlsruhe, Germany) were used in all PCRs. Oligonucleotides were purchased from Eurofins MWG operon (Ebersberg, Germany). The amount of DNA in cloning experiments was quantified using a NanoDrop photometer (ND-1000, NanoDrop Technologies, Wilmington, DE, USA). Plasmid extraction and PCR purification kits were purchased from Macherey-Nagel (Düren, Germany). Sunrise plate reader (Tecan Group AG, Männedorf, Switzerland) was used for absorbance detection. Microtiter plates (Greiner Bio-One GmbH, Frickenhausen, Germany) were incubated in a Multitron II Infors shaker (Infors AG, Bottmingen, Switzerland).

2.1.1. Target gene

The gene *p*-nitrobenzyl esterase (*p*NBEBL) (GenBank number: AAU39577.1) from *B. licheniformis*, composed of 491 amino acids, has a molecular weight of ~54 kDa[93]. The gene of *p*NBEBL was ordered as a synthetic gene (GeneArt, Regensburg, Germany). The sequence has a sequence identity of 60.8 % to a *B. subtilis p*-nitrobenzyl esterase (PDB 1CFI)[75].

2.1.2. Strains and plasmids

The *E. coli* strains DH5α and BL21-Gold (DE3) were purchased from Agilent Technologies (Santa Clara, USA) and used either as hosts for DNA manipulation or for recombinant protein expression. The plasmid pET22b(+) from Novagen (Darmstadt, Germany) was used to construct an expression vector. The used strains and plasmids were summarized in Table 3 and Table 4.

Table 3 Bacterial strains used in this work.

Strain	Description	References
E. coli DH5α	F-*mcr*A Δ(*mrr-hsd*RMS-*mcr*BC) *end*A1 *rec*A1 ϕ80d*lac*ZΔM15 Δ*lac*X74 *ara*D139 Δ(*ara,leu*)7697 *gal*U *gal*K *rps*L *nup*Gλ *ton*A	Agilent Technologies
E. coli BL21-Gold (DE3)	F^- *ompT hsdS*(r_B^- m_B^-) *dcm*$^+$ Tet^r *gal* λ(DE3) *endA* Hte	Agilent Technologies

Table 4 Plasmid used in this work.

Plasmid	Description	References
pET22b(+)	Expression vector, Amp^R	Novagen

Amp^R: Ampicillin resistance gene

2.1.3. Oligonucleotides

The oligonucleotides were ordered from Eurofins MWG Operon (Ebersberg, Germany) in salt-free form and are summarized in Table 5 - Table 8.

Table 5 Primers for epPCR (small letters indicates phosphorothioate nucleotides).

Primer name	Sequence 5'-3'
FW_eppnBDSM_PTO	cttgtcgacggaGCTCGAATTCTTATTA
RV_eppnBDSM_PTO	atacaactgtcgAAACACGCTTCGG

Table 6 Primers for vector backbone (small letters indicates phosphorothioate nucleotides).

Primer name	Sequence 5'-3'
FW_pET22_PTO	cgacagttgtatCATACATCAT
RV_pET22_PTO	tccgtcgacaagCTTGC

Table 7 Primers for site-saturation mutagenesis library (Underlined indicates randomized codons).

Primer name	Sequence 5'-3'
Fw_SSM_298	GGCGCGGCAAAA**NNK**ATCAATCTATTAATCGG
Rv_SSM_298	CCGATTAATAGATTGAT**MNN**TTTTGCCGCGCC
Fw_SSM_377+378	CGGCTCAATCACGATAT**NNKNNK**GTCTTTATGTACCGG
Rv_SSM_377+378	CCGGTACATAAAGAC**MNNMNN**ATATCGTGATTGAGCCG

Table 8 Primer for site-directed mutagenesis (Underlined indicates mutagenized codons).

Primer name	Sequence 5'-3'
Fw_Ala377Met	CTCAATCACGATAT**ATG**TCTGTCTTTATGTACCGG
Rv_Ala377Met	CCGGTACATAAAGACAGA**CAT**ATATCGTGATTGAG
Fw_Ser378Pro	CTCAATCACGATATGCA**CCT**GTCTTTATGTACCGG
Rv_Ser378Pro	CCGGTACATAAAGAC**AGG**TGCATATCGTGATTGAG

2.1.4. Cell culture medium and cultivation

Cells were cultivated and expressed in Luria Broth (LB) media supplemented with the respective antibiotics. For isolation of plasmid the cells were incubated (ON, 37°C). For the expression pre-culture the cells were incubated (ON, 37°C), subsequently the main culture was incubated (37°C) until an OD_{600} of 0.6 was reached and then expressed (4 h, 30°C). Transformants were cultivated on a LB-agar plate. Differentiation of active and inactive clones was done on LB-agar plates supplemented with tribuytrin. All medias and antibiotics are listed in Table 9 and Table 10.

Table 9 Medium and agar plates used in with work.

Medium/Agar plate	Composition
LB-medium (1 l)	10 g tryptone
	5 g yeast extract
	10 g NaCl
LB-agar plates (1 l)	LB-medium + 15 g agar
LB-ager plates (0.8 l) with tributyrin	Solution A:
	15 g yeast extract
	10 g tryptone
	5 g NaCl
	15 g agar
	Adjust pH to 7.5
	Solution B:
	1.5 g gummi arabicum
	30 ml tribuytrin

Table 10 Antibiotic used for cell culture in this work.

Antibiotics	Stock [mg/mL]	Solvent	Working concentration [µg/mL]
Ampicillin	100	Milli Q Water	100

2.2. Methods

2.2.1. Cloning

Chemically competent cells of *E. coli* DH5α and *E. coli* BL21-Gold (DE3) were produced in-house with a transformation efficiency of $2.2*10^6$ and $1.8*10^7$ using the rubidium chloride technique[94]. The gene p*nbebl* (GenBank: AAU39577.1), was ordered as a synthetic gene together with the pelB leader sequence (GeneArt, Regensburg, Germany) and transformed into *E. coli* DH5α[93, 95-96]. Plasmid was extracted using the plasmid isolation kit from Machery & Nagel (Düren, Germany) and plasmid, containing the synthetic gene, and the pET22b(+) expression vector were digested using *Xba*I (100 U) and *Eco*RI (100 U) restriction enzymes. After purification of the specific genes, the digested *pelB*-p*nbebl* gene and vector pET22b(+) were ligated using T4 DNA ligase (5 U) resulting in pET22b(+)-pelB-*p*NBEBL. For generation of plasmid construct without the pelB leader sequence pET22b(+)-pelB-*p*NBEBL was digested with *Nde*I (100 U) and the backbone was religated. Plasmid was verified by sequence analysis (Eurofins MWG Operon, Ebersberg, Germany) and Clone Manager 9 Professional Edition (Sci-Ed software, Cary, USA). For expression experiments the plasmids were additionally transformed into *E. coli* BL21-Gold (DE3).

2.2.2. Construction of epPCR library with PLICing

The random mutagenesis library was generated by using the standard epPCR[17]. For the mutagenic PCR of the insert *p*NBEBL the followed program was used (Table 11).

Table 11 epPCR program for *p*NBEBL.

Step	Temperature [°C]	Time [sec]	Cycle [-]
Initial denaturation	94	60	1x
Denaturation	94	30	
Annealing	58	30	25x
Elongation	72	90	
Final elongation	72	600	1x

The PCR reaction mixture comprised of Taq DNA polymerase (2.5 U), dNTP mix (10 mM), plasmid template (pET22b(+)-*p*NBEBL, 30 ng), $MnCl_2$ (0.04-0.20 mM) and phosphorothioate DNA primers (Table 5) (20 µM). For the vector backbone amplification the following PCR program was used (Table 12).

Table 12 PCR program for vector backbone amplification.

Step	Temperature [°C]	Time [sec]	Cycle [-]
Initial denaturation	98	30	1x
Denaturation	98	10	
Annealing	54	30	25x
Elongation	72	240	
Final elongation	72	600	1x

For the reaction the following mixture was used: Phu DNA polymerase (2.5 U), dNTP mix (10 mM), plasmid template (pET22b(+)-*p*NBEBL, 30 ng) and phosphorothioate DNA primers (Table 6) (20 µM). Agarose gel electrophoresis was performed to confirm the corresponding size of the amplified insert and vector backbone constructs[97]. The PCR products were digested with *Dpn*I (20 U) (ON, 37°C), *Dpn*I was subsequently inactivated (20 min, 80°C)[98]. The PCR products were purified using QIAquick PCR Purification Kit (Qiagen GmbH, Hilden, Germany). The cloning was performed by PLICing and hybridized DNA fragments were transformed into *E. coli* BL21-Gold (DE3)[99-100].

2.2.3. Generation of site-saturation and site-directed mutagenesis libraries

Site-saturation mutagenesis library consist of amino acid position 298, 377 and 378. For site-directed mutagenesis position 377 and 378 were chosen. According to Wang and Malcolm a mutagenic “two-stage” PCR was performed for SSM and SDM, where the first step contains two reaction mixture for separation of the forward and revers oligonucleotide[101]. Subsequently, in the second step both reactions mixtures were combined and the PCR program shown in Table 13 was continued.

Table 13 "Two-stage" PCR program for site-saturation and site-directed mutagenesis.

Step 1	**Temperature [°C]**	**Time [sec]**	**Cycle [-]**
Initial denaturation	98	60	1x
Denaturation	98	30	
Annealing	55[a]/61[b]	30	3x
Elongation	72	420	
Step 2	**Temperature [°C]**	**Time [sec]**	**Cycle [-]**
Initial denaturation	98	60	1x
Denaturation	98	30	
Annealing	55[a]/61[b]	30	15x
Elongation	72	300	
Final elongation	72	300	1x

[a] 55°C for SSM, [b] 61°C for SDM

For the PCR mixture PfuS DNA polymerase (2.5 U), dNTP mix (10 mM), plasmid template (pET22b(+)-*p*NBEBL, 30 ng) and oligonucleotides listed in Table 7 and Table 8 (20 µm) were used. The resulted PCR products were digested with *Dpn*I (20 U) and afterwards purified using a PCR clean-up Gel extraction kit. Transformation was performed into *E. coli* BL21-Gold (DE3) for expression.

2.2.4. Detection of esterolytic activity on tributyrin plates

LB-agar plates with tributyrin were supplemented with 0.1 mM isopropyl thio-β-D-galactoside (IPTG) and Amp. The semi-quantify assay was used to detect enzymatic activity via halo formation. Colonies showing esterolytic activity were transferred in a microtiter plate (MTP).

2.2.5. Growth conditions and expression in microtiter plates

Colonies displaying active enzyme variants (2.2.4) were transferred into a 96-well MTP (flat bottom) containing 150 µl LB-medium supplemented with Amp and cultivated in a microtiter plate shaker (ON, 37°C, 900 rpm, 70 % humidity) (pre-culture). For the main-culture 150 µl LB-medium supplemented with Amp were inoculated with 10 µl pre-culture (v-bottom MTP). The main-culture was incubated (2.5 h, 37°C, 900 rpm, 70 % humidity) until OD_{600} was reached 0.6. Protein expression was induced by adding 0.1 mM IPTG and incubated (4 h, 30°C, 900 rpm, 70 % humidity). Afterwards cells were harvested by centrifugation (15 min, 4°C, 3220 g), medium supernatant was removed and cell pellets were stored overnight at -20°C. Cell pellets were resuspended in 150 µL PBS buffer (137 mM NaCl, 2.7 mM KCl, 10 mM Na_2HPO_4, 2 mM KH_2PO_4, pH 7.4) supplemented with lysozyme (1 mg/ml) and incubated for cell disruption (1 h, 37°C, 900 rpm, 70 % humidity). Afterwards the MTPs were centrifuged (15 min, 4°C, 3220 g) and the supernatant containing active enzyme was transferred in a fresh MTP and used for enzyme activity assays.

2.2.6. Expression in flask and purification by anion exchange chromatography

Enzyme WT and identified variants were expressed for purification and further characterization. Therefore, pre-cultures were grown (ON, 37°C, 250 rpm). Subsequently, 1 % of the pre-culture was used to inoculate the main-culture (200 ml LB-medium supplemented with Amp). The cultures were incubated in 1000 ml flasks (37°C, 250 rpm) until an OD_{600} of 0.6 was reached. Overexpression was induced by adding 0.1 M IPTG and incubated (4 h, 30°C, 250 rpm). Cells were harvested by centrifugation (30 min, 4°C, 3220 g) and cell pellets were frozen overnight at -20°C. For purification the cell pellets were resuspended in 20 ml HEPES-buffer (10 mM, pH 7). Cell disruption was carried out by using Vibra-Cell VCX130 (Sonics, Newtown, CT, USA) the received lysate was centrifuged (30 min, 4°C, 3220 g). Supernatant containing the enzyme was concentrated with Amicons (10 kDa cut off, Merck Millipore, Darmstadt, Germany) and washed three times with 10 ml HEPES buffer (10 min, 4°C, 3220 g). The concentrated sample was filtered (0.45 µM) and loaded into a Toyopearl Super Q 650c anion exchange column (*p*NBEBL: pI ~4.7, http://web.expasy.org/cgi-bin/compute_pi/pi_tool) connected to an Äktaprime plus FPLC system (GE Healthcare, Solingen, Germany). The protein was eluted with 19 % NaCl (1 M). Fractions showing esterolytic activity were pooled, concentrated and total protein concentration was determined by Pierce™ BCA protein assay kit (Thermo scientific, Waltham, MA USA)[102] and the homogeneity analysed by capillary electrophoresis (Experion system, BioRad, München, Germany).

2.2.7. Sodium dodecyl sulfate polyacrylamide gel electrophoresis (SDS-PAGE)

The SDS-PAGE was used to confirm the expression and the corresponding size of the expressed *p*NBEBL. A stacking gel (5 % (w/v) acrylamide) and a separating gel (12 % (w/v) acrylamide) were used for separation[103]. Subsequently, the SDS-PAGE was stained with Coomassie brilliant blue.

2.2.8. Continuous *B. licheniformis* esterase 4-aminoantipyrine screening system (cBLE-4AAP) for microtiter plates

The continuous *B. licheniformis* 4-aminoantipyrine screening system (cBLE-4AAP) is modification of the 4-aminoantipyrine assay (4AAP assay)[104-105]. For esterolytic activity detection the assay was performed at room temperature (RT) using the supernatant after cell disruption. Additionally, a detection solution and a substrate solution are needed, which have to be prepared fresh. The detection solution must be prepared in the following order: 20 µl NaOH (0.01 M), 15 µl of potassium peroxodisulfate (5 mg/ml) in phosphate-buffered saline (PBS-buffer, 137 mM NaCl, 2.7 mM KCl, 10 mM Na_2HPO_4, 2 mM KH_2PO_4, pH 7.4) and 15 µl of 4AAP (5 mg/ml) in PBS-buffer (pH 7.4). The substrate solution contained 17.5 µl PBS-buffer (pH 7.4) supplemented with 2.5 µl 100 mM phenyl benzoate solved in acetonitrile. The final assay mixture comprises 160 µl PBS buffer (pH 8.5), 20 µl supernatant containing *p*NBEBL, 50 µl of the detection solution and 20 µl substrate solution. The release of 1,5-dimethyl-4-(4-oxo-cyclohexa-2,5-dienylidenamino)-2-phenyl-1,2-dihydro-pyrazol-3-one was continuously monitored at 509 nm (60 cycles, 30 sec, shaking 3 sec before first measurement) in a microtiter plate reader.

2.2.9. Screening for improved thermal resistance

Identification of variants showing an increased thermal resistance was performed by incubating 50 µl supernatant of cell lysate containing *p*NBEBL in a 96-well MTP PCR-plate for (30 min, 55°C) in a Mastercycler proS (Eppendorf, Hamburg, Germany). After cooling down on ice (5 min) the residual esterolytic activity was determined at RT by the cBLE-4AAP assay (2.2.8). Residual activity was calculated by dividing activity value of treated supernatant of cell lysate with activity value of non-treated supernatant of cell lysate.

2.2.10. Characterization of purified *p*NBEBL for thermal resistance

The final characterization of the identified *p*NBEBL variants was done with purified enzyme (2.2.6) diluted to a final concentration of 180 ng/µl. Characterization regarding thermal resistance was done in a temperature range from 50°C to 85°C with 50 µl pure enzyme for 30 min (2.2.9). Afterwards the samples were cooled on ice (5 min) and the remaining esterolytic activity was determined at RT with the cBLE-4AAP screening system (2.2.8). The specific activity was calculated in Units, using the extinction coefficient for quinoneimine dye (6.58 $l*mmol^{-1}*cm^{-1}$) (Oriental Yeast Co., Ltd., Japan). One Unit was defined as the amount of esterase that catalyses the conversion of 1 nmol phenyl benzoate per minute.

2.2.11. Computational studies on *p*NBEBL by YASARA to understand increased activity

The software YASARA (Yet Another Scientific Artificial Reality Application, www.yasara.org[106]) was used to generate the homology model based on the crystal structure of 1QE3, 1C7I, 1C7J (*p*-nitrobenzyl esterase from *B. subtilis*[75]) and 2OGT (carboxyl esterase from *Geobacillus stearothermophilus*[107]). The molecular dynamic simulations of the generated variants were done by FoldX[108] as implemented plugin in YASARA[109].

2.2.12. Differential scanning calorimetry (DSC) for understanding of increased thermal resistance

The differential scanning calorimetry (DSC) (DSC 8000, Perkin Elmer, Waltham, USA) was used to detect the amount of Joule (J) which is needed to denature the protein. Pure protein (40 µl, 20 mg) was filled in stainless steel sample containers (large volume capsules, Perkin Elmer, Waltham, USA) and closed by pressure. The reference sample was filled with 40 µl PBS pH 7.4. The purified protein was analysed with the following method: heating from 25°C to 70°C with 10°C/min.

3. Results

In this work, the cBLE-4AAP medium throughput screening system was established and the performance parameters in MTPs were determined for the quantification of esterolytic activity. Subsequently, the *p*NBEBL was used for a directed evolution campaign to validate the cBLE-4AAP screening platform. Finally improved *p*NBEBL variants were purified and characterized.

3.1. Cloning and expression of *p*NBEBL

The wildtype (WT) gene *p*NBEBL was ordered as a fusion protein with the N-terminal leader sequence pelB. PelB was firstly isolated from *Erwinia carotovora* as the pectate lyase B with 22 amino acids which is a periplasm destination peptide[110-111]. The synthetic gene was delivered by GeneArt in the vector pMK-RQ. The fusion protein pelB-*p*NBEBL was subcloned into the expression vector pET22b(+) containing the T7-bacteriophage system[112]. For restriction *Eco*RI and *Xba*I were used, subsequent the ligation was performed with the T4 DNA ligase and resulted in the construct pET22b(+)-pelB-*p*NBEBL (Figure 7A). The construct pET22b(+)-pelB-*p*NBEBL was digested with *Nde*I and religated to generate a construct without the pelB leader sequence (Figure 7B). The successful cloning was confirmed by sequence analysis.

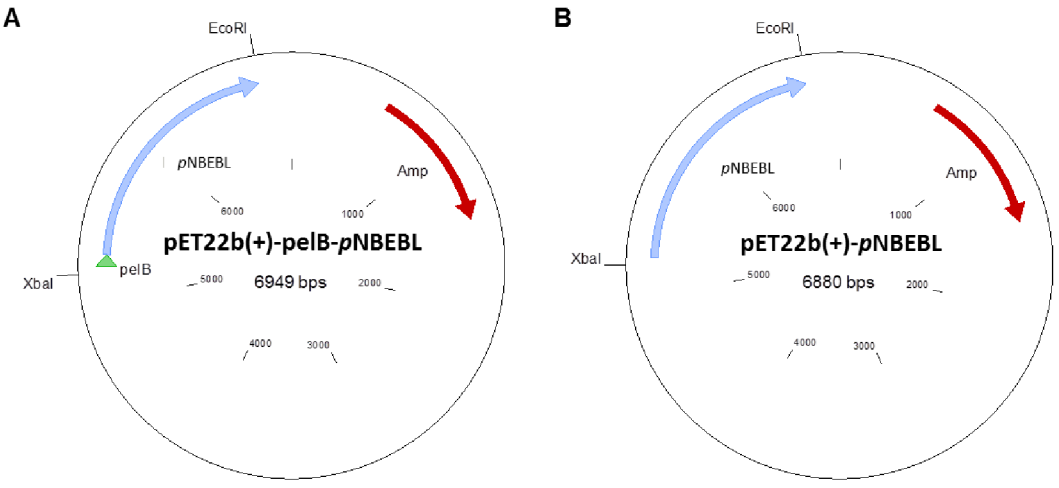

Figure 7 Vector map of the generated construct pET22b(+)-pelB-*p*NBEBL (**A**) and pET22b(+)-*p*NBEBL (**B**). PelB sequence (green); *p*NBEBL (blue) and Amp (red).

The final constructs pET22b(+)-pelB-*p*NBEBL and pET22b(+)-*p*NBEBL were transformed for expression in chemically competent *E. coli* BL21-Gold (DE3) cells, and subsequently expressed for 4 h at 30°C. The expression level was determined using pET22b(+) empty vector (EV) as a reference. Protein production was analysed using SDS-PAGE electrophoresis (Figure 8).

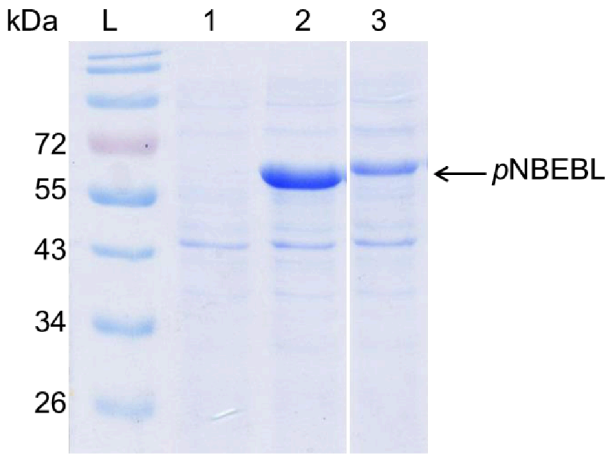

Figure 8 SDS-PAGE analysis confirmed successful expression of *p*NBEBL. Enzyme was expressed for 4 h at 30°C. 7.5 µl of cell lysate containing the expressed protein was loaded on the SDS-PAGE. **L**: ladder in kDa, **1**: pET22b(+), **2**: pET22b(+)-*p*NBEBL, **3**: pET22b(+)-pelB-*p*NBEBL (merged). Estimated protein size ~54 kDa.

Figure 8 shows that construct with pelB leader sequence has lower expression level compared to construct without pelB. Therefore, the construct pET22b(+)-*p*NBEBL was used in further experiments.

3.2. Continuous *B. licheniformis* esterase 4-aminoantipyrine screening system (cBLE-4AAP)

The 4-aminoantipyrine (4AAP) assay is commonly applied to detect phenols[113]. Here it was used to develop a novel screening system, a continuous 4-aminoantipyrine assay applied to *B. licheniformis* esterase (cBLE-4AAP). The screening system determines esterolytic activity using phenyl benzoate as a substrate. The phenyl benzoate was identified as a substrate with higher similarity to PET. Esterase converts phenyl benzoate into phenol and benzoic acid. Phenol reacts with 4AAP and the released final product 1,5-dimethyl-4-(4-oxo-cyclohexa-2,5-dienylidenamino)-2-phenyl-1,2-dihydro-pyrazol-3-one which has red colour and can be monitored spectrophotometrically at 509 nm (Figure 9).

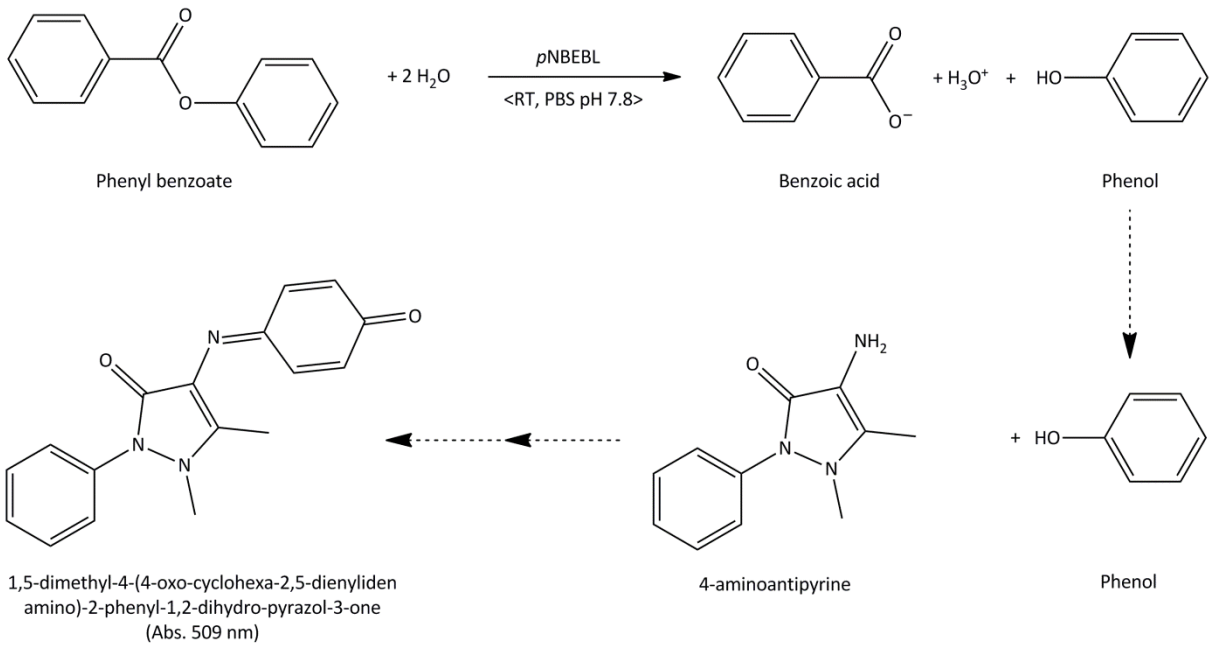

Figure 9 Principle of cBLE-4AAP screening system. The esterase *p*NBEBL catalyses the hydrolysis of the substrate phenyl benzoate to phenol (product) and benzoic acid (by product). The released phenol reacts with 4-aminoantipyrine and the released final product 1,5-dimethyl-4-(4-oxo-cyclohexa-2,5-dienylidenamino)-2-phenyl-1,2-dihydro-pyrazol-3-one can be spectrophotometrically determined at 509 nm[76]. (With kind permission from Springer Science and Business Media).

3.2.1. Determination of assay parameters

A successful assay development is based on optimization of assay parameters such as low background, pH optimum, linear detection range, and standard deviation. Besides this, the first challenge was the solubility of the phenyl benzoate. Schwaneberg *et al.* showed that nontoxic organic solvents can increase the solubility of hydrophobic substrates[114]. Therefore, dimethyl sulfoxide (DMSO) and acetonitrile (AcN) were used to dissolve the phenyl benzoate. Phenyl benzoate dissolved in DMSO showed precipitation which interferes with the spectrophotometric measurements at 509 nm whereas phenyl benzoate dissolved in AcN showed no precipitation and was selected as a solvent for phenyl benzoate. Besides the selection of the organic solvent, the pH range of the assay was determined. Therefore, phosphate-buffered saline (PBS-buffer) with a pH range from 5.8 to 11.7 was investigated (Figure 10).

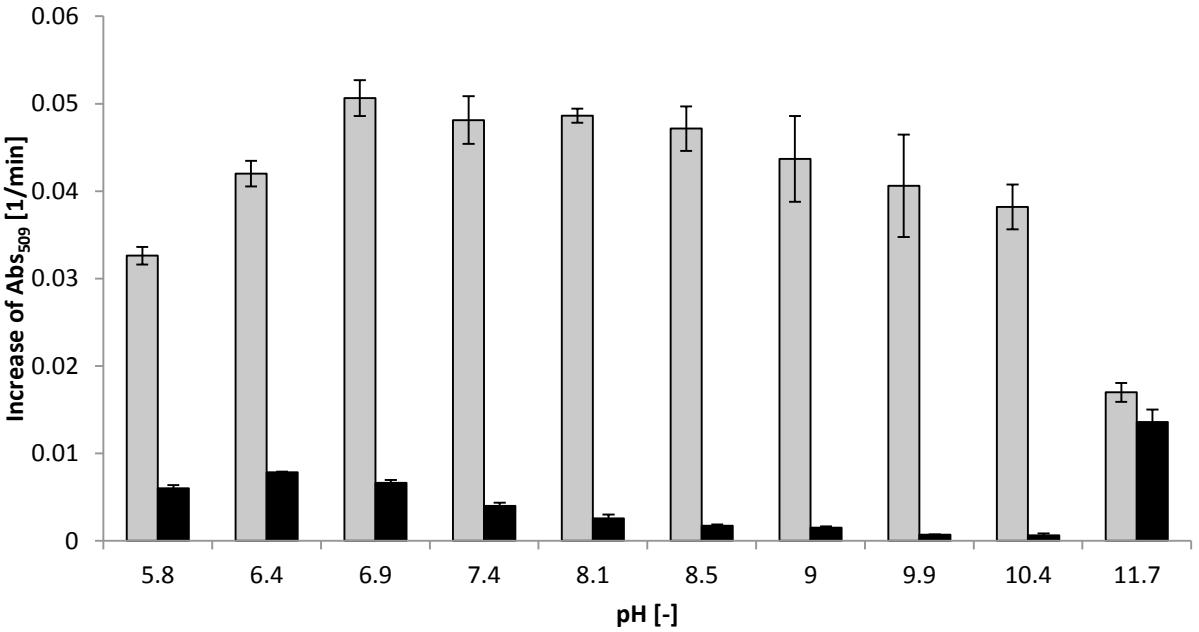

Figure 10 Esterolytic activity in different pH values applying the cBLE-4AAP screening system. PBS-buffer in a pH range from 5.8 to 11.7 were used to determine the assay conditions, where the difference in activity between the supernatant of cell lysate containing *p*NBEBL WT (▫) and EV (■) is high and the standard deviation low. The reported values are the average of three measurements and deviations are calculated from the corresponding mean values, modified from[76]. (With kind permission from Springer Science and Business Media).

Figure 10 showed that overall the assay is working in a broad pH range from 5.8 to 10.4. At pH 11.7 the activity of the supernatant of cell lysate containing EV showed a very high background, whereas *p*NBEBL WT showed a reduced activity. Considering the signal to noise ratio (WT/EV) and the standard deviation assay conditions pH 8.5 was selected as optimal for the cBLE-4AAP detection system. The optimal pH value of 8.5 complements washing conditions in laundry detergents (liquid detergents).

In addition, the interference of benzoic acid on colour formation in the cBLE-4AAP system was monitored. In Figure 11 samples containing benzoic acid, 4AAP and *p*NBEBL WT or EV lysates or buffer control were compared. Activity values showed no colour formation upon mixing benzoic acid and 4AAP indicating that the pH shift due to the acid production does not lead to a spontaneous colour formation. Furthermore, influence of lysate components was tested on colour formation upon reaction of phenol and 4AAP. Presence of endogenous compounds in the crude cell extract quenched absorbance signal for ~30 % when phenol, 4AAP, and supernatant of cell lysates are mixed compared to control reaction without lysate. The observed phenomenon was not studied in detail since there is a significant difference (27-fold) between colour development coming from *p*NBEBL WT and pET22b(+) EV (both measured in the presence of lysate, see Figure 10).

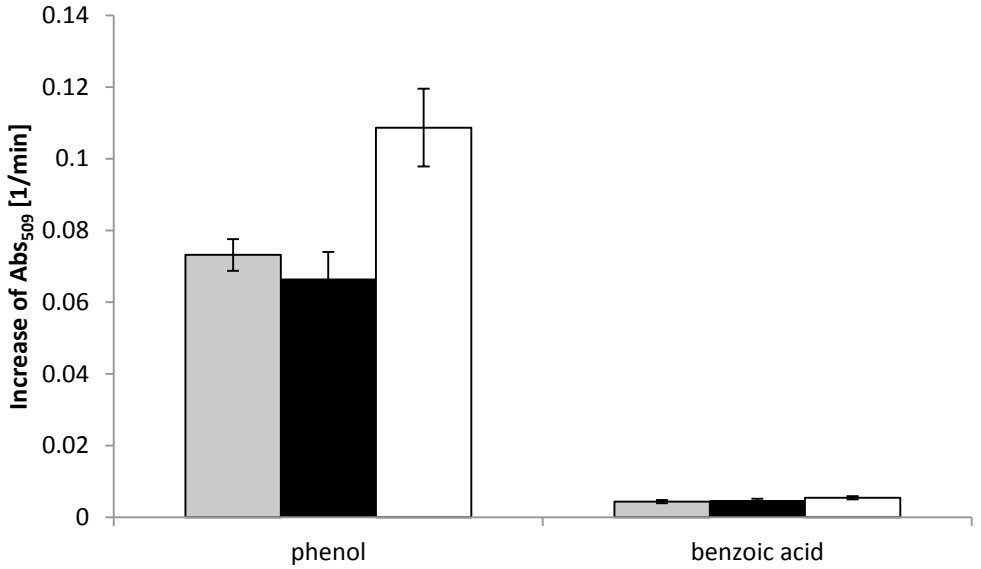

Figure 11 cBLE-4AAP screening system supplemented with phenol or benzoic acid instead of substrate phenyl benzoate. The supernatant of cell lysate containing *p*NBEBL WT (▫), pET22b(+) EV (■), or buffer control (▫) and 4AAP were supplemented with either 1 mM phenol or 1 mM benzoic acid, both were released during hydrolysis of phenyl benzoate. The reported values are the average of three measurements and the shown average deviations are calculated from the mean values, modified from[76]. (With kind permission from Springer Science and Business Media).

Furthermore, the correlation between different phenyl benzoate concentrations and the absorbance values were analysed. The results are shown in Figure 12.

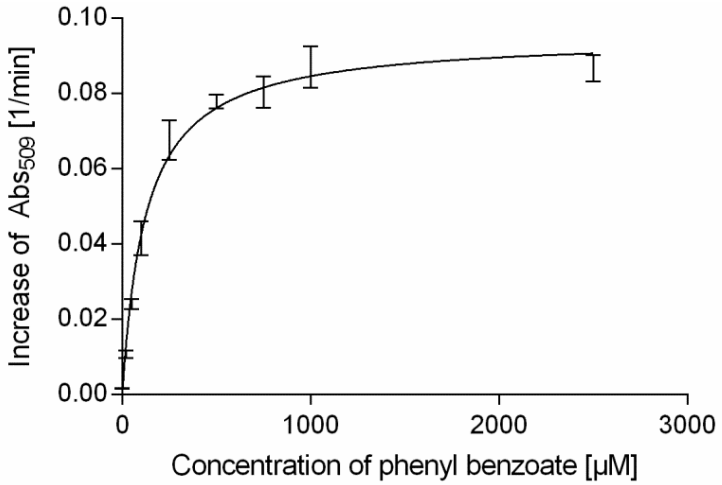

Figure 12 Continuous cBLE-4AAP screening system at different phenyl benzoate concentrations. The increase in absorbance at 509 nm is plotted to different phenyl benzoate concentrations (concentration range 0-2500 µM). The reported values are the average of three measurements and average deviations from the mean values are shown, modified from[76]. (With kind permission from Springer Science and Business Media).

The graph indicates a hyperbolic correlation between the rate of reaction and the concentration of phenyl benzoate. There is a steep increase in the rate of reaction with increasing phenyl benzoate concentration. Since the phenyl benzoate concentration used in the screening system (1000 µM) is 8-fold higher than K_M of *p*NBEBL WT (125 µM) the hydrolysis rate of the assay is not limited by the phenyl benzoate amount. Therefore, the

rate of formation of product depends on the activity of *p*NBEBL itself, and adding more phenyl benzoate will not affect the rate of reaction.

In the last step of the screening system characterization the detection limit of the cBLE-4AAP assay was determined. Therefore, different phenol concentrations were applied to the assay and the release of 1,5-dimethyl-4-(4-oxo-cyclohexa-2,5-dienylidenamino)-2-phenyl-1,2-dihydro-pyrazol-3-one was spectrophotometrically monitored at 509 nm (Figure 13).

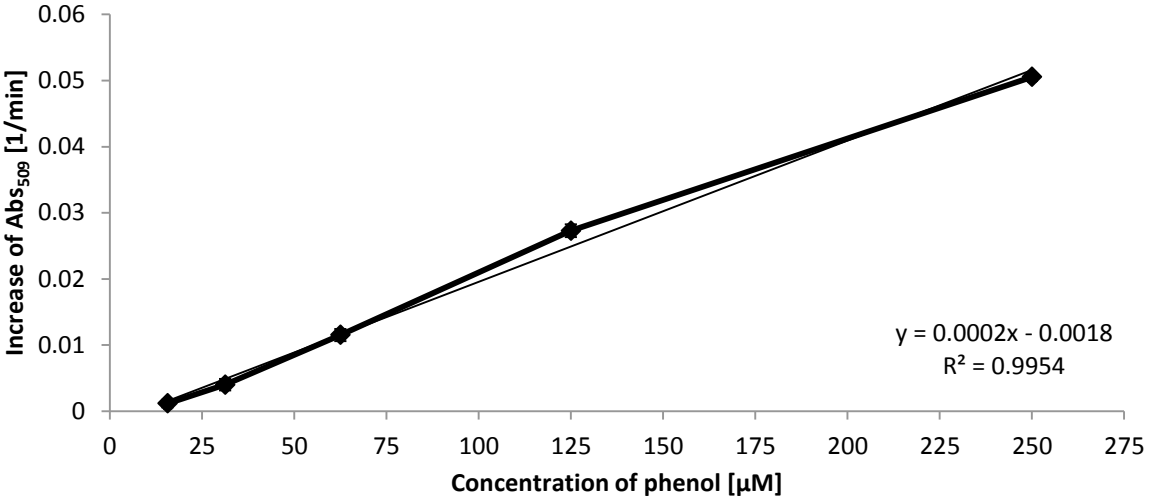

Figure 13 Determination of the linear detection limit of the continuous 4AAP assay. Phenol concentrations from 0 to 1000 µM were used to determine the linear detection range. The reported values are the average of three measurements and average deviations from the mean values are shown, modified from[76]. (With kind permission from Springer Science and Business Media).

The lower detection limit of the screening system is at 15 µM phenol and the linear detection range covered a span from 15 µM to 250 µM phenol.

3.2.2. Thermal resistance of *p*NBEBL

In the first step a temperature profile for the *p*NBEBL WT was determined, in order to define the temperature where *p*NBEBL WT loses activity. Therefore, supernatant of cell lysate containing *p*NBEBL WT was incubated for 30 min at respective temperatures ranging from 30°C to 75°C. Subsequently, the lysate was cooled on ice and the activity measurement with the cBLE-4AAP screening system was performed at RT (2.2.9) (Figure 14).

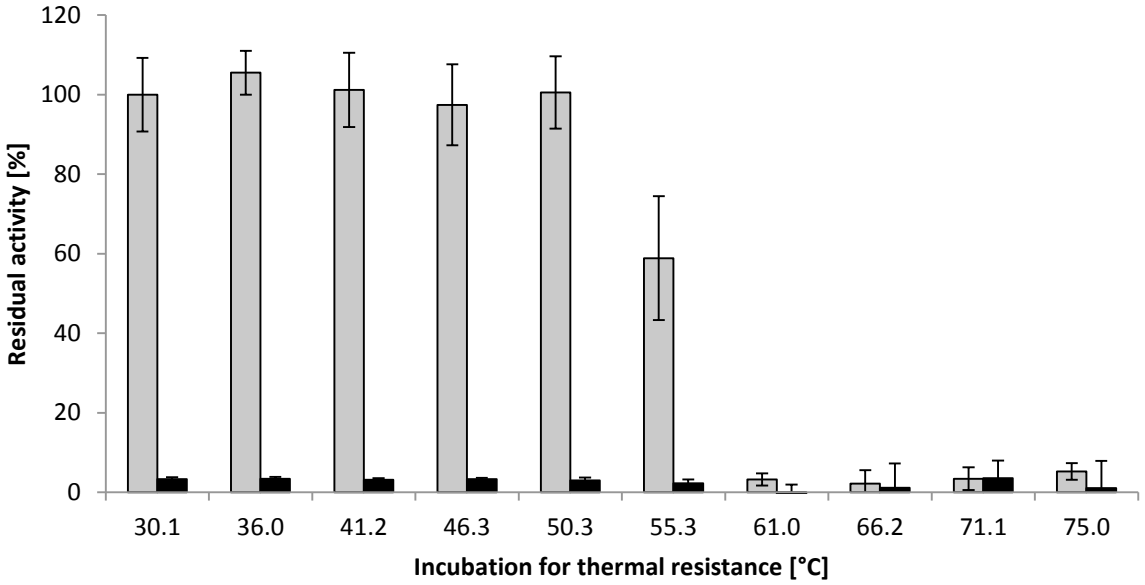

Figure 14 Determination of the temperature for thermal resistance screening. The cell lysate containing *p*NBEBL WT (▫) and pET22b(+) EV (■) were incubated for 30 min in a temperature range from 30°C to 75°C. The reported values are the average of three measurements and average deviations from the mean values are shown, modified from[76]. (With kind permission from Springer Science and Business Media).

For calculating the residual activity, the activity at 30.1°C was set to 100 %. Residual activities for elevated temperatures were calculated by dividing activity value at specific incubation temperature with activity value at 30.1°C and respective percentage was shown in Figure 14. In the temperature range from 30 to 50°C no loss in *p*NBEBL activity was detected. Further increase in temperature causes drop in enzyme activity to ~50 % (at 55°C) and at incubation temperatures above 60°C (61.0°C to 75.0°C) the *p*NBEBL can be considered as inactive.

3.2.3. Standard deviation of the cBLE-4AAP screening system

After determining the final assay conditions (4 h expression at 30°C, cell disruption in 150 µl PBS pH 7.4, incubation of 50 µl supernatant of cell lysate containing *p*NBEBL WT at 55°C or RT, 5 min cooling on ice, 160 µl PBS pH 8.5, 20 µl incubated supernatant of cell lysate containing *p*NBEBL, 50 µl detection solution, 20 µl substrate solution with a final AcN concentration of 1 %, measured at 509 nm) the standard deviation in 96-well format was determined at RT and 55°C (Figure 15).

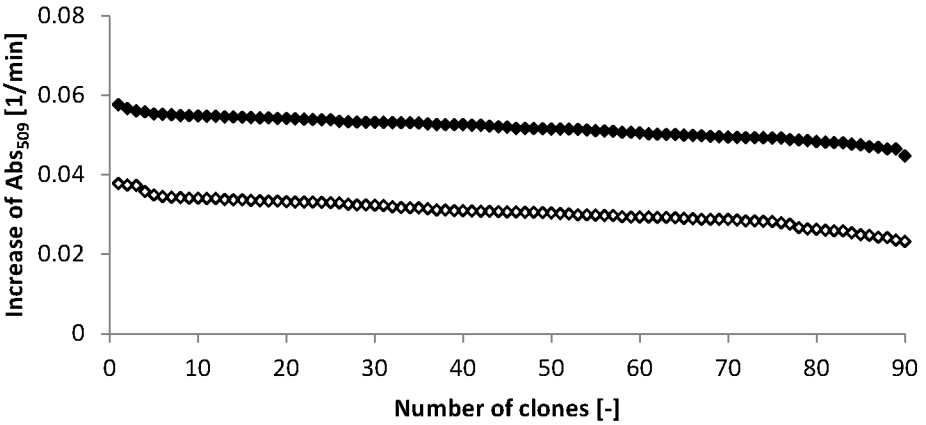

Figure 15 Determination of standard deviation of cBLE-4AAP screening system in 96-well MTP format. Activity values of *p*NBEBL WTs are shown in descending order at two temperatures (RT (◇), 55°C (◆)). *p*NBEBL WT was expressed in 90-wells (six wells with pET22b(+) EV). Supernatant of cell lysates harbouring the expressed *p*NBEBL WT were used to determine the standard deviation in the cBLE-4AAP screening system (5 % at RT, 10 % at 55°C), modified from[76]. (With kind permission from Springer Science and Business Media).

The standard deviation of the cBLE-4AAP assay in the 96-well MTPs was optimized to 5 % at RT and to 10 % at 55°C. Thereby, the established assay can be used for a directed evolution campaign where screening systems with standard deviation ~10 % are routinely employed[115].

3.3. Directed evolution campaign

After a successful optimization and establishment of the novel cBLE-4AAP screening system, a directed evolution campaign was performed using a *p*NBEBL mutant library in order to validate the proposed screening system. In Figure 16 the strategy of the directed evolution campaign is represented.

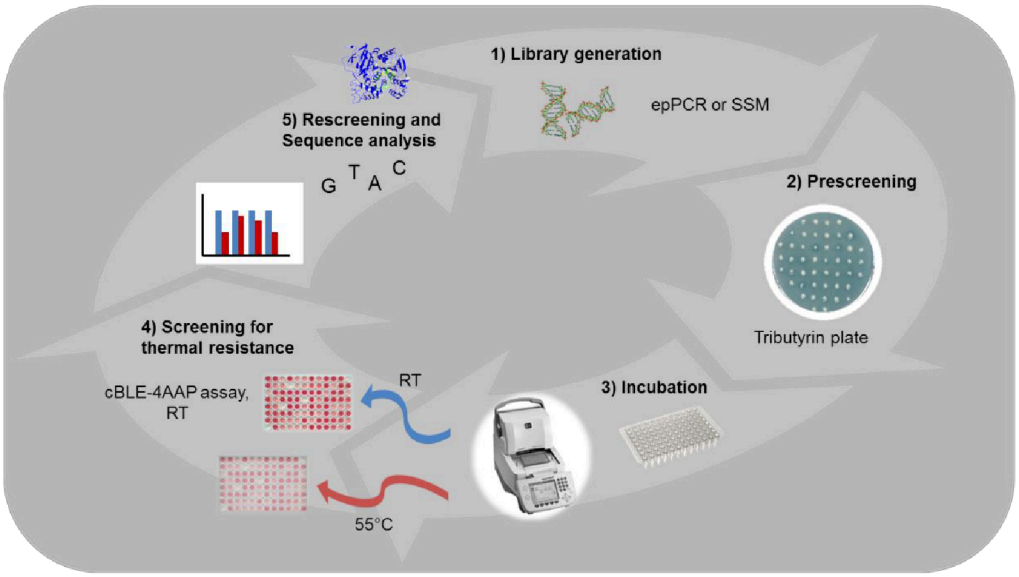

Figure 16 Strategy for the directed evolution campaign of *p*NBEBL. **1**) library generation by epPCR or site saturation mutagenesis, **2**) prescreening of active *p*NBEBL variants on tributyrin agar plates, **3**) incubation of supernatant of cell lysate containing *p*NBEBL at RT or 55°C, **4**) screening for thermal resistance by using the before incubated supernatant of cell lysate for assay performance at RT, **5**) rescreening of improved thermal resistance variants and subsequent sequence analysis, modified from[76]. (With kind permission from Springer Science and Business Media).

In the first step of the directed evolution campaign a random mutant library was generated by epPCR (Step 1). The received plasmid DNA was transformed in chemically competent *E. coli* BL21-Gold (DE3) and grown for prescreening on tributyrin plates (Step 2). Active variants showing halo formation were transferred into MTPs for expression. Supernatant of ell lysate containing *p*NBEBL were incubated for 30 min at 55°C or RT (Step 3). Subsequently, the residual activity of the supernatant of cell lysate containing *p*NBEBL was determined by the cBLE-4AAP screening system and the ratio of activity ($activity_{55°C}/activity_{RT}$) was calculated to eliminate expression mutants (Step 4). Identified variants were rescreened and afterwards sequence analysed to determine the amino acid exchanges occurring in improved variants (Step 5).

3.3.1. Generation and screening of epPCR library

The random mutagenesis library was generated by the standard epPCR[17] and cloned using PLICing[99] (2.2.2). The mutational frequency in epPCR *p*NBEBL mutant library was tuned by varying concentrations of $MnCl_2$ and the percentage of active and inactive mutants in the library was analysed using cBLE-4AAP screening system (Table 14).

Table 14 Ratio of activity of *p*NBEBL variants after mutangenic epPCR with different $MnCl_2$ concentrations. For each concentration one MTP was analysed by the cBLE-4AAP screening system.

$MnCl_2$ [mM]	**0.00**	**0.04**	**0.08**	**0.10**	**0.15**
Active clones [%]	>99	42	40	29	6

The concentration of Mn^{2+} (0.04 mM) at which ratio of active *vs*. inactive clones was approximately 50 % (42 %) was selected for generation of epPCR library. The ratio of 50 % active *vs.* inactive clones is an internal standard value for generation of epPCR libraries (one or two amino acid substitutions per round of mutagenesis and screening)[115].

For the final library generation prescreening was performed on tributyrin agar plates to select only active *p*NBEBL variants for an efficient screening in MTPs (2.2.4). After cell disruption of the expressed *p*NBEBL variants, supernatant of cell lysate containing the expressed protein was incubated at 55°C for 30 min, cooled on ice and absorbance increase per min was measured at RT (2.2.9). In total, 2000 variants were screened. Sequence analysis revealed mutational hotspots at amino acid positions Glu298, Ala377 and Ser378. For calculating the relative activity the residual activity (defined as the ratio of activity after incubation at 55°C and RT) of variants was divided by WT residual activity. The three identified variants showed an increase in relative activity of 2.7-fold (P5C8: His103His, Asp222Asn, Glu298Gly), 3.1-fold (P13C: Asp150Gly, Ser378Pro), and 3.3-fold (P9G4: Met357Val, Ala377Ala) (Table 15).

Table 15 Sequence analysis of improved thermal resistance *p*NBEBL variants (silent mutations are shown in grey). The relative activity (%) was calculated for *p*NBEBL WT and each variant.

Variant	Amino acid exchange	Relative activity* [%]
*p*NBEBL	---	100
P5C8	His103His, Asp222Asn, Glu298Gly	276
P9G4	Met357Val, Ala377Ala	334
P13C6	Asp150Gly, Ser378Pro	312

*Relative activity is calculated as the ratio of residual activity of variants divided by WT residual activity. Relative activity of WT was set to 100 %, and relative activities of other three variants were transferred to percentages. Residual activity is defined as the ratio of activity after incubation at 55°C and RT.

3.3.2. Site-saturation mutagenesis and site-directed mutagenesis at mutational hotspots

The homology model showed that three of the identified amino acid positions are in close proximity and interact with each other. In order to explore cooperative effect all three positions (298, 377, and 378) were simultaneously saturated. Therefore, the site-saturation mutagenesis (SSM) method was used to generate one library in two subsequent rounds (298 on top of library 377 and 378) (2.2.3). After screening for thermal resistance 990 active clones and rescreening of 15 most promising variants, the variant T1 having 4.8-fold increase in residual activity at 55°C compared to wildtype was identified (Figure 17).

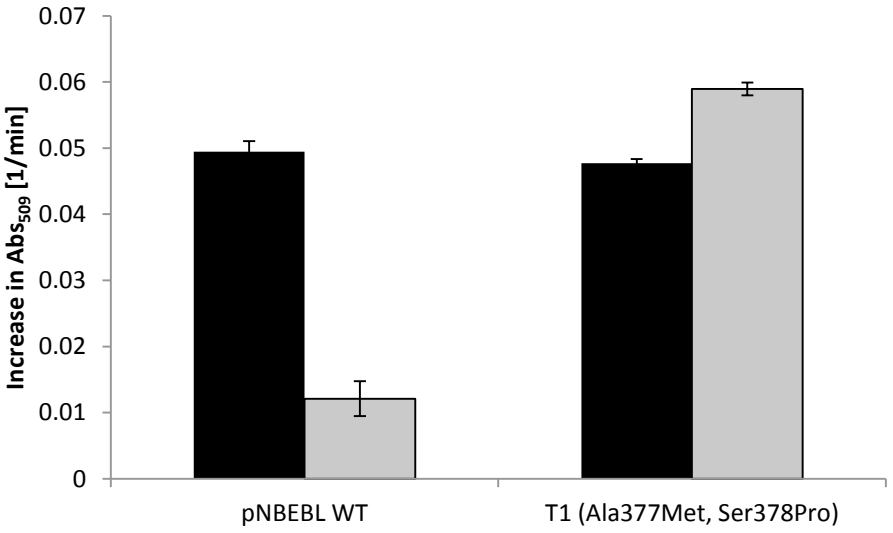

Figure 17 Rescreening and sequence analysis of SSM library (298, 377, and 378) screening for thermal resistance. The supernatant of cell lysate containing *p*NBEBL WT and variant T1 were incubated for 30 min at RT (■) or 55°C (■) and subsequent cooled on ice for later analysed with the cBLE-4AAP screening system. The reported values are the average of three measurements and average deviations from the mean values are shown, modified from[76]. (With kind permission from Springer Science and Business Media).

The sequencing analysis of T1 revealed amino acid exchanges Ala377Met and Ser378Pro while at position 298 Glu silent mutation occurred. In order to elucidate the individual impact of each amino acid substitution (377, 378) site-directed mutagenesis (SDM) experiments were performed to achieve the *p*NBEBL variants T2 (Ala377Met) and T3 (Ser378Pro) (2.2.3). The scheme of the mutants generation is shown in Figure 18.

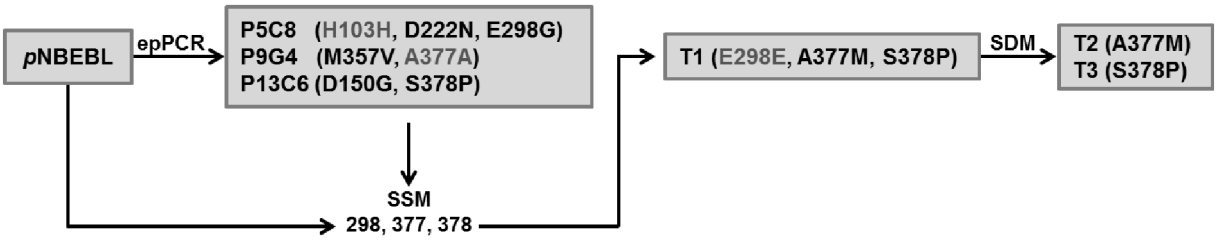

Figure 18 Scheme of the identified and generated *p*NBEBL variants. epPCR was used to introduce mutations and the mutational hotspots 298, 377 and 378 were combined in one SSM library. Subsequent SDM was done to introduce single amino acid exchanges to generate variant T2 and T3. Silent mutations are shown in grey.

All generated variants (T1, T2, and T3) as well as *p*NBEBL WT were expressed and the supernatant of cell lysate containing the expressed protein was used for determining a temperature profile (temperature range from 41.7°C to 60.1°C). The supernatant of cell lysate containing the expressed protein was incubated for 30 min and afterwards cooled for 5 min on ice. Subsequently, the activity was analysed by the cBLE-4AAP detection system. In Table 16 the ratio of activity is shown, and the *p*NBEBL WT activity after incubation at 41.7°C was set to 100 %.

Table 16 Activity comparison of improved *p*NBEBL variants with *p*NBEBL WT after screening for thermal resistance. The supernatant of cell lysate containing *p*NBEBL WT and *p*NBEBL variants T1 (Ala377Met, Ser378Pro), T2 (Ala377Met), and T3 (Ser378Pro) were incubated at defined temperatures and activity with cBLE-4AAP was determined at RT. The shown relative activity (%) is the activity ratio of improved variant and WT.

Variant	Temperature [°C]						
	41.7	**45.8**	**51.1**	**53.8**	**56.2**	**58.1**	**60.1**
***p*NBEBL WT**	100.0	95.2	97.0	75.6	9.4	1.8	1.8
T1 (Ala377Met, Ser378Pro)	121.8	118.5	112.8	116.2	**109.0**	61.7	24.2
T2 (Ala377Met)	109.3	109.2	67.9	33.5	11.2	5.0	3.5
T3 (Ser378Pro)	115.7	117.7	110.4	112.8	**105.3**	77.6	50.7

The activity of *p*NBEBL WT showed significant decrease in activity of almost 90 % upon incubation at 56.2°C (100 % at 41.7°C to 9.4 % at 56.2°C). The relative activities of variants T1 and T3 showed no dramatically changed activity values till 56.2°C with approx. 50 % reduction in activity at temperature higher than 56.2°C. Variant T2 showed a similar behaviour as *p*NBEBL WT and lost its activity dramatically at incubation temperature of 56.2°C. The above shown results indicate that amino acid substitution at position Ala377Met does not govern increase in thermal resistance. Only the single substitution Ser378Pro was identified to have an impact on the thermal resistance increase. Further analyses were performed with purified variants to confirm data obtained in crude cell extract.

3.4. Characterization of improved variants

3.4.1. Purification by anion exchange chromatography of *p*NBEBL WT and variants T1, T2, and T3

Three esterase variants having increased thermal resistance (T1, T2, and T3) and *p*NBEBL WT were purified for further kinetic characterization. Purification enables the possibility to remove impurities like unspecific proteins and eliminate differences in expression levels among different esterase variants. The purification was done using an anion exchange chromatography where the esterase (pI ~4.7) binds to the positive charged matrix. Prior to the application of the sample to the anion exchange column *E. coli* cells expressing *p*NBEBL WT and variants T1, T2 and T3 were sonicated and filtered supernatant was loaded on the Toyopearl Super Q 650c column pre equilibrated with running buffer (2.2.6). The *p*NBEBL was recovered at 19 % of elution buffer and fractions were analysed on a SDS-PAGE (Figure 19, Figure 20).

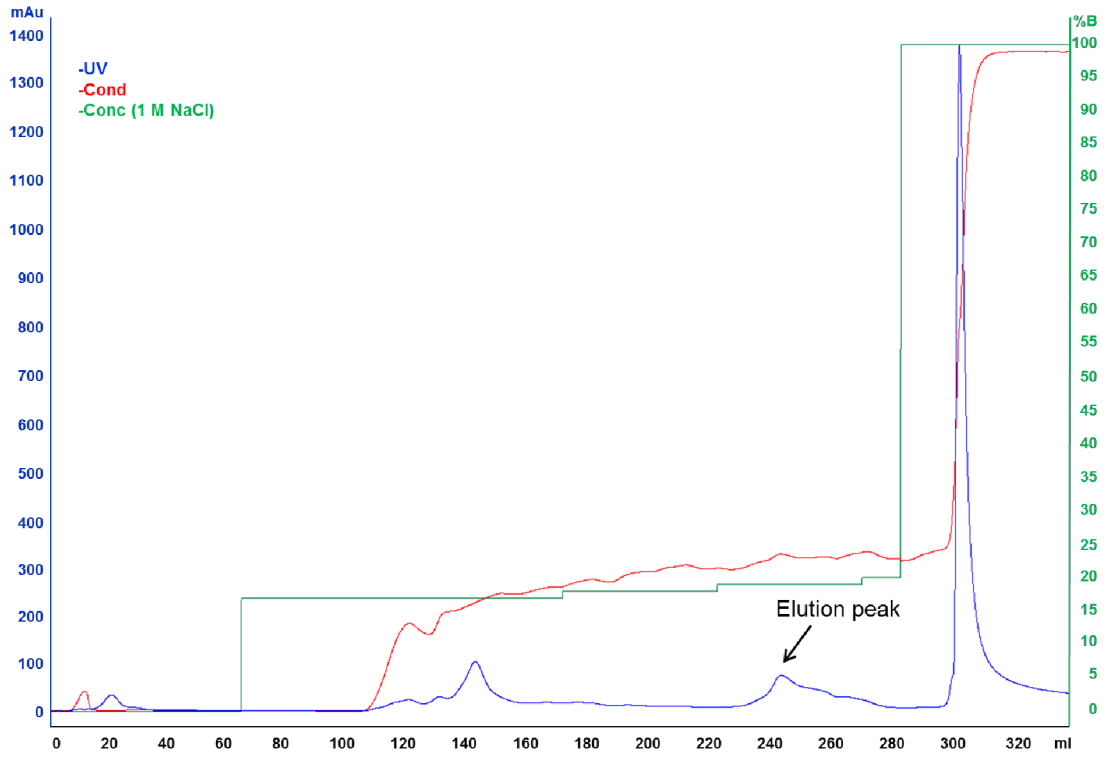

Figure 19 Anion exchange chromatography profile of *p*NBEBL WT. The peak marked with an arrow represents the eluted fractions with esterolytic activity observed at 19 % 1 M NaCl. The concentration (green) is measured before the column, whereas the conductivity (red) is measured after the column. The column volume is ~20 ml.

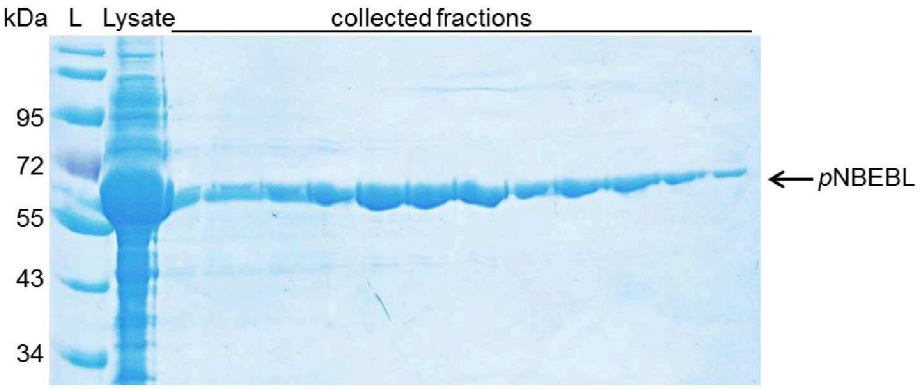

Figure 20 SDS-PAGE analysis of the *p*NBEBL anion exchange purification. **L**: ladder in kDa, Lysate: cell lysate containing expressed protein, which was loaded on the column for purification, collected fractions: pure proteins with the corresponding size, which was eluted with 19 % NaCl.

Fractions showing esterolytic activity were pooled and concentrated. Subsequently, the homogeneity was analysed by capillary electrophoresis (Experion Pro260 Analysis Kit) (Figure 21).

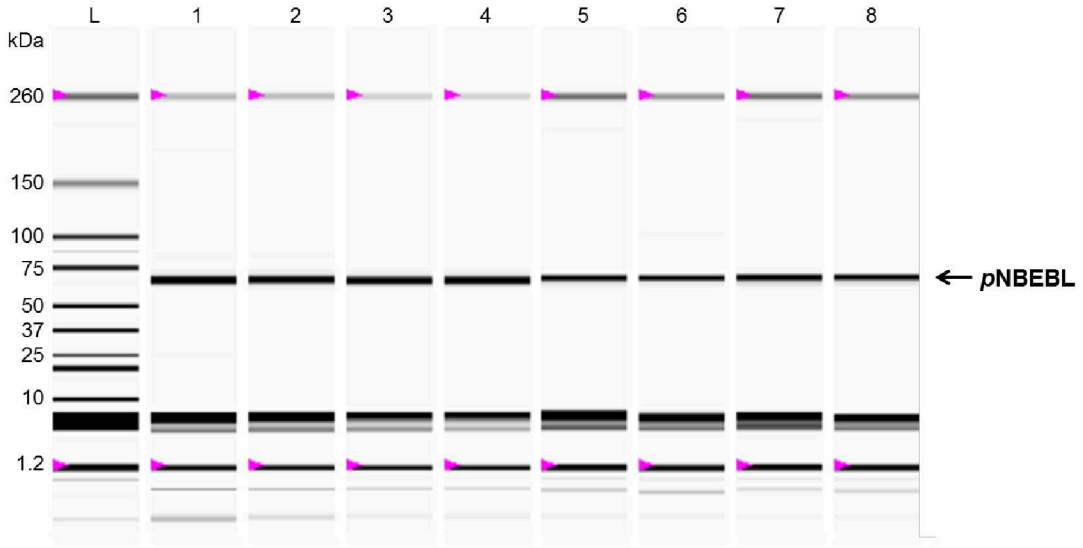

Figure 21 Experion™ analysis of purified *p*NBEBL WT and variants T1, T2, and T3. Samples were prepared as described in the manufactures protocol and analysed in duplicate. **L**: ladder in kDa; **1**, **2**: *p*NBEBL WT (dilution 1:20); **3**, **4**: T1 (dilution 1:20); **5**, **6**: T2 (dilution 1:10); **7**, **8**: T3 (dilution 1:10).

The obtained purity of the purified *p*NBEBL WT and variants was >98 %. The total protein concentration was calculated using the BCA assay (Pierce™ BCA protein assay kit). Both results combined revealed in the specific protein concentration shown in Table 17.

Table 17 The specific protein concentration was calculated after purification, homogeneity and total protein concentration determination. The results for *p*NBEBL WT and all variants are shown.

Variant	Specific concentration [mg/ml]
*p*NBEBL WT	3.1
T1 (Ala377Met, Ser378Pro)	4.5
T2 (Ala377Met)	1.2
T3 (Ser378Pro)	1.9

3.4.2. Characterization of purified variants for thermal resistance

Temperature profile of *p*NBEBL WT and its variants was determined in a temperature range from 50.3°C to 75.9°C. Upon incubation at different temperatures *p*NBEBL WT and the variants were cooled on ice and the residual activity was measured at RT with the cBLE-4AAP detection system (2.2.10). The specific activity of each variant is shown in Figure 22.

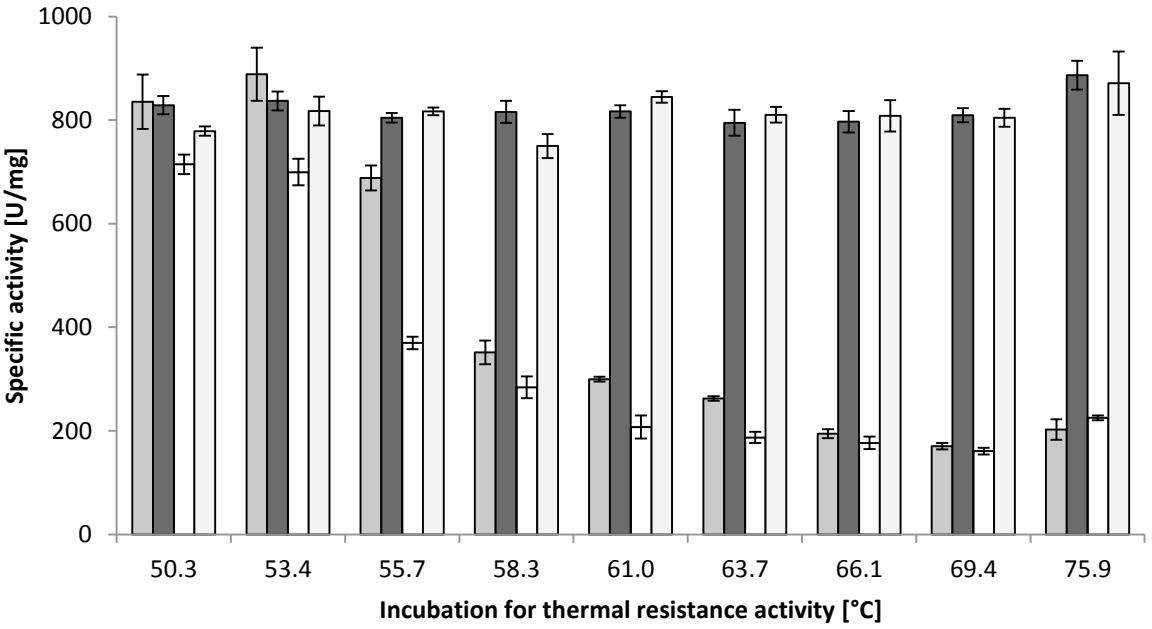

Figure 22 Specific activity (U/mg) of all generated variants. Purified enzyme (*p*NBEBL WT (▫), T1 (Ala377Met, Ser378Pro, ▪), T2 (Ala377Met, ▨), T3 (Ser378Pro, □)) was incubated for 30 min at broad temperature range from 50.3 to 75.9°C. The activity was determined at room temperature by applying the cBLE-4AAP detection system. The reported values are the average of three measurements and average deviations from the mean values are shown. One Unit was defined as the amount of esterase that catalyses the conversion of 1 nmol phenyl benzoate per minute, modified from[76]. (With kind permission from Springer Science and Business Media).

After incubation at 50.3°C *p*NBEBL WT showed a residual activity of 835 U/mg, though it showed a significant decrease in residual activity after incubation at temperatures ≥58.3°C (≤351 U/mg). A similar behavior as *p*NBEBL WT was shown for variant T2 having a significant decrease in residual activity (50.3°C: 829 U/mg; 58.3°C: 284 U/mg). The specific activity of variants T1 and T3 remained constant over the assessed temperature range (50.3-75.9°C). The residual activity of variant T3 is at 69.4°C was 4.7-fold improved (WT: 170 U/mg. T3: 804 U/mg) compared to the WT. Additionally, the specific activity of *p*NBEBL WT and the

variant T3 was measured at RT, showing no loss in initial activity at RT (*p*NBEBL WT: 863.16 U/mg; T3: 831.03 U/mg). All variants and *p*NBEBL WT showed a slightly increased activity at 75.9°C compared to 69.4°C, but as shown in 3.4.3 it is not caused by refolding. Only the single mutation at position Ser378Pro showed to be responsible for the improved thermal resistance. In order to study and obtained better understanding of structural changes in protein upon Ser378Pro substitution a homology model of the variant T3 was generated for further computational analysis.

The homology model of *p*NBEBL WT was generated by YASARA and showed a structural similarity of 77.4 % to the *p*-nitrobenzyl esterase from *B. subtilis* (PDB 1CFI) and a sequence identity of 60.8 %. Variant T3 was compared with the WT regarding changes in the structure and hydrogen bond formation (Figure 23)[75, 106].

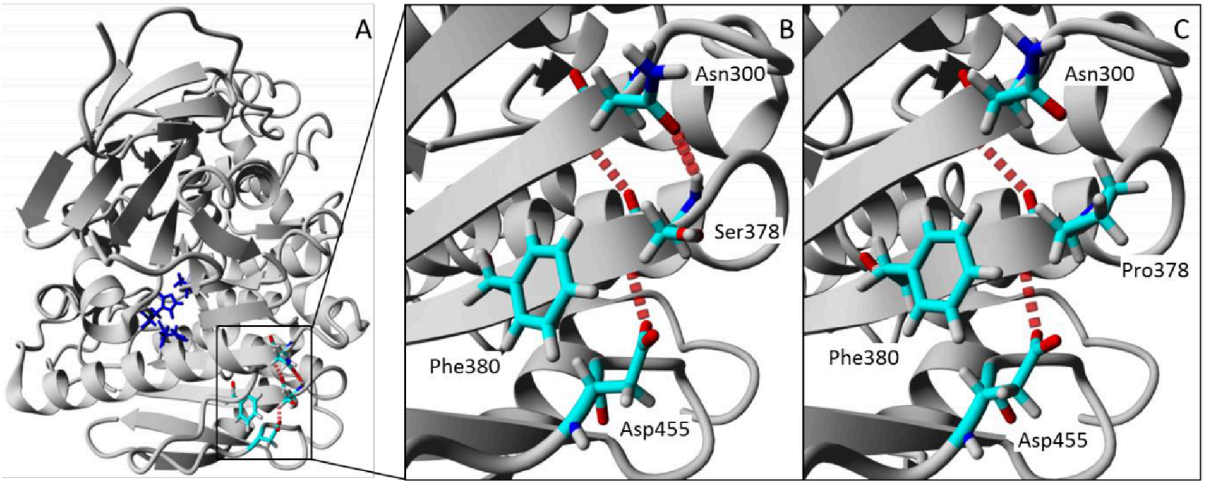

Figure 23 Energy minimization of *p*NBEBL WT and amino acid exchange Ser378Pro. **A**: *p*NBEBL WT with the catalytic triad Ser188, His400 and Glu309 in blue. B and C were predicted with YASARA and the FoldX plugin, the hydrogen bonds were displayed in red segmented lines. **B**: Amino acid Ser378 forms two hydrogen bonds with Asn300, and one with Asp455. **C**: Substitution of amino acid Ser378 by Pro forms only one hydrogen bond with Asn300, the hydrogen bond with Asp455 still exists.

Figure 23 shows the homology model of *p*NBEBL WT with the catalytic triad Ser188, His400 and Glu309 in blue and the amino acid Ser378 and their surrounding amino acids Asn300, Phe380 and Asp455 highlighted in light blue. Hydrogen bond is formed between Ser378 and Asn300 with a distance of 2.32 Å in WT. The FoldX analysis of Pro378 showed the absence of this hydrogen bond due to missing hydrogens in Pro. Additionally, calculated distances between Asn300 Cα to Pro378 Cα of 5.25 Å and for Pro378 Cα to Asp455 Cα of 7.26 Å confirms absence of hydrogen bonds. On the other hand, the WT shows shorter distances Asn300 Cα to Ser378 Cα of 5.19 Å and for Ser378 Cα to Asp455 Cα of 6.67 Å which enable formation of hydrogen bond.

3.4.3. Differential scanning calorimetry of *p*NBEBL WT and variant T3

In order to examine whether the increased resistance in variant T3 is due to enzyme stability or faster refolding differential scanning calorimetry (DSC) experiment was performed with *p*NBEBL WT and variant T3. The pure protein was analyzed against PBS buffer as reference with the following method: heating from 25 to 70°C with a heating rate of 10°C/min (2.2.12) (Figure 24).

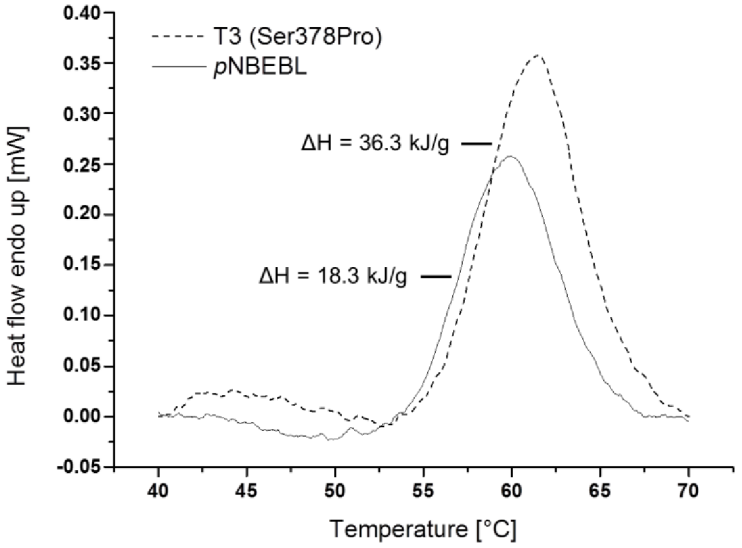

Figure 24 Differential scanning calorimetry of *p*NBEBL WT (–) and variant T3 (··). The samples were measured by heating from 25°C to 70°C with a heating rate of 10°C/min. The reported values are the average of three measurements[76]. (With kind permission from Springer Science and Business Media).

In Figure 24 the diagram of the released enthalpy over the temperature range from 40°C to 70°C is shown. The results were plotted as a curve of heat flow versus temperature. The area under the peak (mJ) was multiplied with the calorimetric constant, which varies for each instrument and enthalpy ΔH was obtained. The released enthalpy increased form 18.3 kJ/g for *p*NBEBL WT to 36.3 kJ/g for the variant T3. In addition, DSC measurements revealed a temperature shift of 1.1°C in the optimum values (*p*NBEBL WT: 60.0°C; T3: 61.1°C).

4. Discussion

High throughput screening systems play a pivotal role in isolating new enzymes as well as in improving existing enzymes regarding specific industrial requirements (*e.g.* thermal resistance). The until now existing and well established continuous screening systems based on *p*-nitrophenyl- (*e.g. p*-nitrophenyl acetate) or umbelliferyl-esters are commonly used in directed esterase evolution campaigns. However, aliphatic esters like *p*-nitrophenyl-based substrates cannot represent the complexity of a substrate like polyethylene terephthalate which is based on aromatic structures. Therefore, ongoing challenge in directed evolution campaigns of esterases is the establishment of screening systems with a broad substrate spectrum. For the first time a continuous high throughput screening system in 96-well microtiter plate (MTP) format based on the hydrolysis of aromatic esters (phenyl benzoate) is reported for a directed esterase evolution.

Within the cBLE-4AAP assay the esterase *p*NBEBL catalysed the hydrolysis of phenyl benzoate. Thereby, the intermediate products benzoic acid and phenol are released. In the following reaction the produced phenol reacts with 4-aminoantipyrine (4APP) to 1,5-dimethyl-4-(4-oxo-cyclohexa-2,5-dienylidenamino)-2-phenyl-1,2-dihydro-pyrazol-3-one. The reaction can be monitored spectrophotometrically at 509 nm. The continuous cBLE-4AAP assay allows for the first time the detection of esterase activity of phenol production and could offer the opportunity to enlarge the substrate spectra to complex aromatic substrates with non-substituted para-positions[105]. Furthermore key performance parameters of the cBLE-4AAP screening system were evaluated, which are necessary for a robust and reliable high throughput screening system. Thereby, low standard deviation (<14 % at 55°C; and 5 % at RT), high sensitivity (15 µM), minimal background, broad pH profile (7.4-10.4), and linear detection range of phenol (15-250 µM) were achieved.

For the validation of the cBLE-4AAP screening system a single round of directed evolution was performed improving the residual activity of *p*NBEBL after a thermal denaturation step. Thermal resistance corresponds well to storage and process stability, which are key parameters for the use of enzymes in industrial processes. The directed evolution campaign revealed the variant T1 (Ala377Met, Ser378Pro), which showed an increased residual activity after incubation at 55°C compared with *p*NBEBL WT. The effect of the individual contribution of each amino acid substitution was investigated by generating the variants T2 (Ala377Met) and T3 (Ser378Pro). After final characterization of all variants only amino acid substitution Ser378Pro (T3) increased the thermal resistance, resulting in a 4.7-fold improved residual activity after incubation at 69.4°C compared to WT (170 U/mg to 804 U/mg). Surprisingly the improvement was caused by only one single substitution. However, this enormous increase in thermal resistance was not obvious during differential scanning calorimetry (DSC). Thereby, only a slightly higher thermal stability for variant T3 compared to *p*NBEBL WT was determined, and no peak was detected in the cooling cycle from 70°C to 4°C, indicating no obvious refolding of the protein. A refolding contribution cannot be excluded by DSC

measurements, because activity measurement for thermal resistance screening was done at room temperature instead of elevated temperature.

The increase in T_M obtained by DSC measurements of 1.1°C is similar to the one found in a directed esterase (*p*-nitrobenzyl esterase from *B. subtilis*) evolution with *p*-nitrophenyl-ester based screening system (0.9°C)[44]. The influence on entropy was reported for prolines, which have a stabilizing effect on the secondary protein structure[116]. Furthermore, it was reported that 26 % of all prolines are located in β-sheets and were followed by a valine[117]. The visual inspection by homology modeling showed that the amino acid substitution Ser378Pro behaves like the prolines in the review article. It is the first amino acid of a ß-sheet followed by valine and therefore matching with the above mentioned results.

As a conclusion, the development of the novel continuous esterase assay offers the possibility to screen large libraries with PET mimicking substrates. The identified and optimized esterase variants are a milestone for the implementation of esterases for PET degradation, since elevated temperatures lead to more flexible and solvent exposed polymer chains. The reported increased temperature resistance of an esterase of about 15°C could allow a greener and more energy saving process compared to established chemical and mechanical methods.

The novel cBLE-4AAP screening system is the first continuous screening system with a PET-like model substrate which is not like the *p*-nitrophenyl based substrates. The functionality of the assay was proven by the identification of a 4.7-fold improved variant. Therefore, a first milestone was achieved to tackle the global PET degradation challenge by directed evolution.

Part III: Exploring novel strategies - A flow cytometry-based screening system developed on the example of an esterase

The principle of this work was developed by Christian Pitzler (PhD candidate, RWTH Aachen, Institute of Biotechnology). In cooperation with Christian Pitzler the technology was advanced and transferred to other hydrolases, the work was equally distributed and accomplished. Parts of this chapter were published by the authors in the journal of ChemComm. Reproduced by permission of The Royal Society of Chemistry.

"Lülsdorf N.[*], Pitzler C.[*], Biggel M., Martinez R., Vojcic L. and Schwaneberg U. (2015) *A flow cytometer-based whole cell screening toolbox for directed hydrolase evolution through fluorescent hydrogels*. ChemComm, 51, 8679-8682"

[*]shared first authorship

Goals and main results

In this part of the thesis the further advancements of a high throughput screening system based on flow cytometry which overcomes the limitation of medium throughput screening systems is described. Previously published principle of Fur-Shell technology on directed phytase evolution as model was further advanced by employing three additional hydrolase and screening of epPCR libraries[118]. As outcome, improved hydrolases were identified with improvement ranging from 1.3–7.0-folds. Esterase variant showed highest catalytic activity (7.1-fold higher k_{cat}) and 2-fold reduced K_M compared to WT enzyme. The presented Fur-Shell technology showed a potential to be used as universal screening platform for hydrolases.

1. Introduction

Tailored enzymes *e.g.* generated within a directed evolution approach which are screened with standard methods like MTPs provide a throughput of only up to 10^4 variants per day[119]. This limitation can be overcome by the use of high or ultra-high throughput screening systems where more than 10^7 enzyme variants can be screened per one hour[28, 120]. The main advantage compared to MTP-based screening systems is to cover more of the generated sequence space. Reliable high throughput screening systems are reported for microfluidic-based systems or flow cytometry[28, 121]. Compartmentalization techniques *e.g.* double emulsions (water-in oil-in water) are applied for providing genotype-phenotype linkage in case a gene library is expressed cell free or the product readily diffuses through the cell membrane. Despite the extremely high throughput and high sensitivity the compartmentalization techniques are still rarely used in directed evolution campaigns[122]. Main reasons are the stability of the compartment systems, polydispersity of emulsions and the diffusion of the fluorescent substrate or product from the compartments in the

surrounding[123-125]. Whole cell-based screening systems can overcome this limitation when a substrate is applied which can diffuse inside the cells and remain entrapped upon conversion into fluorescent product[30, 32, 126-127]. The latter was successfully applied in directed evolution campaigns for three different enzymes (P450 monooxygenase, N-acetylgalactosaminidase, protease)[30, 32, 127]. Nevertheless, an establishment of flow cytometer-based screening in directed evolution campaigns requires novel, general applicable screening systems.

In previous studies, fluorescent-labelled hydrogels were applied in eight-well strip plate format for antigen detection representing a new fluorescent based-screening technology[128]. The properties of the hydrogel as high water content, softness and biocompatibility makes it interesting for further industrial application *e.g.* drug delivery[129-131]. A further improvement in flow cytometer-based screening systems could be a fluorescent-labelled hydrogel, which is covalently bound around cells expressing active enzymes. Recently, in our group fluorescent-labelled hydrogels were combined with whole cell screening system leading in a new technology called Fur-Shell. A proof of concept for the novel screening principle Fur-Shell based on fluorescent hydrogel formation around *E. coli* cells with a phytase as an example (*Yersinia mollaretii* phytase, YmPh) was recently reported[118]. The Fur-Shell technology enables the possibility to screen with natural substrates in case a cellulolytic is used. Fur-Shell overcomes all named limitations of compartmentalization and leakage of fluorescent substrate or product, as the fluorescence signal is connected to the cells expressing active enzyme through the hydrogel[118].

In this work, the published screening technology Fur-Shell was advanced by applying it to three additional hydrolases (*i.e.* esterase, cellulase, and lipase). Further development and validation of screening platform was done by screening a epPCR library of a *p*NBEBL esterase and identification of improved variants by using β-D-(+)-glucose pentaacetate as β-D-glucose donor substrate.

2. Material and methods

2.1. Material

See Part II section 2.1 with the exception of Methacryloxyethylthiocarbamoyl-rhodamine B (PolyFluor® 570), which was purchased from Polysciences Inc. The Tecan Infinite M1000 Pro (Tecan Group AG, Männedorf, Switzerland) was used for detection of fluorescence.
For the used target gene, strains and plasmids, oligonucleotides and cell culture methods see Part II section 2.1.1 until 2.1.4, as well as Table 5 and Table 6.

2.2. Methods

For expression in flasks and purification by anion exchange chromatography see Part II section 2.2.6. The growth conditions and expression in 96-well microtiter plate are explained in Part II section 2.2.5. For homology model analysis by YASARA see Part II section 2.2.11.

2.2.1. Construction of mutagenesis epPCR by PLICing

Cloning was done like mentioned in Part II section 2.2.1, for the PCR protocol and program see Part II section 2.2.2, Table 11 and Table 12.
The $MnCl_2$ concentration was varied between 0.1 and 0.3 mM, the optimal concentration regarding mutagenesis frequency and hydrogen formation (2.2.2) was analysed by flow cytometry and cell sorting (2.2.4) as well as sequence analysis.

2.2.2. Hydrogel formation

E. coli BL21-Gold (DE3) cells containing pET22b(+)-pelB-*p*NBEBL were grown (ON, 37°C, 250 rpm). For inoculation of the main culture (20 ml LB-medium supplemented with Amp) 1 % of the overnight culture was used. *E. coli* cells were induced at an OD_{600} of 0.6 with 0.1 mM IPTG and expressed (4 h, 30°C, 250 rpm). Afterwards *E. coli* cells were harvested by centrifugation (10 min, 4°C, 3220 g). The obtained cell pellet was washed two times (10 min, 4°C, 3220 g) in 10 ml PBS (137 mM NaCl, 2.7 mM KCl, 10 mM Na_2HPO_4, 2 mM KH_2PO_4, pH 6). Subsequently, cell density was adjusted to an OD_{600} of 2 with PBS. For the hydrogel formation 960 µl of *E. coli* cells containing the expressed *p*NBEBL were incubated (10 min) with 24.8 % PEG_{575}-DA, 2.5 % 1-vinyl-2-pyrrolidone, 20 µl (0.5 % stock concentration) PolyFluor® 570, 2 µl (25 µM stock concentration) $Fe_2SO_4*7H_2O$ dissolved in ddH_2O, 200 µl (200 mM stock concentration) β-D-(+)-glucose pentaacetate dissolved in ddH_2O, and 2 µl glucose oxidase (GOx) type II dissolved in PBS pH 6.0 (1.58 mM stock concentration) in a total reaction volume of 1.5 ml. Hydrogel formation was stopped by three times washing (1 min, 11363 g) with 1 ml PBS pH 6.0. Finally the prepared samples were used for confocal microscopy (2.2.3) and flow cytometry analyses (2.2.4).

2.2.3. Confocal microscopy analysis

Hydrogel formation was analysed by confocal microscopy (Leica TCS SP8, Leica Microsystems) using 63x oil immersion objective. For excitation a continuous wave laser (DPSS, 20 mW: 561 nm) was used and for emission (570 nm) a highly sensitive prism spectral detector filter. *E. coli* cells containing an EV were analysed first in order to set the gain to a minimal signal (530).

2.2.4. Flow cytometry analysis and cell sorting

Flow cytometry was carried out using a BD Influx cell sorter (BD Biosciences) with an installed 100 mm nozzle. PBS pH 7.5 (1.05 mM KH_2PO_4, 3 mM Na_2HPO_4, and 155 mM NaCl) was used as sheath fluid and for a 1:10 sample dilution. Samples were additionally filtered with 0.4 µM filter. Stream of events was adjusted to 5000 events s^{-1}, to reach a throughput of $1.8x10^{-7}$ per h. Active events were sorted regarding forward and side scatter and to its fluorescence intensity (Ex. 561 nm/Em. 585 nm) and collected [118]. After sorting plasmids were recovered by centrifugation (1 min, 11363 g) and subsequent plasmid isolation. The obtained plasmids were transformed into competent *E. coli* Bl21-Gold (DE3) cells and plated on LB-agar plates supplemented with Amp. Colonies were transferred in a MTP for expression.

2.2.5. Fluorometric screening system with Amplite™

For detection of esterolytic activity the Amplite™ Red Kit (AAT Bioquest, Sunnyvale, USA) was applied. This assay detects glucose, by formation of a highly fluorescent product (Ex. 540 nm, Em. 590 nm). By oxidation of β-D-glucose due to GOx, hydrogenperoxide is released and activates horse radish peroxidase (HRP), which activates a sensitive fluorogenic substrate and subsequently the detected product is generated. MTP format was used to determine the activity of 25 µl supernatant of cell lysate containing the expressed *p*NBEBL. Subsequently, 25 µl of β-D-(+)-glucose pentaacetate (stock concentration 60 mM) was added and the reaction was started with 25 µl mastermix (430 µl assay buffer, 10 µl HRP, 10 µl GOx and 2 µl Amplite™). The conversion of the fluorescent substrate was followed at Ex. 540 nm, Em. 590 nm in a microtiter plate reader.

2.2.6. Michaelis-Menten kinetic of purified protein

The final characterization of the identified *p*NBEBL variants was done with purified enzyme (Part II 2.2.6). Therefore, 25 µl of 0.4 µg/µl pure protein (total amount 10 µg) was used for Michaelis-Menten kinetic. Subsequently, 25 µl of β-D-(+)-glucose pentaacetate in varied concentrations (0–50 mM in ddH_20) and 25 µl Amplite mastermix (2.2.5) were supplemented to start the reaction. The conversion of the fluorescent substrate was monitored at 540 nm/590 nm in a microtiter plate reader. The product formation rates were calculated using a standard curve obtained by measuring fluorescence values of a D-glucose dilution series (0-10 mM in ddH_2O). The determination of enzyme kinetics was performed with Prism 6 software (GraphPad) using a Michaelis-Menten kinetic derivation. One unit of *p*NBEBL catalysed the conversion of 1 mmol β-D-(+)-glucose pentaacetate per second.

3. Results

In the first part of this chapter a high throughput screening system based on Fur-Shell technology platform was established for *p*NBEBL in order to generate a reliable prescreening system. In the second part the assay was validated by prescreening a mutagenesis library, which was afterwards analysed in a MTP format regarding improved activity. Finally improved variants were characterized regarding kinetic constants (k_{cat}, and K_M).

3.1. Development of an *in vivo* flow cytometry screening system

The Fur-Shell technology developed firstly for a phytase was advanced for an esterase. Thereby several steps in the technology had to be optimized *i.e.* expression vector, substrate, cell recovery and MTP screening system. Figure 25 shows a schematic overview of the advanced Fur-Shell technology for the esterase. The library was generated by epPCR and the insert and vector fragments were cloned by PLICing. Subsequently the mutant library was transformed in *E. coli* cells (Step I)[99]. In Step II the substrate β-D-(+)-glucose pentaacetate is converted by *p*NBEBL into β-D-glucose. Finally the three monomers were polymerized to a fluorescent hydrogel. The fluorescent hydrogel shell surrounds *E. coli* cells expressing active enzyme variants and can be analysed and sorted by flow cytometer at rates of around 5000 events per second (Step III). The plasmid of the sorted *E. coli* cells expressing active esterase was isolated in Step IV to overcome the low cell survival rate of *E. coli* cells (<8 %) to rescue mutated genes that encoded improved hydrolase variants in non-viable *E. coli* cells[118]. Isolated plasmids are subsequently transformed into *E. coli* cells and screened in 96-well MTP format with the Amplite™ screening system.

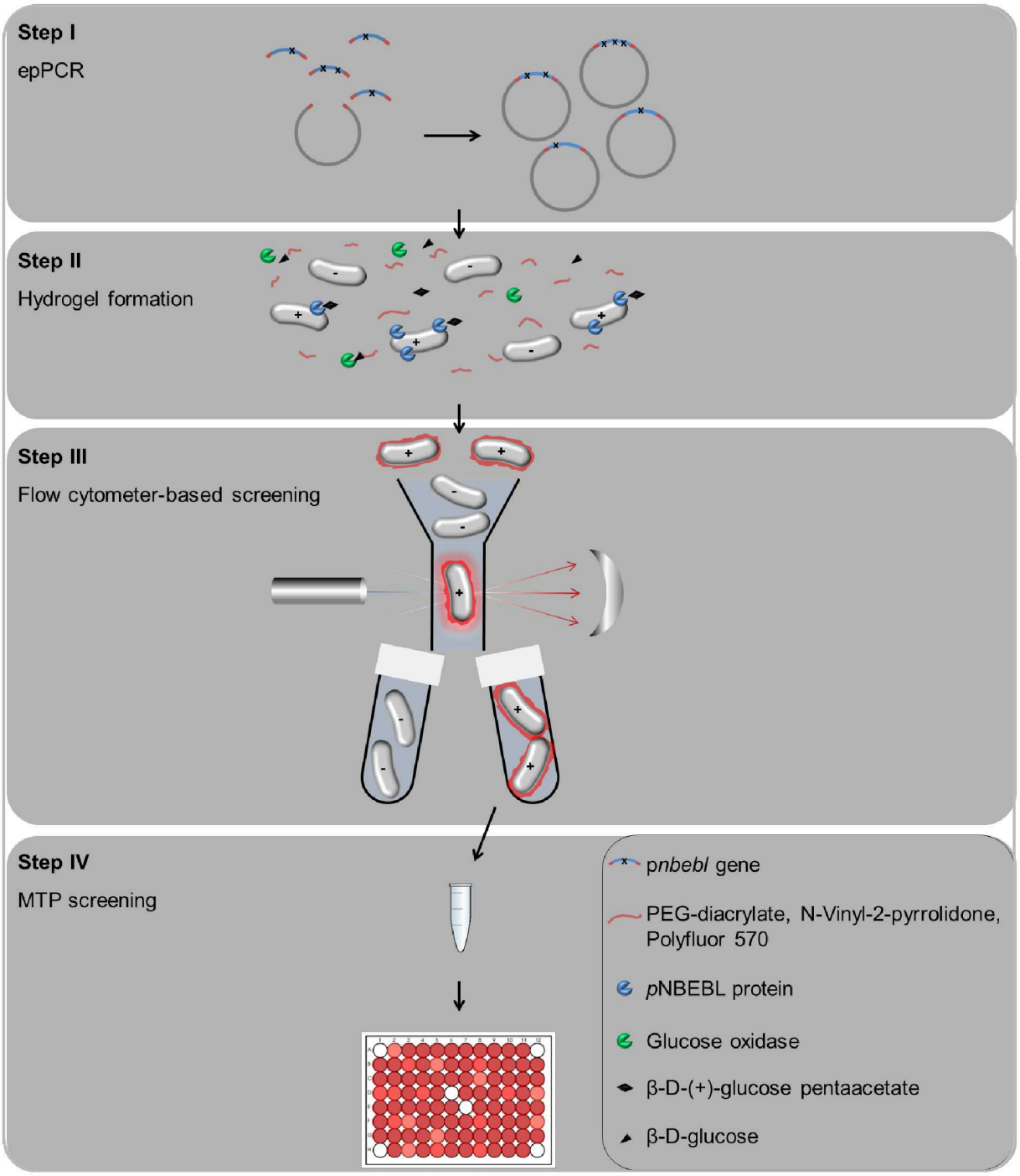

Figure 25 Flow cytometer-based sorting principle in four Steps of the Fur-Shell toolbox for *p*NBEBL. **Step I**: Library generation by epPCR and subsequent cloning by PLICing and transformation, **Step II**: *E. coli* cells producing *p*NBEBL variants are incubated with β-D-(+)-glucose pentaacetate, glucose oxidase and fluorescent labelled monomers (PolyFluor® 570). Cells expressing active enzyme variants (+) were surrounded by a fluorescent hydrogel which allows in **Step III** analysis and sorting (enrichment) by flow cytometer. Finally the *E. coli* cells are used for plasmid isolation and transformation (**Step IV**), followed by transferring clones into MTPs for final screening, modified from[122]. (Reproduced by permission of The Royal Society of Chemistry).

3.1.1. Fluorescent labelling reaction

Pitzler *et al.* developed a whole cell screening system which was optimized for a phytase performance[118]. For the transfer of this protocol an adaptation regarding esterase substrate selection was necessary. Therefore, β-D-(+)-glucose pentaacetate was used, which has the

required ester bond and upon esterase catalysed cleavage donates β-D-glucose (Figure 26) (2.2.2). The glucose oxidase (GOx) catalyzed the conversion of β-D-glucose into D-glucono-δ-lactone[118]. Thereby, H_2O_2 is released and subsequent converted in a Fentons reaction into a hydroxyl radical which initiates the polymerisation reaction of the three monomers poly(ethylene glycol)-diacrylate (PEG), 1-vinyl-2-pyrrolidinone and the fluorescent labelled PolyFluor® 570 on the surface of the *E. coli* cells[118, 132]. The produced polymer formes a layer around the *E. coli* cells and the fluorescence can be detected due to the integrated PolyFluor® 570.

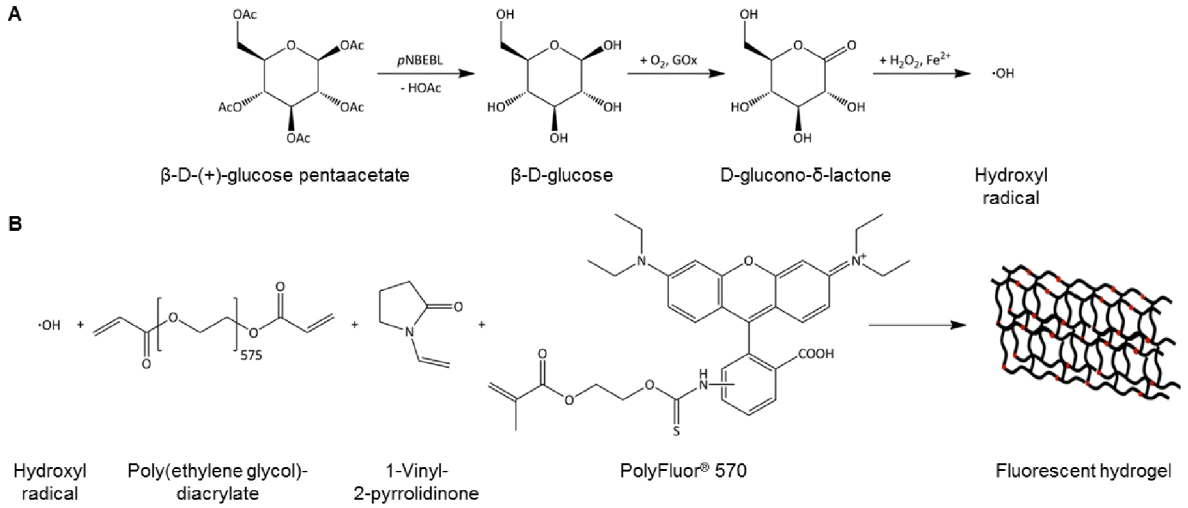

Figure 26 Reaction schema of Fur-Shell technology. **A**: *p*NBEBL hydrolysed the substrate β-D-(+)-glucose pentaacetate into β-D-glucose and acetic acid. β-D-glucose and molecular oxygen are converted by glucose oxidase (GOx) to D-glucono-δ-lactone and in a Fenton reaction a hydroxyl radical is released. **B**: The hydroxyl radical starts the polymerization reaction of three different monomers leading to a fluorescent hydrogel, modified from[118].

3.1.2. Flow cytometry analysis

The first flow cytometer analysis was done to determine the necessity of the pelB leader sequence. The pelB leader sequence leads to a periplasmic expression of the encoded protein, which can have a positive influence on the hydrogel formation around the *E. coli* cells. Therefore, *E. coli* cells expressing pET22b(+)-*p*NBEBL were compared with *E. coli* cells expressing pET22b(+)-pelB-*p*NBEBL in order to elucidate the influence of pelB regarding the intensity of fluorescent signal. Figure 27 shows the flow cytometry plots with fluorescent siganl versus forward scatter.

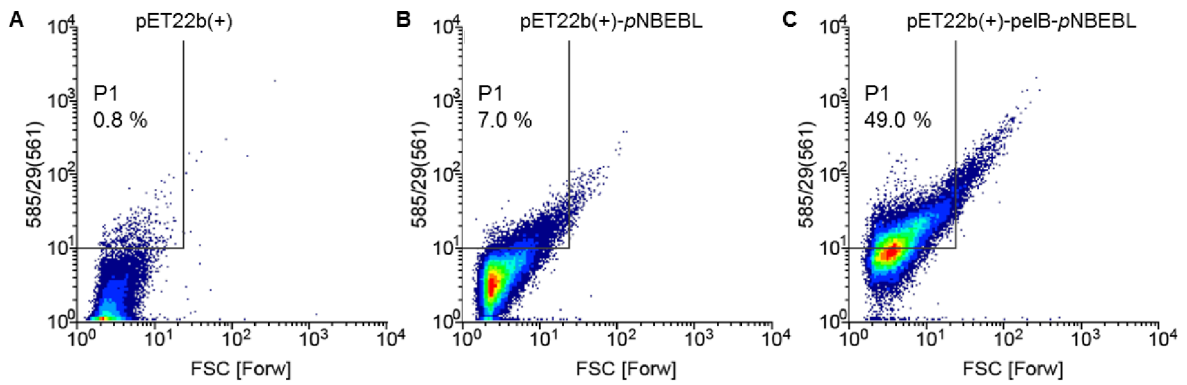

Figure 27 Flow cytometry plots of Fur-Shell labelled cells. Fur-Shell reaction was performed with *E. coli* BL21-Gold (DE3) cells harbouring pET22b(+) (**A**), expressing pET22b(+)-*p*NBEBL (**B**), or expressing pET22b(+)-pelB-*p*NBEBL (**C**). The forward scatter (FSC) was analysed versus the fluorescent signal (Ex. 561 nm, Em. 585 nm, filter +/- 29 nm). Events in gate P1 were fluorescent events with a size <3µm, modified from[122]. (Reproduced by permission of The Royal Society of Chemistry).

P1 gate was set according to negative control fluorescent signal by minimizing background (0.8 %) coming from *E. coli* cells harbouring pET22b(+) EV and size of events <3 µm in order to eliminate associated *E. coli* cells (Figure 27A). *E. coli* cells expressing pET22b(+)-*p*NBEBL showed a fluorescence signal of 7.0 % (Figure 27B), whereas *E. coli* cells expressing pET22b(+)-pelB-*p*NBEBL showed a fluorescence signal of 49.0 % (Figure 27C), which is 61-fold higher than EV and 7-fold higher than the construct without pelB. The results impressivly indicate that a pelB leader sequence is needed to generate a fluorescent signal in order to minimaze background and successfully discriminate among positive and negative events.

3.1.3. Confocal microscope analysis

The formation of the fluorescent hydrogel (2.2.2) around the *E. coli* cells expressing pET22b(+)-pelB-*p*NBEBL was analysed by confocal microscopy. Therefore, the fluorescence signal of *E. coli* cells harbouring pET22b(+) EV was compared by *E. coli* cells expressing pET22b(+)-pelB-*p*NBEBL. The overlay of transmission and fluorescence images showed a strong fluorescent signal for *E. coli* cells expressing pET22b(+)-pelB-*p*NBEBL indicating the formed hydrogel layer (Figure 28A). Whereas *E. coli* cells harbouring pET22b(+) showed a negligible fluorescent (Figure 28B).

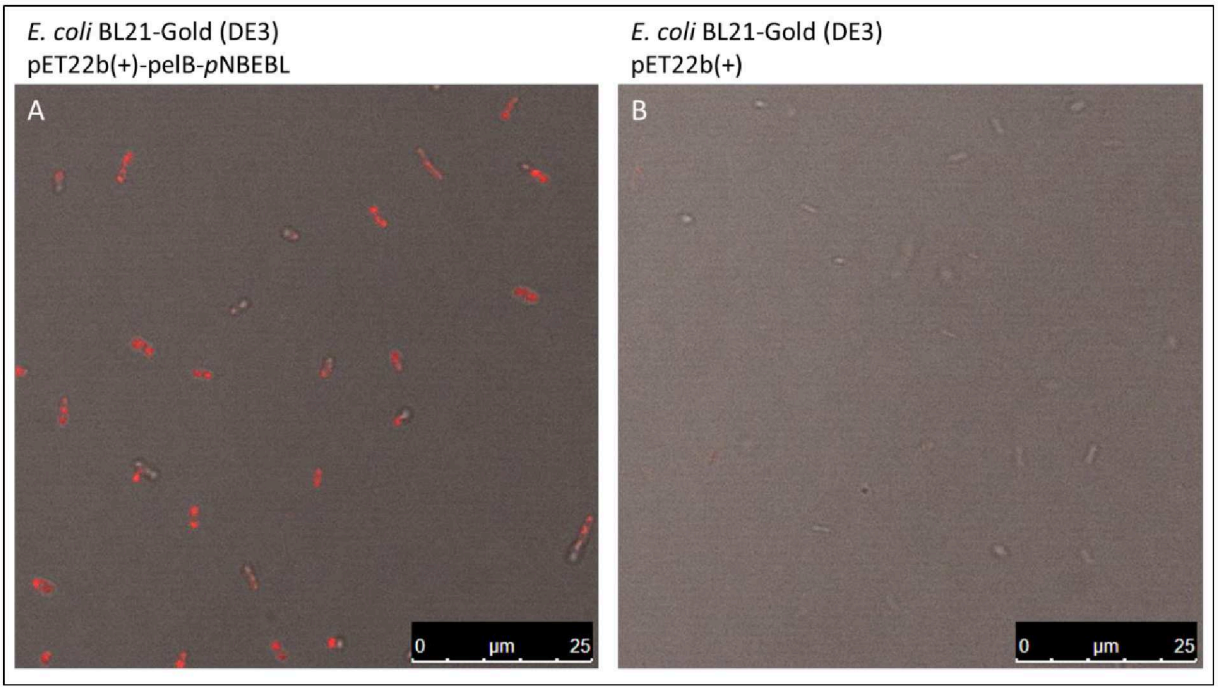

Figure 28 Confocal microscope analysis of *E. coli* cells expressing pET22b(+)-pelB-*p*NBEBL (**A**) and pET22b(+) (**B**) after hydrogel formation. An overlay of the transmission and fluorescence image is shown, modified from[122]. (Reproduced by permission of The Royal Society of Chemistry).

3.1.4. Establishing a MTP screening system with β-D-(+)-glucose pentaacetate

The Fur-Shell screening system is based on conversion of β-D-(+)-glucose pentaacetate as substrate. In order to have the same prescreening and screening conditions for esterase regarding substrates it was necessary to develop a new β-D-(+)-glucose pentaacetate based screening system for MTP format. Upon conversion of β-D-(+)-glucose pentaacetate by esterase released β-D-glucose is further oxidized by a GOx. In a subsequent reaction the Amplite™ Red Kit (AAT Bioquest, Sunnyvale, USA) was used as a sensitive fluorogenic substrate. Oxidation of Amplite fluorogenic compound is mediated by horseradish peroxidase and the fluorescence can be followed at Ex. 540 nm, Em. 590 nm.

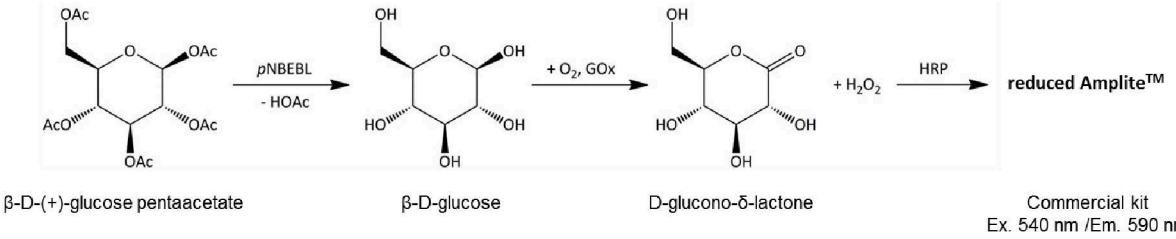

Figure 29 Reaction scheme of Amplite™ screening system. Substrate β-D-(+)-glucose pentaacetate is hydrolysed by *p*NBEBL into β-D-glucose and acetic acid (HOAc). β-D-glucose is converted by the glucose oxidase (GOx) into D-glucono-δ-lactone and H_2O_2, which is used by the horseradish peroxidase (HRP) to reduce Amplite™ to a fluorescent product. Reduced Amplite™ can be measured spectrophotometrically at Ex. 540 nm/Em. 590 nm.

MTP adapted Amplite™ Kit was further optimized regarding expression time, enzyme concentration linear detection range, and standard deviation (Figure 30, 2.2.5).

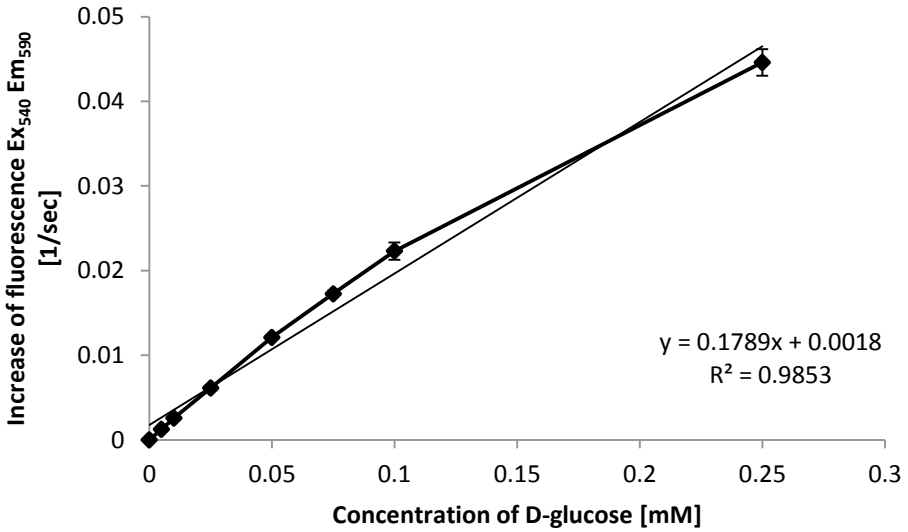

Figure 30 Determination of the linear detection limit of the continuous Amplite™ screening system. D-glucose concentrations from 0 mM to 0.25 mM were used to determine the linear detection range. The reported values are the average of three measurements and average deviations from the mean values are shown.

The linear detection range of D-glucose was determined to cover a span from 0.005 mM to 0.25 mM, thereby 0.005 mM D-glucose represents the lower detection limit of the screening system indicating that at least 0.005 mM β-D-(+)-glucose pentaacetate has to be converted.

After determining the final assay conditions (4 h expression at 30°C, cell disruption in 150 µl PBS pH 7.4, 25 µl supernatant of cell lysate containing *p*NBEBL, 25 µl 60 mM β-D-(+)-glucose pentaacetate, 25 µl mastermix Amplite™ kit, measured at Ex. 540 nm, Em. 590 nm) the standard deviation was calculated to be 10 % in 96-well MTP plate. (Figure 31).

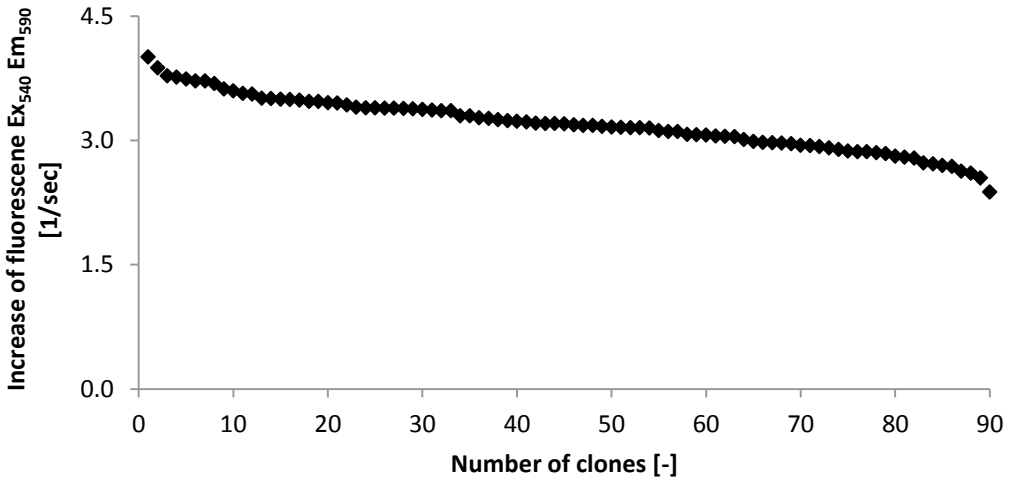

Figure 31 Determination of standard deviation of Amplite™ screening system in 96-well MTP format. Activity values (increase in fluorescence signal (RFU/sec)) of *p*NBEBL WTs by converting β-D-(+)-glucose pentaacetate are shown in descending order. 90 wells were used for mean value calculation (six wells with pET22b(+) EV).

Standard deviations ~10 % are routinely employed in directed evolution campaigns[115].

3.1.5. Sorting of *p*NBEBL reference libraries

Upon performing Fur-Shell reaction using β-D-(+)-glucose pentaacetate as substrate flow cytometry analysis was performed using different ratios of *E. coli* cells expressing pET22b(+)-pelB-*p*NBEBL and *E. coli* cells harbouring pET22b(+) (10:90 and 40:60). Active to inactive *E. coli* mixed populations were sorted and enrichment factor were calculated by dividing the percent number of active cell fraction after sorting with the percent number of active cell fraction before sorting. Therefore, ~200 clones before sorting and ~100 clones after sorting were screened by the Amplite™ screening system and percentages of active cell fraction were calculated (Table 18). The calculated enrichment factors for 10:90 and 40:60 active to inactive ratio were 6-fold, and 1.8-fold, respectively.

Table 18 Enrichment of a 10 % and 40 % reference library analysed with the Amplite™ screening system (n=number of clones).

Expected amount of active clones [%]	Active clones before sorting [%]	Active clones after sorting [%]	Enrichment [fold]
10	10.0 (n=180)	60.0 (n=70)	6.0
40	45.2 (n=230)	81.3 (n=107)	1.8

3.2. Generation and screening of random mutagenesis library by flow cytometry

In order to validate the Fur-Shell technology platform for directed esterase evolution, a standard epPCR (0.1 mM $MnCl_2$, 3.25 mutations per gene) was screened[17]. *E. coli* cells expressing pET22b(+)-pelB-*p*NBEBL 0.1 mM epPCR library were analysed and active variants were sorted by flow cytometry (2.2.4). Sorting strategy comprised minimising a background signal coming from *E. coli* cells harbouring pET22b(+) by P1 gating where all the events with a size <3 µM were included. The *E. coli* cells expressing pET22b(+)-pelB-*p*NBEBL 0.1 mM epPCR library showed a 17.3-fold higher fluorescent signal (15.6 %) compared to *E. coli* cells harbouring pET22b(+) (0.9 %) (Figure 32).

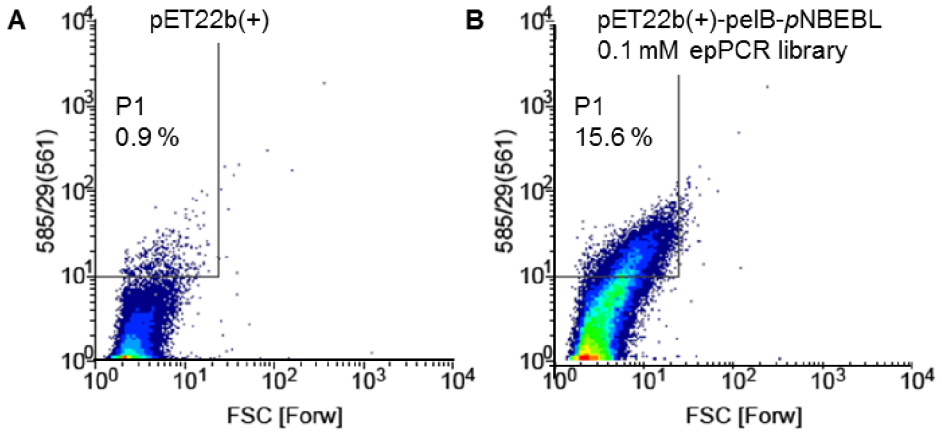

Figure 32 Flow cytometry analysis of the mutant library of Fur-Shell labelled cells. The density plots showed forward scatter (FSC) against the fluorescent signal (Ex. 561 nm, Em. 585 nm, filter +/- 29 nm). Fur-Shell reaction was performed with *E. coli* cells expressing pET22b(+)-pelB-*p*NBEBL 0.1 mM $MnCl_2$ epPCR library (**B**) and *E. coli* cells harbouring pET22b(+) (**A**). Gate P1 was set according to background signal of *E. coli* cells harbouring pET22b(+) and the respective size of the events <3µm[122]. (Reproduced by permission of The Royal Society of Chemistry).

In total, $1*10^7$ *E. coli* cells expressing pET22b(+)-pelB-*p*NBEBL 0.1 mM epPCR library were analysed out of which $5*10^5$ active *E. coli* cells expressing *p*NBEBL were sorted. The DNA was recovered by plasmid isolation and transformed in *E. coli* cells for MTP screening using Amplite™ screening system. In total, 180 *E. coli* clones were screened to determine initial number of active clones before sorting and 360 clones after sorting. The enrichment factor was calculated by dividing the percent number of active fraction after sorting with percent number of active fraction before sorting and yielded 1.3-fold (Figure 21).

Table 19 Comparison of the amount of active variants before and after flow cytometry sorting revealed in the enrichment value.

Active variants before sorting [%]	Active variants after sorting [%]	Enrichment [fold]
31	41	1.3

The eight variants showing highest activity values were rescreened in Amplite™ MTP screening assay. Variant E1 showed 13.7-fold and variant E2 showed 7.9-fold higher activity compared to *p*NBEBL WT in supernatant of cell lysate (Figure 33A). SDS-PAGE analysis was performed for variants E1, E2, and WT to assess the differences in expression levels. Figure 33B confirmed no difference in expression levels among variants E1, E2 and WT excluding the possibility that increase in activity is due to an increased protein production (Figure 33A).

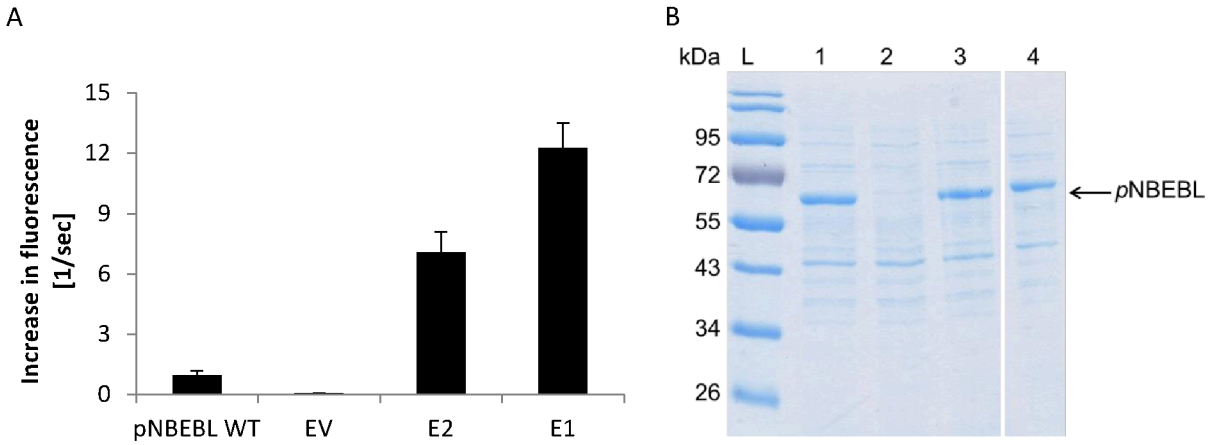

Figure 33 Rescreening analysis of improved *p*NBEBL variants. **A**: Activity (RFU/sec) of variants (E1, E2) is compared with *p*NBEBL WT and EV by applying Amplite™ screening system **B**: SDS-PAGE analysis of *p*NBEBL WT and isolated variants. Enzymes were expressed for 4 h at 30°C. 6 µl of cell lysate containing the expressed protein were loaded on the SDS-PAGE. **L**: ladder in kDa, **1**: pET22b(+)-pelB-*p*NBEBL (WT), **2**: pET22b(+), **3**: pET22b(+)-pelB-*p*NBEBL variant E2, **4**: pET22b(+)-pelB-*p*NBEBL variant E1 (merged), modified from[122]. (Reproduced by permission of The Royal Society of Chemistry).

Sequence analysis was performed to identify amino acids exchanges in variants E1 and E2 (Table 20). Variant E1 contained two amino acid exchanges Glu256Gly, Gly401Val and one silent mutation Arg348, whereas variant E2 contained one amino acid exchange Phe313Ser and five silent mutations Tyr135, Glu213, His214, Ser366, and Gly423.

Table 20 Sequence analysis of *p*NBEBL variants revealed in several amino acid exchanges (silent mutations are shown in grey).

Variant	Amino acid exchange
*p*NBEBL	---
E1	Glu256Gly, Arg348Arg, Gly401Val
E2	Tyr135Tyr, Glu213Glu, His214His, Phe313Ser, Ser366Ser, Gly423Gly

3.3. Kinetic characterization of *p*NBEBL WT and identified variants E1 and E2

3.3.1. Purification by anion exchange chromatography

The identified variants E1 and E2 were purified for a detailed kinetic characterization. The purification was done using an anion exchange chromatography where the esterase (pI ~4.7) binds to the positive charged matrix. *E. coli* cells expressing *p*NBEBL WT, and variant E1, and E2 were sonicated and the filtered supernatant was loaded on the Toyopearl Super Q 650c column pre equilibrated with running buffer (Part II 2.2.6). The protein was eluted at 19 % of elution buffer containing 1 M NaCl and collected in fractions (Figure 34).

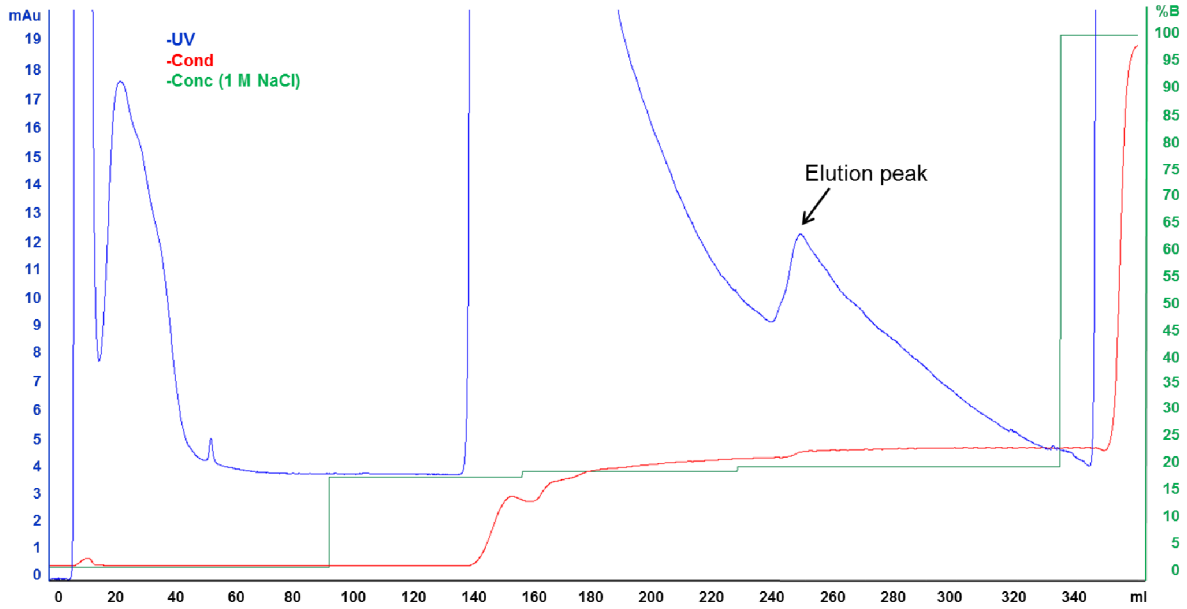

Figure 34 Anion exchange chromatography profile of *p*NBEBL variant E1. The peak marked with an arrow represents the eluted fractions with esterolytic activity observed at 19 % 1 M NaCl. The concentration (green) is measured before the column, whereas the conductivity (red) is measured after the column. The column volume is ~20 ml.

The esterolytic activity of the collected fractions was determined and those showing activity were pooled and concentrated. The homogeneity was analysed by capillary electrophoresis (Experion Pro260 Analysis Kit) (Figure 35).

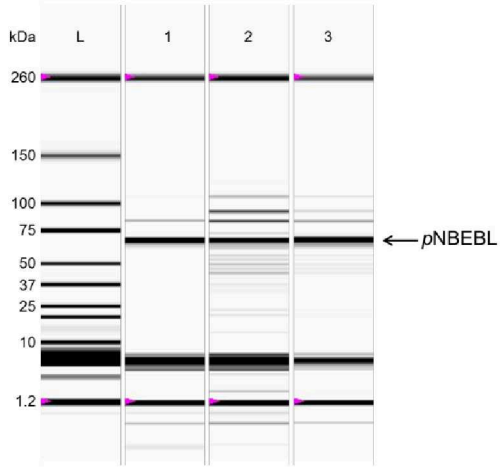

Figure 35 Experion™ analysis of purified *p*NBEBL WT and variants E1 and E2. Samples (0.2 mg/ml) were prepared as described in the manufactures protocol and analysed in duplicate. **L**: ladder in kDa, **1**: *p*NBEBL WT, **2**: *p*NBEBL variant E1, **3**: *p*NBEBL variant E2.

After estimating the purity (WT: 86 %, E1: 48 %, E2: 82 %) the total protein concentration of each sample was determined using the BCA assay. The specific protein concentration was calculated by dividing total protein concentration by purity and is shown in Table 17.

Table 21 The specific protein concentration was calculated after purification, homogeneity and total protein concentration determination. The results for *p*NBEBL WT and all variants are shown.

Variant	Specific concentration [mg/ml]
*p*NBEBL	2.41
E1 (Glu256Gly, Gly401Val)	0.72
E2 (Phe313Ser)	0.66

3.3.2. Determination of kinetic parameters

For kinetic characterization *p*NBEBL WT and improved variants E1 and E2 were used. The conversion of β-D-(+)-glucose pentaacetate to β-D-glucose was followed and subsequent the Michaelis-Menten plots were generated and evaluated with GraphPad (Figure 36) (2.2.6).

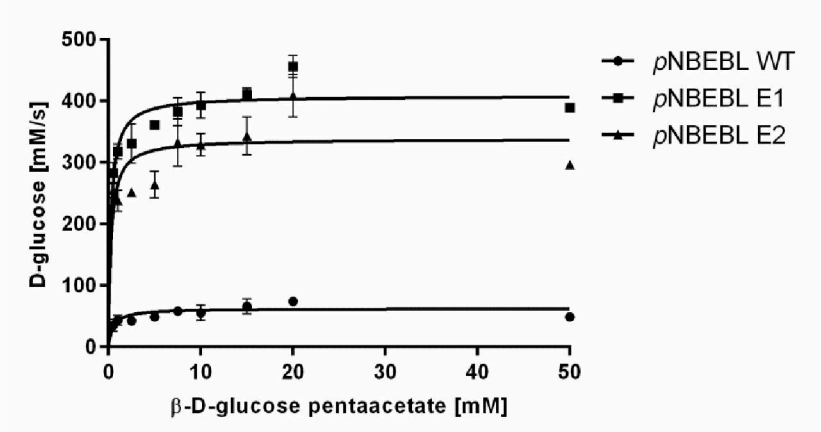

Figure 36 Michaelis-Menten plots of *p*NBEBL WT and improved variants E1 and E2. V_{max} (D-glucose [mM/s]) was plotted against K_M (β-D-(+)-glucose pentaacetate [mM]). Measurements were done in triplicate and the average values and the average deviations from the mean values are shown[122]. (Reproduced by permission of The Royal Society of Chemistry).

Variant E1 showed a 7.1-fold higher k_{cat} (E1: 185.74; WT 26.14) and 2-fold lower K_M (E1: 0.27; WT: 0.54) value compared to *p*NBEBL WT indicating a higher specific activity (Table 22). E2 showed a similar behaviour than E1 a 6.5-fold higher k_{cat} and a 1.8-fold lower K_M.

Table 22 Characterization of isolated and purified variants using the Amplite™ screening system[122].

Enzyme	V_{max} [mM/s]	K_M [mM]	k_{cat} [1/s]	U/g [mmol/s*g]
*p*NBEBL WT	64.07±3.27	0.54±0.17	26.14±1.32	480.53±24.27
E1	409.80±9.00	0.27±0.05	185.74±4.08	3415.00±67.52
E2	341.70±14.26	0.30±0.10	168.96±7.05	3106.36±106.95

3.3.3. Homology model generation and visual inspection

In order to generate in depth molecular understanding of improved thermal resistance in variant E1 its homology model was generated using YASARA[106]. Figure 37 and Figure 38 showing the substitution in comparison to *p*NBEBL WT.

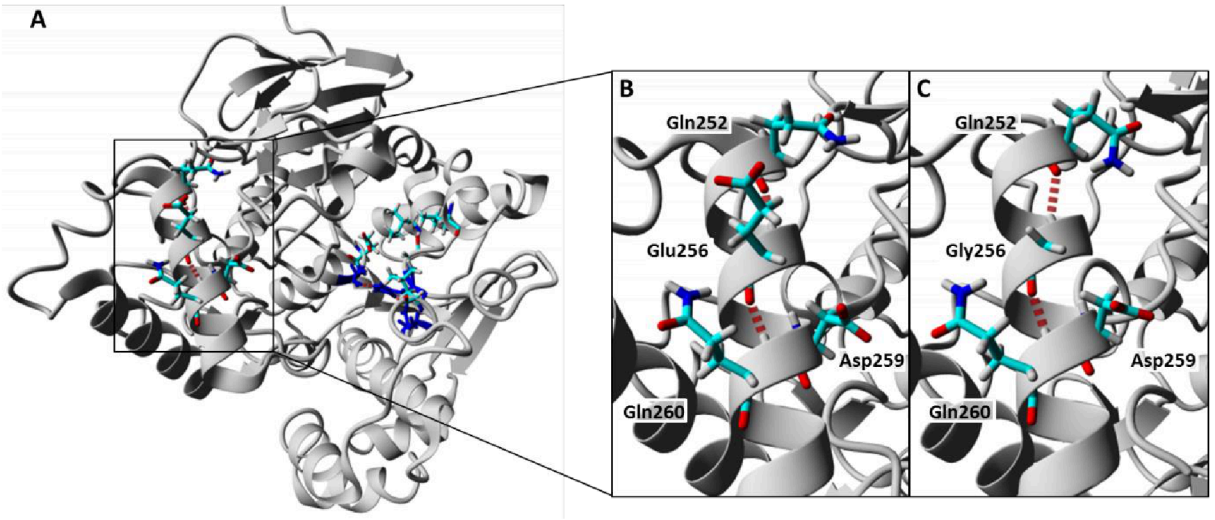

Figure 37 Energy minimization of *p*NBEBL WT and variant E1 with amino acid exchange Glu256Gly. **A**: *p*NBEBL WT with the catalytic triad Ser188, His400 and Glu309 in blue. A-C were predicted with YASARA and the FoldX plugin, the hydrogen bonds were displayed in red segmented lines. **B**: *p*NBEBL WT with Glu256, **C**: substitution Glu256Gly.

The homology model of *p*NBEBL WT with the catalytic triad Ser188, His400 and Glu309 in blue is shown in Figure 37A. The enlarged image of the α-helix including position 256 is shown in Figure 37B and C. Position 256 is located on surface of *p*NBEBL and has not been reported yet. The substitution Glu256Gly leads to no significant changes in the distances of the Cα-atoms of α-helix and no changes in the number of formed hydrogen bonds. Analysis of the possible structure of the mutated α-helix by SWISS-MODEL revealed reduced stability if Glu at position 256 is substituted with Gly[133].

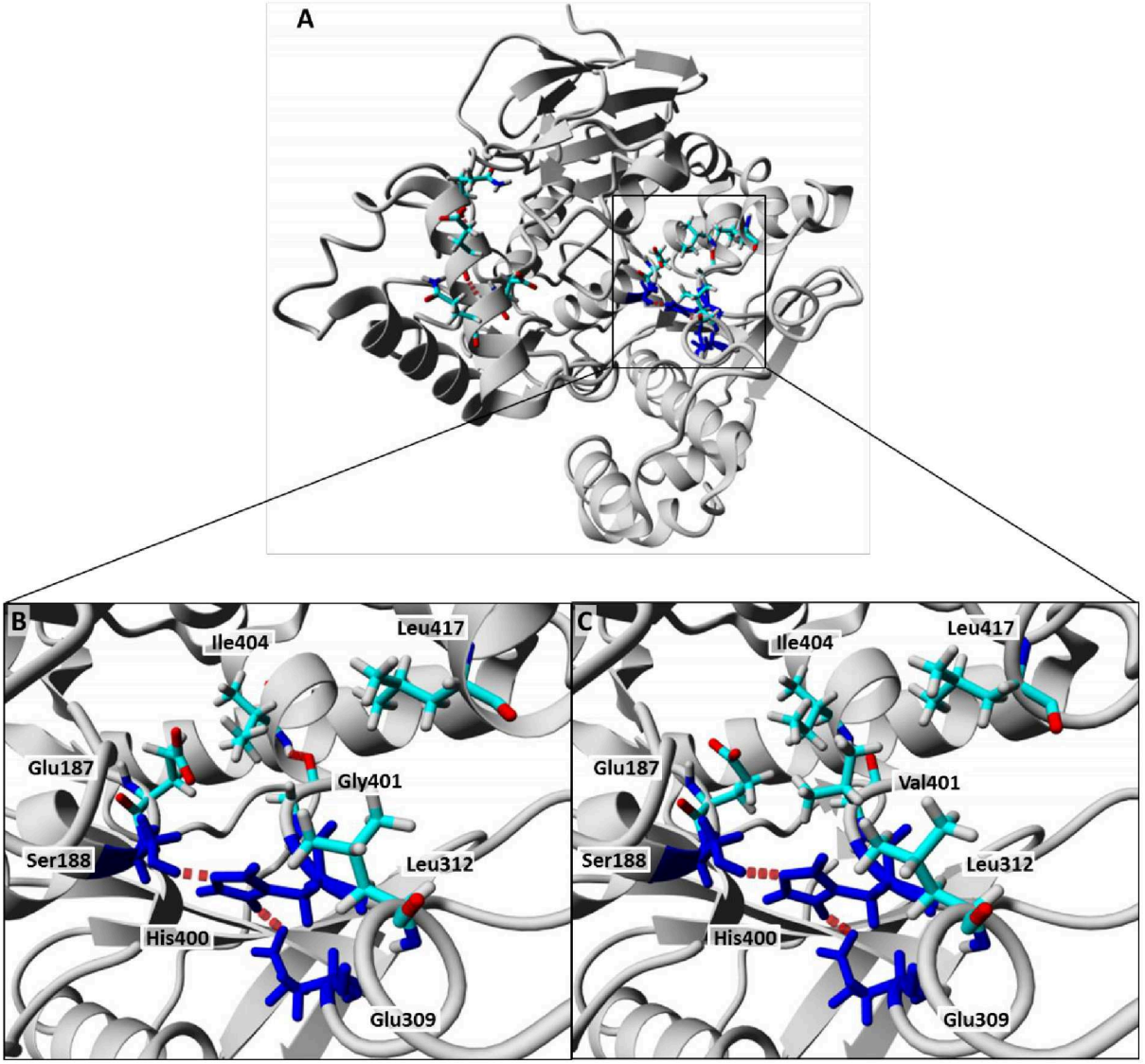

Figure 38 Energy minimization of *p*NBEBL WT and variant E1 with amino acid exchange Gly401Val. **A**: *p*NBEBL WT with the catalytic triad Ser188, His400 and Glu309 in blue. A-C were predicted with YASARA and the FoldX plugin, the hydrogen bonds were displayed in red segmented lines. **B**: *p*NBEBL WT Gly401, **C**: substitution Gly401Val.

The second substitution Gly401Val is shown in detail in Figure 38B and C. Position 401 is located next to the His400 which is part of the catalytic triad, the same position was reported for a *p*-nitrobenzyl esterase to be thermostabilizing[75]. The substitution does not influence the orientation and hydrogen bond formation of the catalytic triad residues. The hydrogen bond between the peptide backbone of Gly401 and Ile404 is missing and the distances between the Cα-atoms of Gly401 and Ile404 (5.75 Å) is enlarged to 6.24 Å (Val401-Ile404).

4. Discussion

Flow cytometers are powerful tools used in high throughput screening offering a high coverage of the generated sequence space by screening throughputs of at least 10^7 events per hour. So far existing flow cytometer-based screening systems are, despite their high throughput rarely used in directed evolutions campaigns. This might be caused by laborious sample preparation steps, like compartmentalization *e.g.* encapsulation of cells or an *in vitro* expression system inside double emulsions. Additionally, retention of the fluorescent product inside the cell membrane or double emulsions dictates the time a sample can be reproducibly analysed via flow cytometry. The herein applied whole cell flow cytometer-based screening system named Fur-Shell overcomes the prevalent drawbacks of screening with flow cytometers.

In Fur-Shell technology, a glucose-derivative is converted by *p*NBEBL into β-D-glucose and supplemented glucose oxidase converts generated β-D-glucose into D-glucono-δ-lactone and hydrogen peroxide. Hydroxyl radicals produced in the Fenton reaction from ferrous ions and hydrogen peroxide, initiate a polymerisation reaction which forms a fluorescent hydrogel around cells expressing active enzymes[118]. The obtained principle overcomes the disadvantage of leakage, because the fluorescent product rhodamine B is covalently bound into the hydrogel. Further improvement of this method was done regarding cell recovery rate after flow cytometer sorting. Cells directly sorted on agar plates showed a survival of less than 8 %[118]. This can be attributed most likely to the polymer shell around the cells, which might hinder cell proliferation. The latter can lead to a reduced number of variants which can be analysed in the final MTP-based screening system. In order to recover all clones coding for active enzyme, regardless of their survival, a plasmid isolation step was added to rescue the DNA of the sorted variants. Afterwards the DNA was re-transformed in competent *E. coli* cells maintaining the diversity of the variants which were analysed in detail in subsequent MTP-based screening system. Therefore, a MTP β-D-(+)-glucose pentaacetate based screening system using reporter fluorogenic substrate Amplite™ was established and validated. The Amplite™ screening system was optimized regarding different assay parameters *e.g.* linear detection range (0.005 mM to 0.25 mM) and standard deviation (10 %). The Amplite™ assay follows, as the Fur-Shell technology, the conversion of β-D-(+)-glucose pentaacetate into β-D-glucose. Thus, by using for both screening systems the same substrate enables on the one hand to screen for improved variants converting β-D-(+)-glucose pentaacetate and on the other hand gives the opportunity to screen for substrate specific activity. Hereby, a significant step to establish the Fur-Shell technology as a valuable prescreening system was made.

Initial experiments with Fur-Shell system and *p*NBEBL in pET22b(+) showed that without a periplasm destination peptide (pelB leader sequence) insufficient fluorescent hydrogel is formed to distinguish cell harbouring an EV and cells expressing *p*NBEBL via flow cytometry. In a former study a phytase with a putative signal peptide for gram-negative microorganisms

was applied in the Fur-Shell reaction indicating a signal peptide being crucial for the Fur-Shell reaction[134]. The requirement of a signal sequence for the Fur-Shell reaction indicates that the hydrolysis of β-D-(+)-glucose pentaacetate might take place in the periplasm or even outside the *E. coli* cell.

In order to validate the established Fur-Shell technology a *p*NBEBL library was analysed and sorted. The identified *p*NBEBL variant E1 (Glu256Gly, Gly401Val) showed a 7.1-fold higher k_{cat} (E1: 185.74; WT 26.14) and a 2-fold lower K_M (E1: 0.27; WT: 0.54) value compared to *p*NBEBL WT. A reduced K_M value is an indication for the requirement of a lower substrate concentration whereas an increase in the turnover number k_{cat}, shows a faster conversion of the substrate. In comparison with other directed evolution campaigns, in which one round of directed evolution leads to an improvement of average 1.5 to 2.5-fold increase in activity, the obtained improvement of 7.1-fold per single round of directed evolution was impressive[135]. The Fur-Shell technology was also applied in a joint project for two other hydrolases with industrial relevance, the *B. subtilis* lipase A (BSLA) and a cellulase (CelA2) isolated from a metagenome library by Streit *et al.*[136-137]. The MTP screening revealed an enrichment of activity for BSLA of 1.5-fold and for CelA2 11.7-fold, which is remarkable and proved once more the effective prescreening. It offers the possibility to isolate active clones from vast populations of inactive clones leading to a minimal MTP-based screening effort. The kinetic characterisation of the improved and purified variants showed 1.3-fold (BSLA variant L1, Tyr139Asp) and 1.9-fold (CelA2 variant C1, Val37Ala, Glu275Gly, Glu398Val) increase in k_{cat} compared to respective wildtypes[122].

In conclusion, the Fur-Shell technology was advanced to a general platform for directed hydrolase evolution, by developing a prescreening system for three hydrolases (*i.e.* esterase, cellulase, and lipase) and validating them in a single round of directed evolution. The developed screening technology is robust and simple and most likely can be expanded to other reaction systems, *e.g.* different microgels and enzyme classes. Large libraries, *i.e.* metagenome libraries will benefit from the fast screening system and separation of active clones.

The Fur-Shell technology was successfully applied to the esterase by adaptation of the reaction substrate. In combination with the Fur-Shell technology and the MTP screening system a variant with an impressive 7.1-fold improvement was identified. The variant has two amino acid substitutions at position 256 located on the surface and at position 401 close to catalytic site.

Part IV: Structure-function analysis of the *p*NBEBL esterase regarding PET degradation

This work was already published in the master thesis of Sandra Knopp "*Rational design study of the substrate specificity of an esterase by saturation mutagenesis*" (2014) and Daniel Sexauer "*Development of a polyethylene terephthalate microtiter plate based screening system*" (2014).

Goals and main results

In Part IV of this work, a MTP-based screening system based on bis(*p*-methylbenzoic acid)-ethylene glycol ester (PET-dimer) was developed in order to tailor esterase towards increased substrate specificity using a model substrate which mimics complex PET polymer structure. Later on, the optimized MTP assay was employed to study structure function relationship of a specific lid like loop in esterase (18AA) and its impact on PET degradation. Analysis was performed by stepwise deletion of pair of two amino acids and monitoring changes in esterase activity towards PET. It was shown that complete deletion of lid like loop yields to an inactive esterase and linear trend was observed between activity decrease and decrease in size of the loop.

1. Introduction

Degradation of polyethylene terephthalate (PET) is performed in the environment by photodegradation, thermooxidative degradation, hydrolytic degradation and biodegradation by microorganisms[138]. Already in 1997 Staples *et al.* showed an overview of microorganisms and fish which are able to degrade phthalate esters and terephthalate esters (Table 23)[139].

Table 23 Overview of phthalate ester and terephthalate ester degrading microorganism or fish[139].

Substrate	Organism	Reference
Dimethyl terephthalate (DMT)	*Aspergillus niger* (Bacteria)	140
Diethyl terephthalate (DET)	*Rhodococcus rhodochorus* (Bacteria)	141
Dimethyl phthalate (DMP)	*Bacillus sp.* (Bacteria)	142
	Lepomis macrochirus (Fish)	143
Diethyl phthalate (DEP)	*Micrococcus sp.* (Bacteria)	144
	Parophyrus vetulus (Fish)	145
Dibutyl phthalate (DBP)	*Micrococcus sp.* (Bacteria)	146
	Cyprinodon variegatus (Fish)	147

The prediction of the biodegradation pathway of phthalate esters in the environment is divided into two possibilities: 1) aerobic conditions, 2) anaerobic conditions (Figure 39)[148]. In

both cases the reaction starts with ester hydrolysis to form the monoester and the corresponding alcohol followed by the production of phthalic acid. In the aerobic pathway protochatechuate is formed via 3,4-dihydroxyphthalate by gram-negative bacteria or 4,5-dihydroxyphthalate by gram-positive bacteria[146, 149]. The ring opening takes place either in meta-position with the final products acetate and succinate or in ortho-position with two pyruvates as products[146, 150-151]. The prediction for the anaerobic degradation showed the formation of benzoyl CoA which is then part of the benzoate pathway, and finally acetate is released[152].

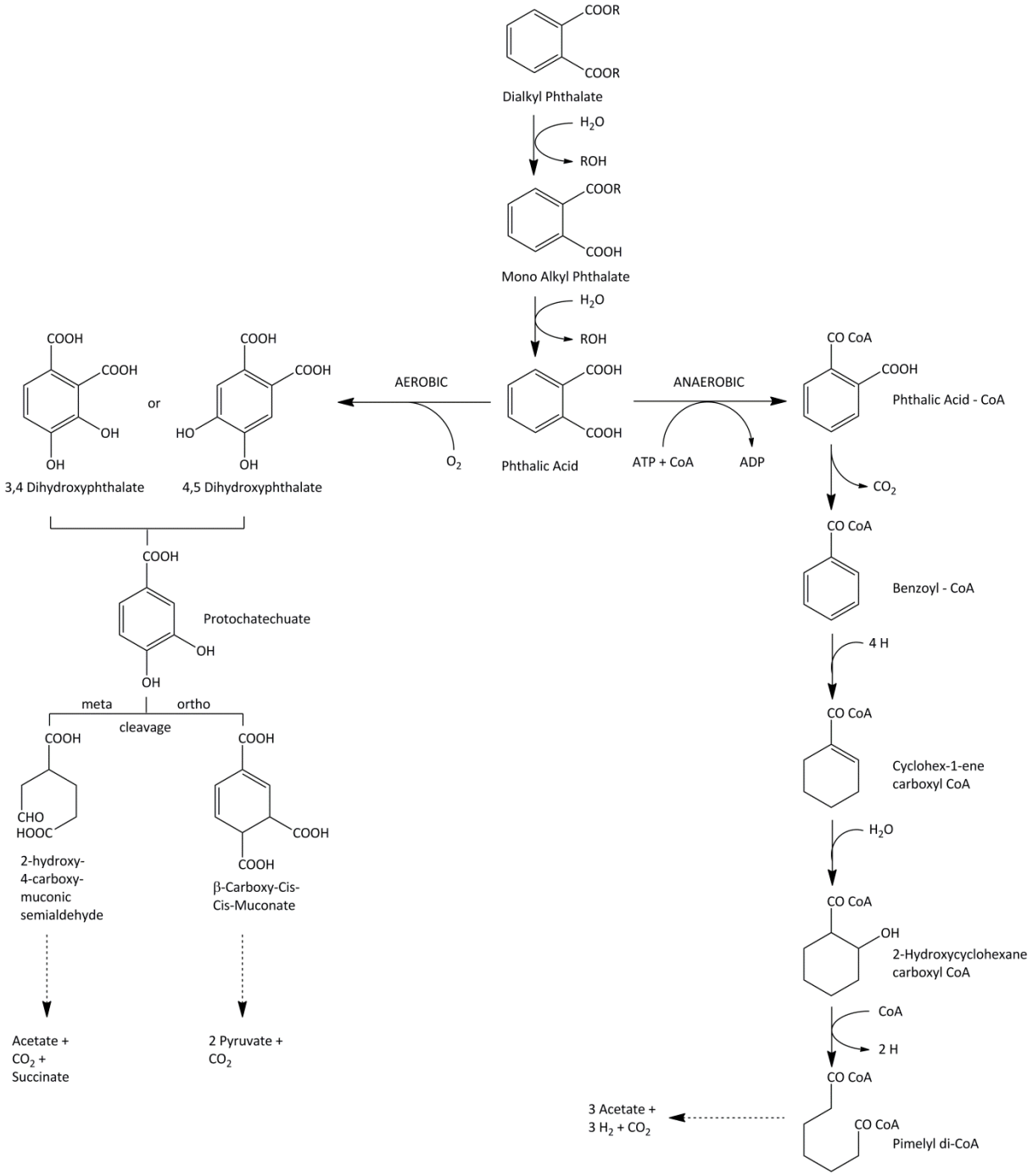

Figure 39 Prediction of the aerobic and anaerobic biodegradation pathway of phthalate esters in the environment, modified from[139].

One of the key prerequisites to identify PET degrading enzymes is the establishment of screening systems in which direct PET degradation can be monitored. Until now PET is seldom represented in screening systems due to its structural complexity and low solubility in aqueous environment. The reported enzymes which showed PET degrading activity were so far grown in enrichment cultures on PET or PET model esters as carbon source[153]. For kinetic characterization HPLC analysis were applied to determine and quantify the released products[154]. Instead of applying PET as substrate in most cases model substrates are used to mimic the complex PET structure. Besides PET-dimer (bis(*p*-methylbenzoic acid)-ethylene glycol ester), PET-trimer (bis(benzoyloxy-ethyl)-terephthalate) and the cyclic PET-trimer (cyclo-tris-ethylene terephthalate) were used which are formed as a side-products during the production of PET in an amount of 1-3 %[153, 155-156]. In agar plate screening system PET-dimer and PET-trimer can be applied to detect activity by halo formation[157]. Main disadvantage of agar plate screening systems is the limited number of variants which can be only qualitatively screened (~10^5)[26].

The degradation of model substrates such as 1,4-bis(benzyloxy)butane, diphenyl adipate, 1,4-bis-cyclohexancarbonyloxy-butane, dicyclohexyl adipate or 1,4-bis-phenylacetoxy-butane was shown for lipases, proteinases and esterases[158]. For hydrolases *e.g.* isolated from *Thermobifida fusca* an screening system was developed where the loss in weight of a PET foil was measured[64]. Furthermore, cutinases *i.e.* from *Fusarium solani pisi* showed activity on PET fibers[159-160]. The hydrolases (*i.e.* lipases, esterases and cutinases) seem to be promising enzymes for further investigation of PET degradation. For all three mentioned enzymes the PET degradation mechanism is not understood and studied in detail. Wei *et al*. performed molecular docking studies with bis(2-hydroxyethyl) terephthalate to investigate the substrate binding pocket of *Thermonospora curvata*. The study revealed that more hydrophobic and less charged amino acids clustered in the vicinity of the substrate binding pocket in comparison to other cutinases[161].

In this work, a MTP screening system using a PET-dimer as model substrate was established. Formation of PET hydrolysis product catalyzed by *p*NBEBL can be spectrophotometrically followed by using a pH indicator. Further on, the optimized assay was used to monitor esterase activity upon systematic deletion of amino acids in one of the loop structures (amino acid position 63-80) located in proximity above the entrance to the active site identified by computational analysis study. In the crystal structure of the *p*-nitrobenzyl esterase from *B. subtilis* (PDB 1CFI), which shared a structural similarity of 77.4 % with *p*NBEBL, a loop from amino acid position 64-71 forming the entrance to the catalytic triad was identified. The same loop was enlarged in the acetylcholine esterase, shrinking the active site and leading to a better hydrolysis of smaller acetylcholine substrates[75]. Based on structural features of *p*NBEBL and already reported work on structurally similar enzymes, structure function relationship study on the loop in close vicinity of the active site and its influence on PET degradation activity was performed. The study comprised systematic deletion of amino acids in pairs and monitoring PET degradation activity using PET-dimer MTP screening system.

2. Material and methods

2.1. Material

See Part II section 2.1 with the exception of PET-dimer (bis(*p*-methylbenzoic acid)-ethylene glycol ester) and PET-trimer (bis(benzoyloxyethyl)-terephthalate) which was synthesized kindly by Dr. Thomas Weber (Henkel AG & Co. KGaA, Düsseldorf, Germany)[55]. See Part II section 2.1.1, 2.1.2 and 2.1.4 for target gene, strains and plasmids, and cell culture methods.

2.1.1. Oligonucleotides

The oligonucleotides were ordered from Eurofins MWG Operon (Ebersberg, Germany) in salt-free form and are summarized in Table 24.

Table 24 Primers for reducing the loop length and used melting temperature (T_M) (small letters indicate phosphorothioate nucleotides).

Primer name	Sequence 5'-3'	T_M [°C]
FW_16 AS loop	GATGGGGTATTGCCTGCGGGGGTTCAAAAG	64
RV_16 AS loop	CTTTTGAACCCCCGCAGGCAATACCCCATC	64
FW_14 AS loop	GCAGCCTGATGGGGTATTGGGGGTTCAAAAGTCTGAGG	55
RV_14 AS loop	CCTCAGACTTTTGAACCCCCAATACCCCATCAGGCTGC	55
FW_12 AS loop	CAGCCTGATGGGGTAGTTCAAAAGTCTGAGGATTGCC	55
RV_12 AS loop	GGCAATCCTCAGACTTTTGAACTACCCCATCAGGCTG	55
FW_10 AS loop	CGCAGCCTGATGGGCAAAAGTCTGAGGATTGCC	55
RV_10 AS loop	GGCAATCCTCAGACTTTTGCCCATCAGGCTGCG	55
FW_8 AS loop	GTTTGTCCGCAGCCTGATAAGTCTGAGGATTGCC	55
RV_8 AS loop	GGCAATCCTCAGACTTATCAGGCTGCGGACAAAC	55
FW_6 AS loop	GTTTGTCCGCAGCCTTCTGAGGATTGCCTTTATTTAAATGTG	65
RV_6 AS loop	CACATTTAAATAAAGGCAATCCTCAGAAGGCTGCGGACAAAC	65
FW_4 AS loop	GGTTTGTCCGCAGGAGGATTGCCTTTATTTAAATGTG	65
RV_4 AS loop	CACATTTAAATAAAGGCAATCCTCCTGCGGACAAACC	65
FW_2 AS loop	GCCCGGTTTGTCCGGATTGCCTTTATTTAAATGTG	65
RV_2 AS loop	CACATTTAAATAAAGGCAATCCGGACAAACCGGGC	65
FW_0 AS loop	ggcccggtttgtTGCCTTTATTTAAATGTGTACGCACCCGAAGAGG	60
RV_0 AS loop	acaaaccgggccAAATTGAAAAGCATCCAGCTCACCTTCC	60

2.1.2. PET-dimer and PET-trimer dispersion

PET-dimer and PET-trimer were received as insoluble powder and a dispersion had to be prepared. Therefore, 6 g/l PET-dimer/trimer was dispersed in 10 g/l triton X 100 and 50 % (v/v) ethanol (96 %) and stirred (15 min, 50°C). The dispersion was added to 2 mM tris-HCl buffer pH 9 and homogenized on ice (25 min). Subsequent, the dispersion was

stirred (16 h, RT) and ethanol was evaporated. The dispersion with a final concentration of 0.6 % (w/v) PET-dimer was stored at RT and resuspended before usage.

2.2. Methods

For cloning see Part II section 2.2.1. The growth conditions and expression are explained in 96-well microtiter plate see Part II section 2.2.5. The expression in flasks and purification by anion exchange chromatography are explained in Part II section 2.2.6.

2.2.1. Construction of loop with reduced length

For loops with a final size of 16-0 amino acids a "two-stage" PCR was performed, where the first step contains two reaction mixture for separation of the forward and revers oligonucleotide[101]. Subsequently, in the second step both reactions mixtures were combined and the PCR program shown in Table 25 was continued.

Table 25 "Two-stage" PCR program loop length reduction. Annealing temperature was set according to the mentioned T_M.

Step 1	**Temperature [°C]**	**Time [sec]**	**Cycle [-]**
Initial denaturation	98	60	1x
Denaturation	98	30	
Annealing	XX[a]	30	3x
Elongation	72	420	
Step 2	**Temperature [°C]**	**Time [sec]**	**Cycle [-]**
Denaturation	98	30	
Annealing	XX[a]	30	15x
Elongation	72	300	
Final elongation	72	300	1x

[a] see T_M in Table 24

For the PCR mixture PfuS DNA polymerase (2.5 U), dNTP mix (10 mM), plasmid template (pET22b(+)-*p*NBEBL, 30 ng) and oligonucleotides listed in Table 24 (20 µm) were used. The resulted PCR products were digested with *Dpn*I (20 U) at 37°C[98]. The PCR products of loop length 16-2 amino acids were purified using a PCR clean-up Gel extraction kit from Macherey-Nagel. The variant *p*NBEBL-loopΔ-0AA was purified by the QIAquick PCR Purification Kit from Qiagen, due to the presence of phosphorothioate oligonucleotides. Afterwards the religation of the linear fragment was performed by PLICing[99]. Hybridized DNA fragments as well as the purified PCR of *p*NBEBL-loopΔ-16-2AA variants were transformed into *E. coli* BL21-Gold (DE3) for expression[100].

2.2.2. Detection of *p*NBEBL activity on agar plates

Agar plate assays were used to semi-quantify enzymatic activity via halo formation. For tributyrin agar plates see Part II section 2.1.4 Table 9 and 2.2.4. For LB-agar plates supplemented with a PET-dimer or PET-trimer a suspension had to be prepared (2.1.2). LB-agar plates (5 g/l yeast, 10 g/l tryptone, 10 g/l NaCl, 15 g/l agar; pH 7.5) were

supplemented with 4.76 % PET-dimer/trimer suspension (final concentration 0.028 % PET-dimer), ampicillin (100 µg/ml), and IPTG (0.1 mM). *E. coli* BL21-Gold (DE3) cells containing pET22b(+)-*p*NBEBL were plated on the plates and incubated (16 h, 37°C, afterwards 24 h, 4°C) for halo formation.

2.2.3. PET-dimer MTP screening system

For detection of PET degradation of esterases an MTP screening system was developed based on the conversion of PET-dimer. The released acid can be followed by colour conversion from orange to yellow due to the applied pH indicator. For preparation of one MTP 0.3 % (w/v) agar was autoclaved in PBS (0.1x; pH 8.5). The lukewarm agar solution was supplemented with 12.8 % (v/v) PET-dimer dispersion (0.076 % final PET-dimer concentration) and 1.96 % (v/v) cresol red (5 mM in ddH_2O). Each well of the MTP was filled with 150 µl of the prepared solution, subsequent plates were stored (ON, 4°C). For detection of esterolytic activity supernatant of cell lysate containing expressed protein (2.2.5) was diluted 1:10 in PBS pH 7.4 and 20 µl were added in each well on top of the agar solution. The degradation of PET-dimer and the subsequent pH shift was monitored as end point measurements spectrophotometrically at 570 nm. During the measurements the plates were incubated at the respective temperature of interest (18°C and 42°C).

2.2.4. Computer based loop analysis

The software YASARA (www.yasara.org) was used to generate the homology model based on the crystal structure of 1QE3, 1C7I, 1C7J (*p*-nitrobenzyl esterase from *B. subtilis*) and 2OGT (carboxyl esterase from *Geobacillus stearothermophilus*)[75, 106-107]. The most detailed description of the loop was given by 1C7I. The alignments of all *p*NBEBL-loopΔ variants to 1C7I were done with the standard program Protein BLAST and the online software Modeller (Bioinformatics Toolkit, Tübingen, Germany)[162] was used to generate models.

2.2.5. Circular dichroism

Circular dichroism (CD) was used to determine the secondary structure of *p*NBEBL WT and to prove the correct folding of *p*NBEBL-loopΔ. The absorption of circularly polarized light by chiral chromophores like peptide bonds, aromatic side chain and disulfide bonds differs and can therefore be used to determine the secondary structure of a protein by comparison with references. The secondary structure of *p*NBEBL was determined with OLIS CD-Spectrophotometer DSM-17 (OLIS Instruments, Bogart, GA, Germany) with nitrogen flow of 10 l/min in the chamber, monochromator and lamp case a slid with of 1 nm and 2 nm bandwidth at 20 nm/min (140 W, water-cooled xenon arc lamp, Hamamatsu, Iwata, Japan). Samples were diluted to 0.4 mg/ml in 0.1 M sodium phosphate buffer pH 8.5 (0.1 M Na_2HPO_4 in ddH_2O, adjust pH 8.5 with 0.1 M NaH_2PO_4 $1xH_2O$ in ddH_2O) and 140 µl were measured in 0.5 mm quartz cuvettes (Suprasil, 106-QS, Hellma) in 1 nm steps and normalized to 0 millidegrees at 240 nm. The baseline was measured with sodium phosphate buffer and subtracted from the sample data. Measurements were done in triplicate and evaluated with the online-software Dichroweb[4] (CONTIN Set 4) which gives an overview about the amount of different secondary structure found in the whole protein[163].

3. Results

In this work a PET-dimer MTP screening system for detection of esterolytic activity was developed. Subsequently, the screening system was used to proof the hypothesis that the lid like loop from *p*NBEBL, covering the entrance to the catalytic triad, has an effect on the degradation of PET-dimer. Influence of lid like loop on PET degradation activity was studied by stepwise reducing the loop length and monitoring change in activity using PET-dimer MTP screening system.

3.1. PET-dimer MTP based screening system

3.1.1. Principle of PET-dimer MTP screening system

PET-dimer was used to design a screening system mimicking complex PET polymer structure. It was shown using GC/MS measurement that prominent PET-dimer degradation products are 4-methylbenzoic acid and 4-methylbenzoic acid ethylene glycol ester[55].

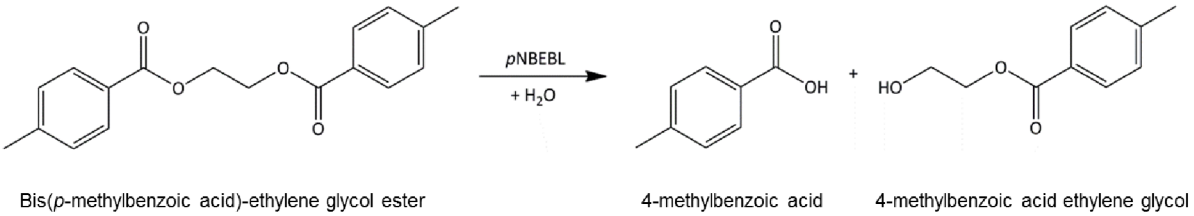

Figure 40 Hydrolysis of bis(*p*-methylbenzoic acid)-ethylene glycol ester (PET-dimer) to 4-methylbenzoic acid and 4-methylbenzoic acid ethylene glycol ester, modified from[55].

Figure 40 shows the hydrolysis products of the substrate bis(*p*-methylbenzoic acid)-ethylene glycol ester (PET-dimer) catalysed by *p*NBEBL. The released products are 4-methylbenzoic acid ethylene glycol ester and 4-methylbenzoic acid. The latter changes the pH of the assay solution which in the presence of pH indicator can be spectrophotometrically monitored. As indicator, cresol red was selected and its transition point (pH 8.8-7.0) is illustrated in Figure 41.

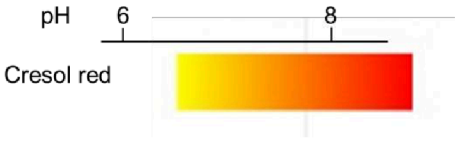

Figure 41 Transition point of the pH indicator cresol red, modified from[164].

Lowering of pH of the assay solution due to PET-dimer degradation causes change of colour from orange/red to yellow and can be followed at 570 nm.

3.1.2. Determination of assay parameters

In order to overcome poor solubility observed for PET-dimer, it was dispersed in agar matrix and used in MTP screening format. Different agar concentrations from 0.1 % till 0.5 % were tested in order to fix the PET-dimer in a kind of matrix to avoid sedimentation on the bottom of the MTP well. It was shown that with 0.1 % agar (w/v) the matrix is not stable enough and PET-dimer precipitates on the bottom of the well. The highest agar concentration (0.5 % w/v) leads to an unequal suspension/distribution within 96-wells of MTP. Furthermore, it decelerates the diffusion rate of the supernatant on the surface of each well. At agar concentration of 0.3 % (w/v) no precipitation and high homogeneity was observed. Afterwards, the volume necessary for covering the complete surface of one well was determined. For better visibility blue coloured water was pipetted on top of the wells (Figure 42).

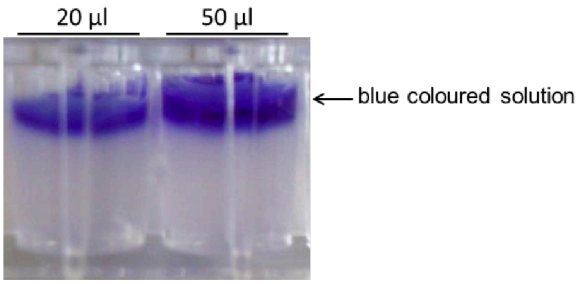

Figure 42 Determination of the volume needed to cover the surface of one well of a 96-well MTP. A blue coloured solution was pipetted on top of two wells left 20 µl solution, right 50 µl solution.

Figure 42 shows two wells of a 96-well MTP where the left well is filled with 20 µl and the right well is filled with 50 µl of blue water. The left well shows that 20 µl are sufficient to cover the complete well surface and therefore will be used for all further assay parameters determination.

In the second step different pH indicator concentrations were analysed. The assay buffer has a pH of 8.5 (identical to the established cBLE-AAP screening system, see Part II 3.2.1) and therefore the pH indicator cresol red was selected with a transition point between pH 8.8 and 7.0 allowing the detection of the released acidic product 4-methylbenzoic acid over the reaction time. The colour change from orange/red (at ~pH 8.8) to yellow (at pH ≤7.0) can be followed spectrophotometrically at 570 nm. In order to determine the optimal concentration of cresol red in the assay, different cresol red concentrations were applied and the activity of *p*NBEBL WT or EV (20 µl lysate) was measured at 18°C (Figure 43). The hydrolysis of PET-dimer was followed over ~5 h and colour change was measured for *p*NBEBL WT and EV at time intervals of 30 min.

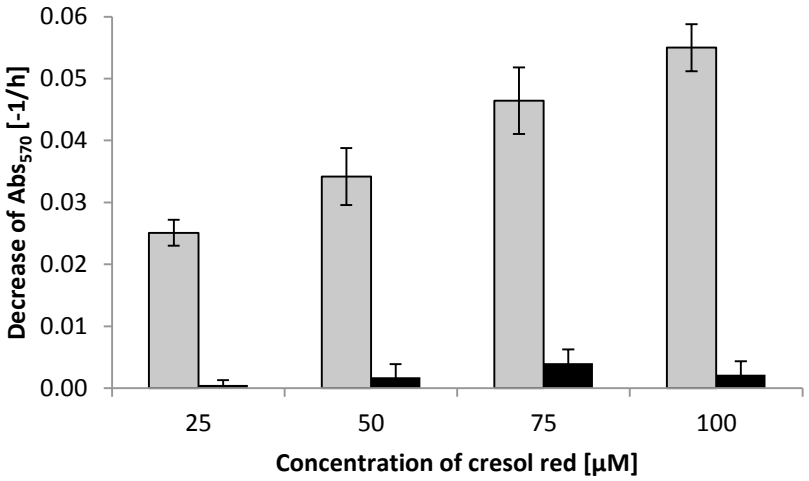

Figure 43 Determination of cresol red concentration for application in the PET-dimer MTP screening system. Different cresol red concentrations (25, 50, 75 and 100 µM) were tested in the assay. The hydrolysis rates of *p*NBEBL WT (▫) and EV (■) lysate (6 µl lysate + 14 µl PBS pH 7.4) at 18°C were followed by measuring decrease of absorbance at 570 nm. The reported values are the average of six (EV) / ten (WT) measurements and average deviations from the mean values are shown.

In concentration range of cresol red from 25 µM to 100 µM the linear increase of *p*NBEBL WT activity was observed. Overall, the background signal produced by incubating the PET-dimer with supernatant containing EV was below 9 % for all cresol red concentrations. At cresol red concentration of 100 µM the *p*NBEBL WT showed 25-fold higher activity than EV and was used as final concentration since it yielded highest decrease of absorbance signal value.

After successful optimization of the concentration of cresol red, different supernatant volumes of the cell lysate containing expressed *p*NBEBL WT were tested (2, 4, and 6 µl) using 0.3 % w/v agar, and 100 µM cresol red. The screening plates were incubated at 18°C and the decrease of absorbance was followed spectrophotometrically at 570 nm (Figure 44). The screening conditions were tested with cell lysate supernatant containing expressed *p*NBEBL WT and EV. The linear increase in activity of *p*NBEBL WT was observed by increasing supernatant cell lysate volume. The background signal from the supernatant containing EV was lower than 24 %. Finally 2 µl of cell lysate supernatant containing *p*NBEBL WT was used. The standard deviation was lower compared to the higher supernatant volumes (6 µl) and most importantly the detection limit of the assay was not reached, enabling identification of more active variants compared to *p*NBEBL WT.

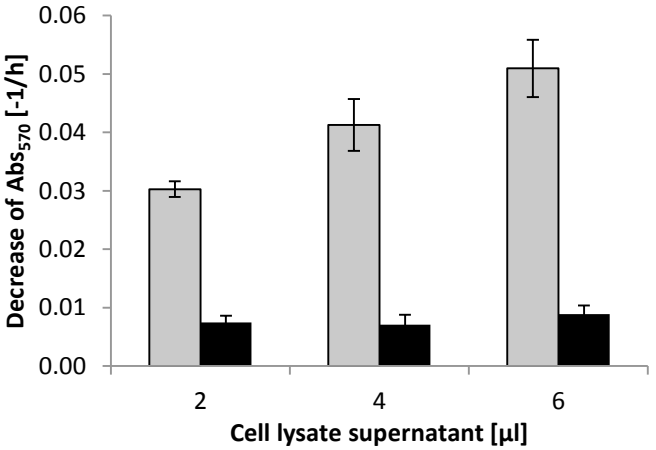

Figure 44 Determination of supernatant concentration for application in the PET-dimer MTP screening system. Different supernatant concentrations (2, 4 and 6 µl) were tested in the assay. The hydrolysis rates of *p*NBEBL WT (▫) and EV (▪) at 18°C were followed by measuring decrease of absorbance at 570 nm. The reported values are the average of five (EV) / ten (WT) measurements and average deviations from the mean values are shown.

3.1.3. Determination of standard deviation of PET-dimer MTP screening assay

The standard deviation of the established PET-dimer MTP screening assay was determined to check its reliability. After determining the final assay conditions (0.3 % (w/v) agar supplemented with 0.076 % (w/v) PET-dimer and 1.96 % (v/v) cresol red; 150 µl solution per well; 2 µl cell lysate supernatant containing expressed *p*NBEBL WT) the standard deviation was determined for 90-wells of *p*NBEBL WT. The plates were incubated at 18°C or 42°C and measurements were done at time intervals of 30 min within 6 h (Figure 45).

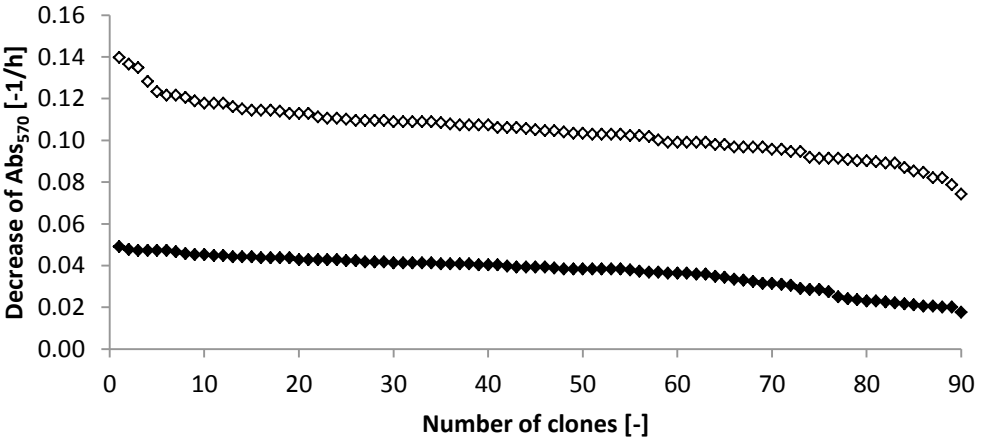

Figure 45 Determination of standard deviation of PET-dimer MTP screening system in 96-well MTP format. Activity values of *p*NBEBL WT are shown in descending order at two temperatures (18°C (♦), 42°C (◇)). *p*NBEBL WT was expressed in 90-wells and supernatant of cell lysates of expressed *p*NBEBL WT were used to finally determine the standard deviations (six wells with pET22b(+) EV).

The standard deviation of the PET-dimer MTP screening system in the 96-well MTPs was optimized to 23 % at 18°C and to 11 % at 42°C. Screening systems with standard deviations ~10 % are routinely used for a directed evolution campaigns[115].

3.2. Strategy for shortening loop length of *p*NBEBL

Computational analysis study on the *p*NBEBL showed the presence of one loop covering the entrance to the catalytic triad. The loop is composed of 18 amino acids (AA) starting at amino acid position 63 till 80. Figure 46 showed the *p*NBEBL WT structure (A) and *p*NBEBL variant with complete loop deletion (*p*NBEBL-loopΔ-0AA, B).

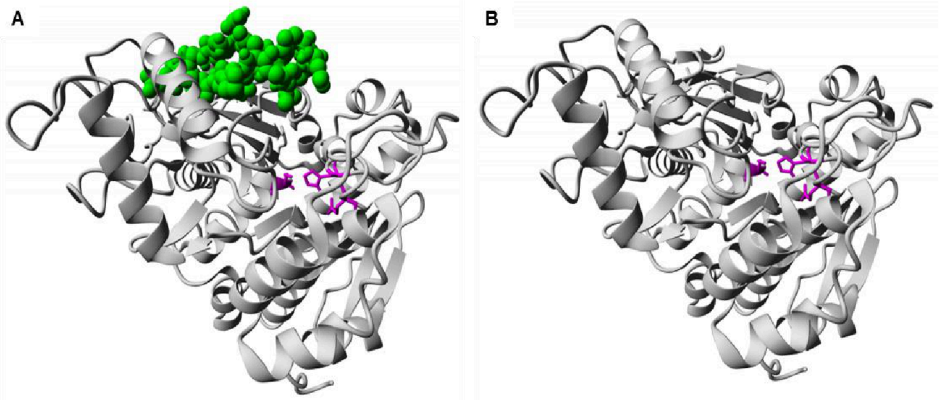

Figure 46 Homology model of *p*NBEBL WT and *p*NBEBL-loopΔ-0AA. **A:** *p*NBEBL WT with the loop from AA position 63 to 80 in green. **B:** *p*NBEBL-loopΔ-0AA. The AAs of the catalytic triad are highlighted in magenta.

In order to analyse the loop (AA 63-80) influence on PET-dimer degradation, the loop length was shortened systematically. Figure 47 shows two possible strategies on shortening the loop even or uneven number of amino acids. In the case that an even number of amino acids is deleted the modified backbone shows the same orientation as in *p*NBEBL WT (Figure 47C). The deletion of an uneven number of amino acids, *e.g.* three amino acids, leads to orientation change of neighbouring amino acids by rotation or flipping of the backbone due to a steric hindrance (Figure 47E-F).

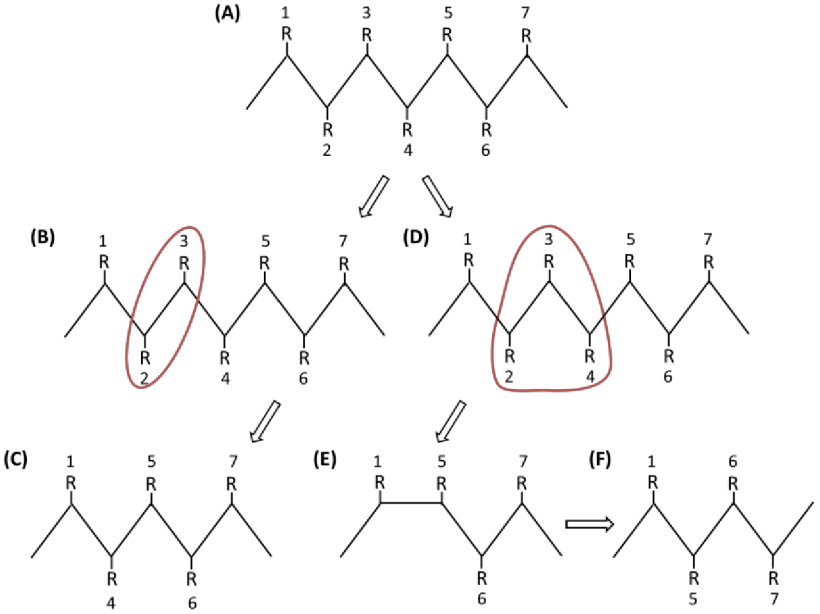

Figure 47 Different strategies of amino acid deletion in the loop of *p*NBEBL WT. The amino acid backbone is shown and R symbolises the rest of the specific amino acids. In the starting backbone (**A**) seven amino acids are shown. A double deletion of two amino acids (**B**) (AAs highlighted in red) lead to a shortened backbone of five amino acids (deletion of number 2 and 3) (**C**). In comparison a deletion of three amino acids (**D**) resulted in an orientation change of neighbouring amino acids by rotation or flipping of the backbone due to a steric hindrance (**E-F**).

In Figure 48 an overview of *p*NBEBL-loopΔ variants is shown. Fulfilling the above mentioned criteria (deletion of even numbers of amino acids) nine constructs have to be generated, each two amino acids shorter than the previous construct. The two amino acids were always deleted from the middle of the loop. Thereby, it was expected to keep the flexibility of the loop as long as possible, since the both cysteine's symbolizing the anchor points of the loop remained.

loopΔ-18AA	CPQPDGVLPESAGVQKSEDC
loopΔ-16AA	CPQPDGVLP~~ES~~AGVQKSEDC
loopΔ-14AA	CPQPDGVL~~PESA~~GVQKSEDC
loopΔ-12AA	CPQPDGV~~LPESAG~~VQKSEDC
loopΔ-10AA	CPQPDG~~VLPESAGV~~QKSEDC
loopΔ - 8AA	CPQPD~~GVLPESAGVQ~~KSEDC
loopΔ - 6AA	CPQP~~DGVLPESAGVQK~~SEDC
loopΔ - 4AA	CPQ~~PDGVLPESAGVQKS~~EDC
loopΔ - 2AA	CP~~QPDGVLPESAGVQKSE~~DC
loopΔ - 0AA	C~~PQPDGVLPESAGVQKSED~~C

Figure 48 Overview of *p*NBEBL-loopΔ variants generated by stepwise deletion of even amino acid numbers. The *p*NBEBL WT loop length is 18 amino acids, 9 constructs were generated to get the final of *p*NBEBL-loopΔ-0AA, and deleted amino acids are highlighted in blue and crossed.

3.2.1. Generation of *p*NBEBL-loopΔ variants with different lengths

The variants with a reduced loop length were generated by PCR (2.2.1) and the resulted constructs were transformed for expression in *E. coli* BL21-Gold (DE3). Subsequently, cell lysates of expressed *p*NBEBL constructs were analysed on a SDS-PAGE to determine the expression levels for each construct (Figure 49).

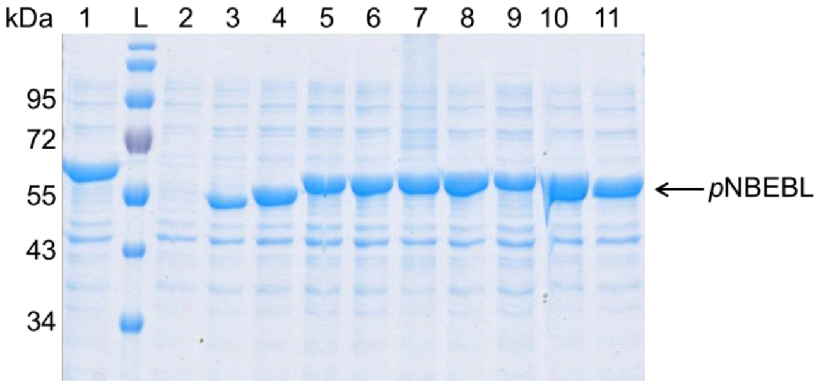

Figure 49 SDS-PAGE analysis of *p*NBEBL WT and generated variants with reduced loop length. Enzymes were expressed for 4 h at 30°C. 6 µl of cell lysate containing the expressed protein were loaded on a 12 % SDS-PAGE. *p*NBEBL WT has an expected size of ~54 kDa, where variants with *p*NBEBL-loopΔ-0AA and *p*NBEBL-loopΔ-2AA showed molecular weight of ~52 kDa. **L**: ladder in kDa, **1**: *p*NBEBL WT, **2**: pET22b(+)-EV, **3**: *p*NBEBL-loopΔ-0AA, **4**: *p*NBEBL-loopΔ-2AA, **5**: *p*NBEBL-loopΔ-4AA, **6**: *p*NBEBL-loopΔ-6AA, **7**: *p*NBEBL-loopΔ-8AA, **8**: *p*NBEBL-loopΔ-10AA, **9**: *p*NBEBL-loopΔ-12AA, **10**: *p*NBEBL-loopΔ-14AA, **11**: *p*NBEBL-loopΔ-16AA.

All generated variants could be successfully expressed, showed comparable expression levels, and differences in activities (Figure 50).

3.2.2. Activity on tributyrin, PET-dimer and PET-trimer agar plates

Esterolytic activity of all *p*NBEBL-loopΔ variants and *p*NBEBL WT was determined by using an agar plate screening system. The agar plates were supplemented with tributryin, PET-dimer or PET-trimer and represent a qualitative detection method, where formed halos around the cells indicate esterolytic activity (Figure 50A, C, and E) (2.2.2). For a better visual effect of the halos the colonies were washed from the plates (Figure 50B, D, and F). The summary of the halo formation for different substrates and loop deletion variants is shown in Table 26.

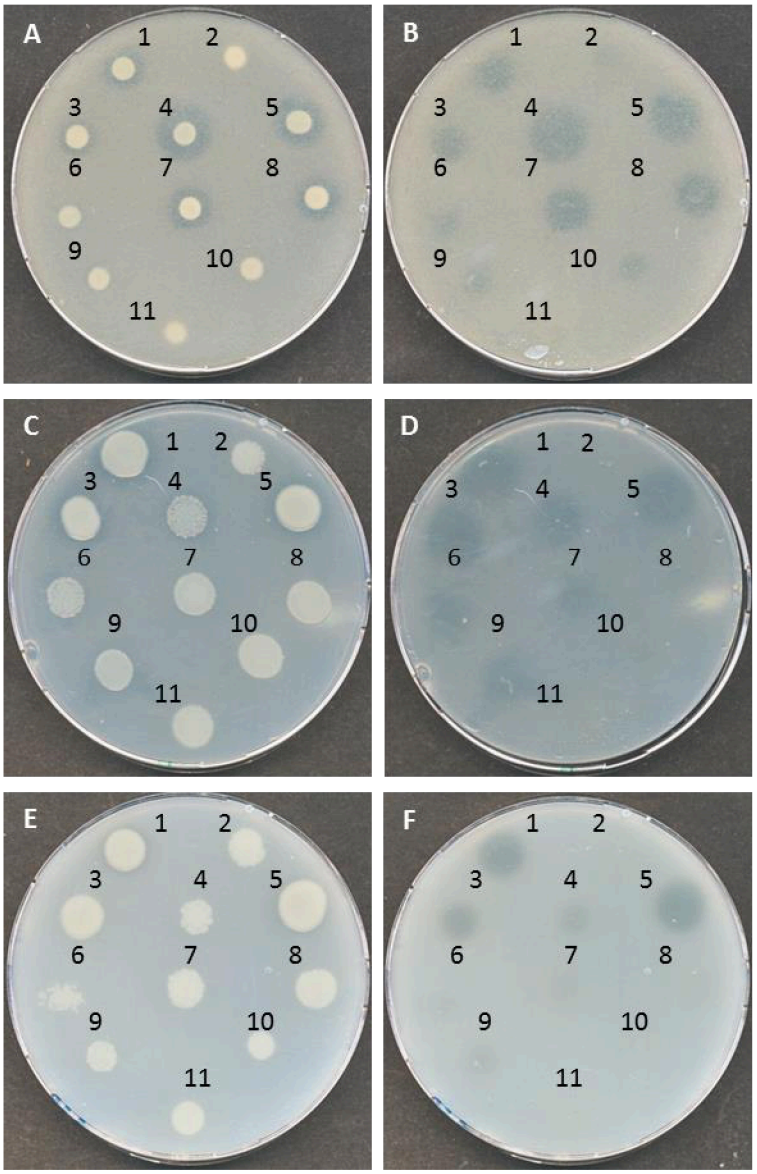

Figure 50 Esterolytic activity determination for *p*NBEBL WT and its *p*NBEBL-loopΔ variants through halo formation on tribuytrin, PET-dimer and PET-trimer plates. Agar plates were supplemented with tributyrin (**A**, **B**), PET-dimer (**C**, **D**) or PET-trimer (**E**, **F**) and incubated after plating *E. coli* cells containing the pET22b(+)-*p*NBEBL variants with different loop lengths for 16 h at 37°C and afterwards at 4°C. **A**, **C**, **E** halo formation around *E. coli* cells, **B**, **D**, **F** visible halos after washing the colonies from the plates. **1**: *p*NBEBL WT, **2:** *p*NBEBL-loopΔ-0AA, **3**: *p*NBEBL-loopΔ-16AA, **4**: *p*NBEBL-loopΔ-14AA, **5**: *p*NBEBL-loopΔ-12AA, **6**: *p*NBEBL-loopΔ-10AA, **7**: *p*NBEBL-loopΔ-8AA, **8**: *p*NBEBL-loopΔ-6AA, **9**: *p*NBEBL-loopΔ-4AA, **10**: *p*NBEBL-loopΔ-2AA, **11**: pET22b(+)-EV.

Table 26 Overview of activities of *p*NBEBL WT and generated *p*NBEBL-loopΔ variants through halo formation on tributyrin, PET-dimer and PET-trimer agar plates.

Variant	Halo formation on		
	Tributyrin plates	**PET-dimer plates**	**PET-trimer plates**
*p*NBEBL WT	X	X	X
*p*NBEBL-loopΔ-16AA	X	X	X
*p*NBEBL-loopΔ-14AA	X	X	X
*p*NBEBL-loopΔ-12AA	X	X	X
*p*NBEBL-loopΔ-10AA	X	X	X
*p*NBEBL-loopΔ-8AA	X	X	-
*p*NBEBL-loopΔ-6AA	X	X	-
*p*NBEBL-loopΔ-4AA	X	X	X
*p*NBEBL-loopΔ-2AA	X	-	-
*p*NBEBL-loopΔ-0AA	-	-	-

X showed halo formation; - no halo formation

The *p*NBEBL WT showed activity on all three different substrates. Whereas, the EV was used as a negative control and showed no halo formation. The *p*NBEBL-loopΔ-0AA showed no activity for all three substrates. The variants *p*NBEBL-loopΔ-16AA till *p*NBEBL-loopΔ-2AA showed activity for tributyrin substrate, and besides the variant *p*NBEBL-loopΔ-2AA all variants were active for PET-dimer substrate. The variants with a loop length of 16AA till 10AA showed activity for PET-trimer substrates as well as the variants with loop length of 4AA (*p*NBEBL-loopΔ-4AA).

3.2.3. Activity on PET-dimer MTP screening system

The established PET-dimer MTP screening system was used for a quantitative analysis of the generated loop variants (2.2.3). The assay was performed in parallel on two temperatures (18°C and 42°C). The optimal temperature for *p*NBEBL WT is 42°C, while 18°C was used to monitor the changes in esterase activity by significantly lowering temperature from its optimum (Figure 51).

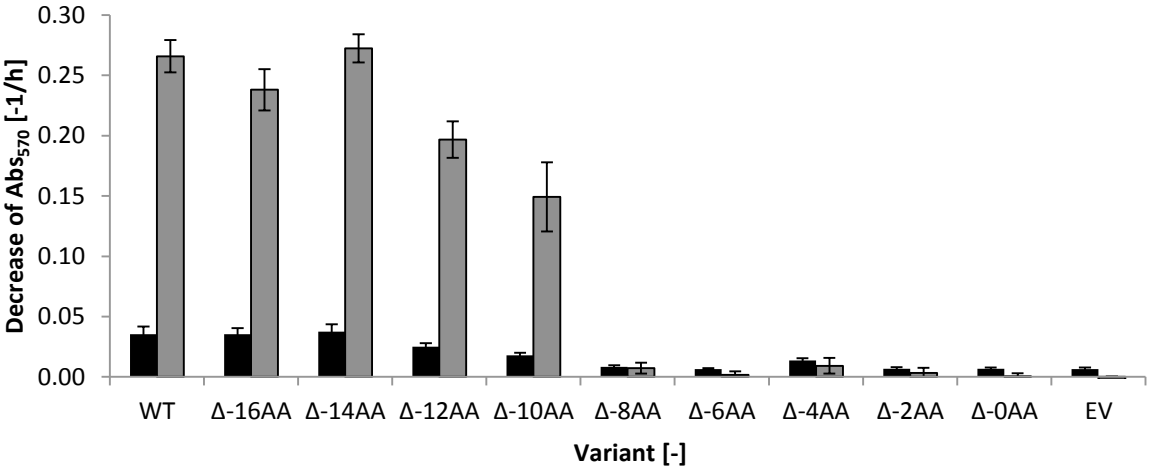

Figure 51 Hydrolysis rates for *p*NBEBL WT and different *p*NBEBL-loopΔ variants using PET-dimer MTP screening system. The assay was performed at 18°C (■) and at 42°C (■), Δ means loopΔ . All *p*NBEBL-loopΔ variants from 16-0 AA were tested as well as *p*NBEBL WT and an EV control. The reported values are the average of three measurements and average deviations from the mean values are shown.

Figure 51 showed comparable *p*NBEBL WT activity levels at 42°C for variants *p*NBEBL-loopΔ-16AA and *p*NBEBL-loopΔ-14AA. The activities of the variants *p*NBEBL-loopΔ-12AA and *p*NBEBL-loopΔ-10AA showed linear decrease in absorbance while variants *p*NBEBL-loopΔ-8AA till *p*NBEBL-loopΔ-0AA can be considered as inactive at 42°C. Activities at 18°C showed comparable profile to activities observed at 42°C for all *p*NBEBL-loopΔ variants. The slight recovery in activity in variant *p*NBEBL-loopΔ-4AA which was observed in PET-dimer plate assay could also be confirmed by the MTP screening system. Summing up, variants until 14AA keep their activity, variants with 12AA and 10AA have an decrease in activity and variants with a loop shorter than 10AA are inactive.

3.2.4. Loop analysis by computational modelling

For further structure-function relationship study, computational modelling analysis was done. The homology model of *p*NBEBL WT was generated by YASARA based on the crystal structure of 1QE3, 1C7I, 1C7J (*p*-nitrobenzyl esterase from *B. subtilis*) and 2OGT (carboxyl esterase from *Geobacillus stearothermophilus*)[75, 106-107]. The structure of the loop from amino acid position 63-80 was not completely solved in the crystal structure. The most detailed description of the loop was given by 1C7I. Figure 52 shows an overlay of the *p*NBEBL WT homology model generated by YASARA and six models generated by the online software Modeller.

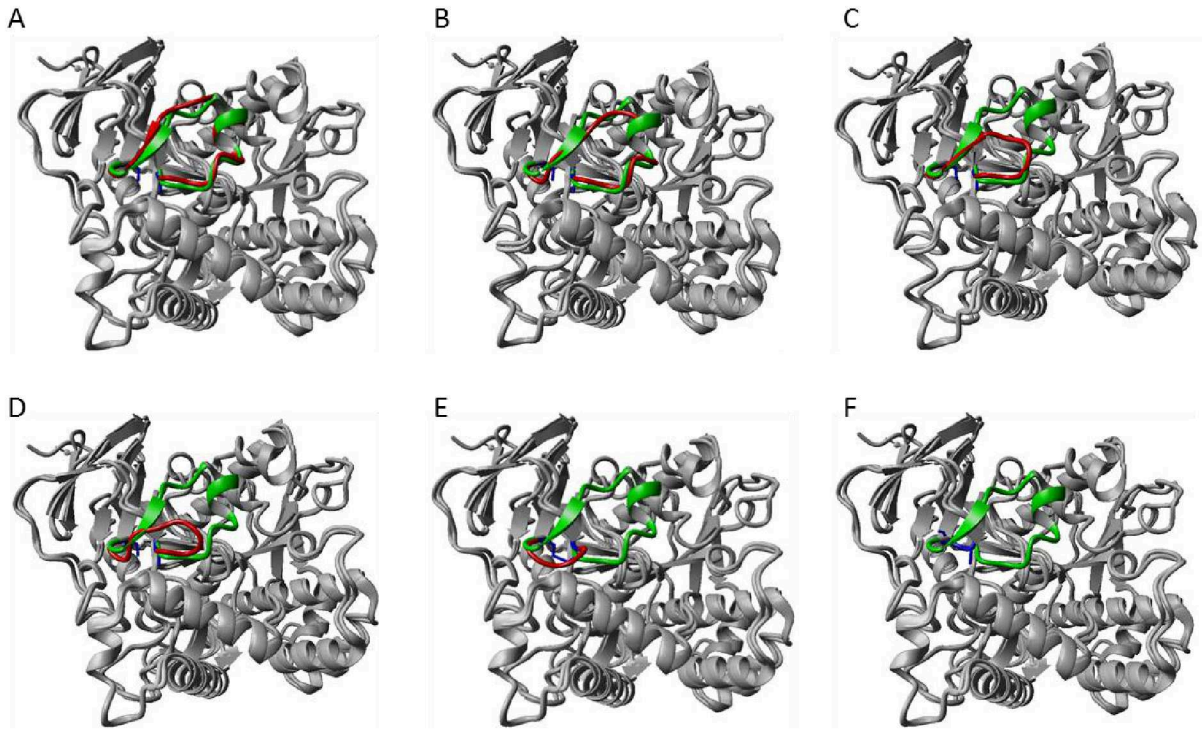

Figure 52 Overlay of homology models of different loop lengths with *p*NBEBL WT. The *p*NBEBL model (green loop) was built with YASARA based on the structure of the *B. subtilis p*-nitrobenzyl esterase (PDB 1CFI)[75]. The models of shortened loops were generated by Modeller (red loop). The cysteine's at position 62 and 81 (shown in blue) are the anchor points of the loop. The *p*NBEBL WT YASARA model was aligned with the models of Modeller, **A**: *p*NBEBL WT, **B**: *p*NBEBL-loopΔ-14AA, **C**: *p*NBEBL-loopΔ-10AA, **D**: *p*NBEBL-loopΔ-8AA, **E**: *p*NBEBL-loopΔ-4AA, **F**: *p*NBEBL-loopΔ-0AA.

Figure 52 shows an overlay of the *p*NBEBL-loopΔ variants containing 14AA (B), 10AA (C), 8AA (D), 4AA (E) and 0AA (F) with *p*NBEBL WT. In Figure 52A the *p*NBEBL WT YASARA model is compared with the *p*NBEBL WT Modeller model in order to show the accuracy of the models generated with Modeller. The loop of the model generated by YASARA is shown in green, in comparison to the loop structure obtained from Modeller (shown in red). A disulfid bond between the both cysteine (amino acid position 62 and 81) could be observed for the short loop model of 4AA and the complete loopΔ (D, F; marked in blue). A difference in loop prediction was only observed for *p*NBEBL-loopΔ-4AA. In the model of *p*NBEBL-loopΔ-4AA the loop was oriented to the opposite way compared to *p*NBEBL WT not covering the entrance to the catalytic site. The loops of the variants with 14AA, 10AA and 8AA are covering the entrance to the binding pocket.

3.2.5. Analysis of secondary structure by circular dichroism

Circular dichroism (CD) was used to determine the changes in secondary structures of proteins. In this method the electric field vector rotates about its propagation direction and generates circularly polarized light. The circularly polarized light is absorbed by chiral chromophores like peptide bonds (>240 nm), disulfid bonds and aromatic side chains (260-230 nm) and based on this the secondary structure can be determined. The excitation at 220 nm caused by a transition of the non-bonding peptide bond orbitals n to the anti-bonding π-orbitals π* and the excitation at 190 nm by the π to π* orbitals is used to

determine the secondary structure of the proteins. The secondary structure of the polypeptide backbone influences the dihedral angles Φ and Ψ and thus corresponds to the energy level of the orbitals. Figure 53 shows the signal obtained by purified protein consist of only α-helix, β-sheet or random coil secondary structures.

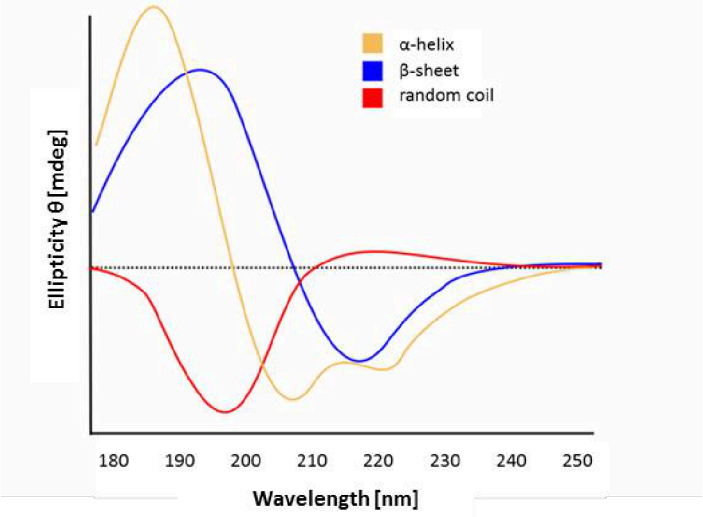

Figure 53 CD spectra of secondary structures. The pure secondary structure of the α-helix (yellow), the β-sheet (blue) and random coil (red) are standard curves and are used as basic principles (modified from http://www.proteinchemist.com/cd/cdspec.html, accessed 24.10.2015).

Upon complete loop deletion, variant *p*NBEBL-loopΔ-0AA showed no activity on agar plates and in the PET-dimer MTP screening system. SDS-PAGE analysis indicates a similar expression level for the *p*NBEBL-loopΔ-0AA compared with *p*NBEBL WT. CD was used to compare folding profile of the *p*NBEBL-loopΔ-0AA variant and the respective changes in the secondary structure. The secondary structure of *p*NBEBL-loopΔ-0AA misses one α–helix (from amino acid position 68 to 73) compared to *p*NBEBL WT due to localization within the deleted loop. *p*NBEBL WT and the *p*NBEBL-loopΔ-0AA variant were expressed, purified, and concentrated in 0.1 M sodium phosphate buffer pH 8.5 to a final concentration of 0.4 mg/ml *p*NBEBL WT and 0.3 mg/ml *p*NBEBL-loopΔ-0AA. The samples were measured by CD and the baseline was subtracted (Figure 54).

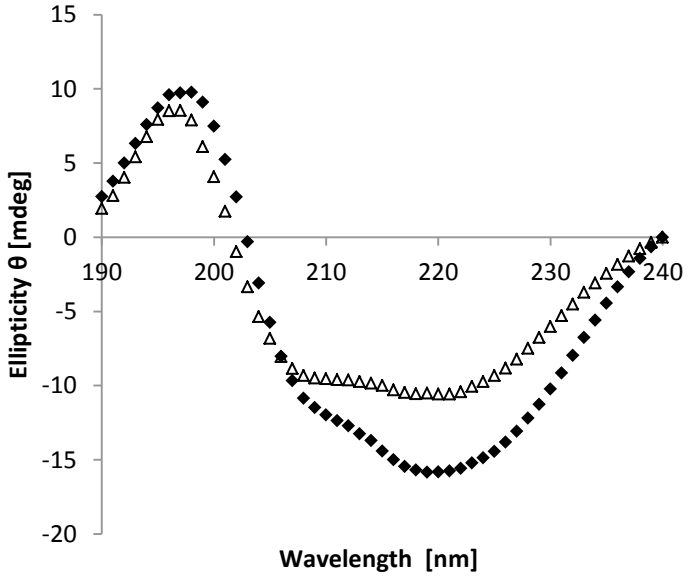

Figure 54 CD spectra of *p*NBEBL WT (♦) and the *p*NBEBL-loopΔ-0AA (Δ). The *p*NBEBL WT (0.4 mg/ml) and *p*NBEBL-loopΔ-0AA (0.3 mg/ml) were prepared in 0.1 M sodium phosphate buffer pH 8.5 and 140 µl were filled in 1 mm cuvettes and measured with CD spectroscopy (JASCO). The baselines were directly subtracted.

The CD spectrum of *p*NBEBL WT differs from the spectrum of the *p*NBEBL-loopΔ-0AA in the intensity of ellipcity θ at 220 nm, where the *p*NBEBL WT showed a more distinct curve (WT: -15.8; loopΔ-0AA: -10.6). The content of the secondary structures were calculated by Dichroweb and summarised in Table 27. The *p*NBEBL-loopΔ-0AA showed nearly no difference in secondary structure compared to the *p*NBEBL WT (α-helix: -1.0 %, β-sheet: +0.4 %, turns: +0.8 %, random coil: -0.1 %). The CD analysis showed for *p*NBEBL-loopΔ-0AA a reduced amount of α-helices which was expected after a structure prediction by homology model.

Table 27 Structure analysis by Dichroweb, CONTIN Set 4. The CD spectra were analysed regarding the amount of each secondary structure which are part of *p*NBEBL WT or *p*NBEBL-loopΔ-0AA.

Enzyme	α-helix [%]	β-sheet [%]	Turns [%]	Random coil [%]
*p*NBEBL WT	26.4	22.4	20.6	30.5
*p*NBEBL-loopΔ-0AA	25.4	22.8	21.4	30.4

No difference in secondary structures between *p*NBEBL WT and *p*NBEBL-loopΔ-0AA corresponds to a correctly folded loop deletion variant. This leads to the conclusion that activity loss originates from the missing loop and not from incorrect folding and is a clear indicator that the loop plays a crucial role in PET-degradation.

4. Discussion

The potential of an esterase to degrade PET polymer was firstly reported by Ribitsch *et al.* in 2011[59]. In order to evolve the *p*NBEBL for PET degradation, it is necessary to use substrates like bis(*p*-methylbenzoic acid)-ethylene glycol ester (PET-dimer) that resemble the aromatic structures of PET. Until now, the PET degradation analysis is done by HPLC. This method is time-consuming and has only a low throughput of samples over analysing time. Therefore, a high throughput screening system is necessary for a successful esterase evolution campaign. Hence, a MTP screening system was established using PET-dimer as model substrate. Due to the insolubility of PET-dimer in water a dispersion was prepared and an agar matrix was included in the screening system to prevent sedimentation of PET-dimer on the bottom of the MTP. The additionally added pH indicator strengthen the detected signal, because beside the decrease in turbidity a color change due to acid release can be measured which simplifies the activity detection.

The established assay offered the possibility to further characterize the esterase regarding their PET degradation activity. Until now it is not known which part of the amino acid sequence plays an important role for the PET degradation. Furthermore, no PET binding domain is known, which could serve as an investigation starting point. By computational analysis of the esterase a loop out of 18 amino acids was conspicuous, due to size and localization above the catalytic triad. The investigation of the loop was started by shortening the amino acid lengths of the loop pairwise in order not to destroy the orientation of the loop which could happen by deleting uneven numbers of amino acids. In total nine different constructs were generated and analysed. The results indicate that the length correlates with the substrate specificity. On tribuytrin agar plates all different loop lengths even the loop with only two amino acids are active. Whereas, on PET-dimer agar plates (halo formation) the loop with two amino acids is inactive and on PET-trimer agar plates the loops shorter than ten amino acids are inactive except the loop with four amino acids, which surprisingly recovered its activity. These results were confirmed by the established PET-dimer MTP screening system. In the PET-dimer MTP screening system the loops shorter than ten amino acids were inactive. This can be attributed to the reaction time. During the PET-dimer MTP screening system the supernatant of cell lysate is incubated (~3 h, 37°C). Whereas, during the agar plate assay the esterase is incubated at least 16 h at 37°C for cell growth, expression and hydrolysis (halo formation). This offers all constructs which are reduced in activity more time to convert the substrate. Thus, a direct comparison of the results between PET-trimer agar plates and PET-dimer MTP screening system is not possible.

The observed differences in substrate conversion – tributyrin versus PET-trimer – leads to the hypothesis that a longer or more complex substrate needs, due to steric hindrance of the bulky substrate, more space to enter the catalytic triad. The generated models of the different loop lengths showed that beside the *p*NBEBL-loopΔ-4AA all loops are covering the entrance to the catalytic site. Therefore, it can be assumed that the differences in activity

are dependent from the loop behaviour *e.g.* flexibility to be able to generate more space. This is why the surface loop is supposed to be a lid or lid like loop which *e.g.* undergoes conformational changes.

Lipases have a lid which moves away from the catalytic triad after an interfacial activation. Structure analysis revealed that the lid consists of a hydrophobic domain, which interacts with hydrophobic substrates like triglycerides[34]. Jennens and Lowe (1994) figured out that changes in the loop come along with increased activity and the variant with the lid deletion still shows activity[165]. Furthermore, they showed an interaction between the lid and another loop which interacts with the oxyanion hole and help stabilizing the oxyanion intermediate. This could negatively influence the substrate binding affinity or substrate turnover. In the case of *p*NBEBL the complete loop deletion was inactive. Contrary to the obtained results - shorter loop is more substrate specific - Carrière *et al.* (1998) showed an increased substrate specificity with a longer domain[166].

The *p*NBEBL-loopΔ-0AA variant was inactive in all assay systems. Therefore, CD measurements were done to proof the folding of the enzyme. The *p*NBEBL-loopΔ-0AA variant and *p*NBEBL WT were correctly folded and inactivity can therefore be attributed to the loop and not to missfolding. This leads to the assumption that for the activity of *p*NBEBL two different points have to be addressed. The first point is the access of the substrate to the catalytic triad. The second point is the flexibility of the loop which most likely fixes the substrate with pressure in the binding pocket. If the loop is missing the substrate is not fixed and subsequent the substrate is not degraded.

As a conclusion, the development of the PET-dimer MTP screening system offers the possibility to screen libraries with PET mimicking substrates. The analysis of the loop from amino acid position 63 to 80 covering the entrance to the catalytic triad resulted in an inactive variant if the complete loop is deleted and therefore the loop plays a pivotal role in PET binding or degradation. The investigation of the loop lead to the assumption that the loop has a lid behavior similar to the one found in lipases.

The research about the *p*NBEBL structure was performed by adaptation of the loop length which is located above the catalytic site. Thereby, a correlation between loop length and PET degradation activity was observed. The obtained knowledge about the importance of the loop is a great progress for the structure function analysis with respect to the substrate binding.

IV. Summary and conclusion

Plastics are widely used for packing *e.g.* food and textiles due to its durability. The production of polyethylene terephthalate (PET)-based plastics is growing since 1960. A global and unsolved challenge is the degradation of micro- and nanometer-sized PET particles derived from *e.g.* washing of textiles. These micro-sized particles are shown to be hazardous to health for maritime organisms.
Hydrolases were identified to have a PET degradation activity with optima ~60°C and not at lower temperatures applied during laundry (especially outside of Europe). Esterases are a class of hydrolases working at lower temperatures at cost of specific activity towards PET. For an economical reasonable application of the esterase for PET degradation a significant higher activity at lower temperatures is required.
A successful protein engineering campaign requires a screening system mimicking PET structures by artificial substrates or, even better, include PET as substrate to be as close as possible to the application conditions. Main prerequisite of a screening system is a sufficient throughput with a standard deviation ~10 % to identify improved variants. However, to best of my knowledge no suitable screening systems for screening of PET degradation has been reported.

In this work two novel screening systems were developed; the novel **continuous cBLE-4AAP screening system** which mimics the PET degradation by applying phenol benzoate as substrate and the ultra-high throughput screening system Fur-Shell. In the continuous MTP screening system cBLE-4AAP the hydrolysis of aromatic ester compounds which produce phenols is monitored. The cBLE-4AAP screening system was established in 96-well format (~2000 clones) and validated by identifying a **4.7-fold improved esterase** variant within one round of directed evolution. Furthermore, enzyme properties such as pH optimum and organic solvent resistance could very likely be improved by applying this novel screening system. Advancements for screening large libraries was achieved by developing ultra-high throughput screening systems (>$1*10^6$ variants) to overcome the limitations of medium MTP screening systems. The ultra-high throughput screening system Fur-Shell is flow cytometer-based and employs the glucose oxidase-based hydrogel formation by using β-D-(+)-glucose pentaacetate as substrate. As first example a **flow cytometer whole cell-based screening system** was applied to an esterase and validated in one round of directed evolution and led to a **7.1-fold improved esterase** variant.
Furthermore, regions involved in the substrate binding were discovered by computational analysis. The targeted loop (AA 63-80) at the entrance to the substrate binding pocket consists of 18 amino acids. A detailed investigation of the influence of loop size on PET degradation (PET-dimer and PET-trimer) by stepwise shortening showed that a minimal size of ten amino acids is required to bind the substrate sufficiently long for activity detection.

A **loop region controlling the activity** of *p*NBEBL was identified and additionally screening systems allows for the first time an efficient evolution for PET degradation.

V. References

1. Jaenicke, R., *Enzymes under Extremes of Physical Conditions.* Ann. Rev. Biophys. Bioeng., **1981,** *10*, 1-67.

2. Cowan, D.; Oxenboll, K. M.; Holm, H. C., *Enzymatic bioprocessing of oils and fats.* Oil Mill Gazetter, **2008,** *113*, 10-13.

3. Lim, B. N.; Choong, Y. S.; Ismail, A.; Glokler, J.; Konthur, Z.; Lim, T. S., *Directed evolution of nucleotide-based libraries using lambda exonuclease.* BioTechniques, **2012,** *53* (6), 357-64.

4. Chen, R., *Enzyme engineering: rational redesign versus directed evolution.* Trends. Biotechnol., **2001,** *19* (1), 13-4.

5. Roccatano, D.; Wong, T. S.; Schwaneberg, U.; Zacharias, M., *Toward understanding the inactivation mechanism of monooxygenase P450 BM-3 by organic cosolvents: a molecular dynamics simulation study.* Biopolymers, **2006,** *83* (5), 467-76.

6. Ding, H.; Gao, F.; Liu, D.; Li, Z.; Xu, X.; Wu, M.; Zhao, Y., *Significant improvement of thermal stability of glucose 1-dehydrogenase by introducing disulfide bonds at the tetramer interface.* Enzyme Microb. Technol., **2013,** *53* (6-7), 365-72.

7. Bornscheuer, U. T.; Pohl, M., *Improved biocatalysts by directed evolution and rational protein design.* Curr. Opin. Chem. Biol., **2001,** *5* (2), 137-43.

8. Stemmer, W. P., *DNA shuffling by random fragmentation and reassembly: in vitro recombination for molecular evolution.* Proc. Natl. Acad. Sci. U. S. A., **1994,** *91* (22), 10747-51.

9. Kuchner, O.; Arnold, F. H., *Directed evolution of enzyme catalysts.* Trends. Biotechnol., **1997,** *15* (12), 523-30.

10. Jackel, C.; Kast, P.; Hilvert, D., *Protein design by directed evolution.* Annu. Rev. Biophys., **2008,** *37*, 153-73.

11. Güven, G.; Prodanovic, R.; Schwaneberg, U., *Protein engineering - an option for enzymatic biofuel cell design.* Electroanal, **2010,** *22* (7-8), 765-+.

12. Schmidt-Dannert, C.; Arnold, F. H., *Directed evolution of industrial enzymes.* Trends. Biotechno.l, **1999,** *17* (4), 135-6.

13. Eckert, K. A.; Kunkel, T. A., *High fidelity DNA synthesis by the Thermus aquaticus DNA polymerase.* Nucleic. Acids. Res., **1990,** *18* (13), 3739-44.

14. Tindall, K. R.; Kunkel, T. A., *Fidelity of DNA synthesis by the Thermus aquaticus DNA polymerase.* Biochemistry, **1988,** *27* (16), 6008-13.

15. Eckert, K. A.; Kunkel, T. A., *DNA polymerase fidelity and the polymerase chain reaction.* Genome Res., **1991,** *1* (1), 17-24.

16. Lin-Goerke, J. L.; Robbins, D. J.; Burczak, J. D., *PCR-based random mutagenesis using manganese and reduced dNTP concentration.* BioTechniques, **1997,** *23* (3), 409-12.

17. Cadwell, R. C.; Joyce, G. F., *Randomization of genes by PCR mutagenesis.* Genome Res., **1992,** *2* (1), 28-33.

18. Cadwell, R. C.; Joyce, G. F., *Mutagenic PCR.* PCR Methods. Appl., **1994,** *3* (6), S136-40.

19. Zaccolo, M.; Williams, D. M.; Brown, D. M.; Gherardi, E., *An approach to random mutagenesis of DNA using mixtures of triphosphate derivatives of nucleoside analogues.* J. Mol. Biol., **1996,** *255* (4), 589-603.

20. Kuipers, O. P., *Random mutagenesis by using mixtures of dNTP and dITP in PCR.* Methods Mol. Biol., **1996,** *57*, 351-6.

21. Cline, J.; Hogrefe, H. H., *Randomize gene sequences with new PCR mutagenesis kit.* Strategies, **2000,** *13*, 157-161.

22. Wong, T. S.; Tee, K. L.; Hauer, B.; Schwaneberg, U., *Sequence saturation mutagenesis (SeSaM): a novel method for directed evolution.* Nucleic Acids. Res., **2004,** *32* (3), e26.

23. Wong, T. S.; Zhurina, D.; Schwaneberg, U., *The diversity challenge in directed protein evolution.* Comb. Chem. High Throughput Screen., **2006,** *9* (4), 271-288.

24. Carter, P., *Site-directed mutagenesis.* Biochem. J., **1986,** *237* (1), 1-7.

25. Dennig, A.; Shivange, A. V.; Marienhagen, J.; Schwaneberg, U., *OmniChange: the sequence independent method for simultaneous site-saturation of five codons.* PloS one, **2011,** *6* (10), e26222.

26. Leemhuis, H.; Kelly, R. M.; Dijkhuizen, L., *Directed evolution of enzymes: Library screening strategies.* IUBMB life, **2009,** *61* (3), 222-8.

27. Ten, L. N.; Im, W. T.; Kim, M. K.; Kang, M. S.; Lee, S. T., *Development of a plate technique for screening of polysaccharide-degrading microorganisms by using a mixture of insoluble chromogenic substrates.* J. Microbiol. Methods, **2004,** *56* (3), 375-82.

28. Griffiths, A. D.; Tawfik, D. S., *Miniaturising the laboratory in emulsion droplets.* Trends Biotechnol., **2006,** *24* (9), 395-402.

29. Lee, S. Y.; Choi, J. H.; Xu, Z., *Microbial cell-surface display.* Trends Biotechnol., **2003,** *21* (1), 45-52.

30. Tu, R.; Martinez, R.; Prodanovic, R.; Klein, M.; Schwaneberg, U., *A flow cytometry-based screening system for directed evolution of proteases.* J. Biomol. Screen., **2011,** *16* (3), 285-94.

31. Zinchenko, A.; Devenish, S. R.; Kintses, B.; Colin, P. Y.; Fischlechner, M.; Hollfelder, F., *One in a million: flow cytometric sorting of single cell-lysate assays in monodisperse picolitre double emulsion droplets for directed evolution.* Anal. Chem., **2014,** *86* (5), 2526-33.

32. Courtois, F.; Olguin, L. F.; Whyte, G.; Theberge, A. B.; Huck, W. T.; Hollfelder, F.; Abell, C., *Controlling the retention of small molecules in emulsion microdroplets for use in cell-based assays.* Anal. Chem., **2009,** *81* (8), 3008-16.

33. Karpushova, A.; Brummer, F.; Barth, S.; Lange, S.; Schmid, R. D., *Cloning, recombinant expression and biochemical characterisation of novel esterases from Bacillus sp. associated with the marine sponge Aplysina aerophoba.* Appl. Microbiol. Biotechnol., **2005,** *67* (1), 59-69.

34. Bornscheuer, U. T., *Microbial carboxyl esterases: classification, properties and application in biocatalysis.* FEMS Microbiol. Rev., **2002,** *26* (1), 73-81.

35. Jaeger, K. E.; Reetz, M. T., *Microbial lipases form versatile tools for biotechnology.* Trends Biotechnol., **1998,** *16* (9), 396-403.

36. Ollis, D. L.; Cheah, E.; Cygler, M.; Dijkstra, B.; Frolow, F.; Franken, S. M.; Harel, M.; Remington, S. J.; Silman, I.; Schrag, J.; et al., *The alpha/beta hydrolase fold.* Protein Eng., **1992,** *5* (3), 197-211.

37. Nardini, M.; Dijkstra, B. W., *Alpha/beta hydrolase fold enzymes: the family keeps growing.* Curr. Opin. Struct. Biol., **1999,** *9* (6), 732-7.

38. Jaeger, K. E.; Dijkstra, B. W.; Reetz, M. T., *Bacterial biocatalysts: molecular biology, three-dimensional structures, and biotechnological applications of lipases.* Annu. Rev. Microbiol., **1999,** *53*, 315-51.

39. Ribeiro, B. D.; de Castro, A. M.; Coelho, M. A.; Freire, D. M., *Production and use of lipases in bioenergy: a review from the feedstocks to biodiesel production.* Enzyme Res., **2011,** *2011*, 615803.

40. Walker, B.; Lynas, J. F., *Strategies for the inhibition of serine proteases.* Cell. Mol. Life Sci., **2001,** *58*, 596-624.

41. Polgar, L., *The catalytic triad of serine peptidases.* Cell. Mol. Life Sci., **2005,** *62* (19-20), 2161-72.

42. de Carvalho, V. M.; Marques, R. M.; Lapenta, A. S.; Machado, M. D. P. S., *Functional classification of esterases from leaves of Aspidosperma polyneuron M. Arg. (Apocynaceae).* Genet. Mol. Biol., **2003,** *26* (2), 195-198.

43. Moore, J. C.; Arnold, F. H., *Directed evolution of a para-nitrobenzyl esterase for aqueous-organic solvents.* Nat. Biotechnol., **1996,** *14* (4), 458-67.

44. Giver, L.; Gershenson, A.; Freskgard, P. O.; Arnold, F. H., *Directed evolution of a thermostable esterase.* Proc. Natl. Acad. Sc.i U. S. A., **1998,** *95* (22), 12809-13.

45. Sayali, K.; Sadichha, P.; Surekha, S., *Microbial esterases: an overview.* Int. J. Curr. Microbiol. App. Sci., **2013,** *2*, 135-146.

46. Kim, G.-J.; Choi, G.-S.; Kim, J.-Y.; Lee, J.-B.; Jo, D.-H.; Ryu, Y.-W., *Screening, production and properties of a stereospecific esterase from Pseudomonas sp. S34 with high selectivity to (S)-ketoprofen ethyl ester.* J. M. Catal. B: Enzym., **2002,** *17* (1), 29-38.

47. Calero-Rueda, O.; Plou, F. J.; Ballesteros, A.; Martinez, A. T.; Martinez, M. J., *Production, isolation and characterization of a sterol esterase from Ophiostoma piceae.* Biochim. Biophys. Acta., **2002,** *1599* (1-2), 28-35.

48. Lee, Y. S., *Role of NADPH oxidase-mediated generation of reactive oxygen species in the mechanism of apoptosis induced by phenolic acids in HepG2 human hepatoma cells.* Arch. Pharmacal Res., **2005,** *28* (10), 1183-9.

49. Fazary, A. E.; Ju, Y. H., *The large-scale use of feruloyl esterases in industry.* Biotechnol. Mol. Biol. Rev., **2008,** *3*, 95-110.

50. Maurer, K. H., *Detergent proteases.* Curr. Opin. Biotechnol., **2004,** *15* (4), 330-4.

51. PlaticsEurope, *Plastics - The Facts 2012.*

52. Köpnick, H.; Schmidt, M.; Brügging, W.; Rüter, J.; Kaminsky, W., Polyesters. In *Ullmann's Encyclopedia of Industrial Chemistry*, Weinheim, Wiley-VCH: **2005**; 233-238.

53. Müller, R. J.; Kleeberg, I.; Deckwer, W. D., *Biodegradation of polyesters containing aromatic constituents.* J. Biotechnol., **2001,** *86* (2), 87-95.

54. Zimmermann, W.; Billig, S., *Enzymes for the biofunctionalization of poly(ethylene terephthalate).* Adv. Biochem. Eng. Biotechnol., **2011,** *125*, 97-120.

55. Pütz, A., *Isolierung, Identifizierung und biochemische Charakterisierung Dialkylphthalat spaltender Esterasen.* Inaugural-Dissertation, Heinrich-Heine-Universität Düsseldorf, **2006**.

56. Hsieh, Y. L.; Cram, L. A., *Enzymatic hydrolysis to improve wetting and absorbency of polyester fabrics.* Text. Res. J., **1998,** *68* (5), 311-319.

57. Leisewitz, A., *Stoffströme wichtiger hormonell wirkender Substanzen.* UBA-Projekt, Nr. 10601076. Im Auftrag des Umweltbundesamtes, **1997**.

58. Gregory, M. R., *Virgin Plastic Granules on Some Beaches of Eastern Canada and Bremuda.* Mar. Environ. Res., **1983,** *10* (2), 73-92.

59. Ribitsch, D.; Heumann, S.; Trotscha, E.; Herrero Acero, E.; Greimel, K.; Leber, R.; Birner-Gruenberger, R.; Deller, S.; Eiteljoerg, I.; Remler, P.; Weber, T.; Siegert, P.; Maurer, K. H.; Donelli, I.; Freddi, G.; Schwab, H.; Guebitz, G. M., *Hydrolysis of polyethyleneterephthalate by p-nitrobenzylesterase from Bacillus subtilis.* Biotechnol. Prog., **2011,** *27* (4), 951-60.

60. Paszun, D.; Spychaj, T., *Chemical recycling of poly(ethylene terephthalate).* Ind. Eng. Chem. Res., **1997,** *36* (4), 1373-1383.

61. Amass, W.; Amass, A.; Tighe, B., *A review of biodegradable polymers: Uses, current developments in the synthesis and characterization of biodegradable polyesters, blends of biodegradable polymers and recent advances in biodegradation studies.* Polym. Int., **1998,** *47* (2), 89-144.

62. Tokiwa, Y.; Suzuki, T., *Hydrolysis of polyesters by lipases.* Nature, **1977,** *270* (5632), 76-8.

63. Gübitz, G. M.; Cavaco-Paulo, A., *Enzymes go big: surface hydrolysis and functionalization of synthetic polymers.* Trends in biotechnology, **2008,** *26* (1), 32-8.

64. Müller, R.-J.; Schrader, H.; Profe, J.; Dresler, K.; Deckwer, W.-D., *Enzymatic degradation of poly(ethylene terephthalate): rapid hydrolyse using a hydrolase from T. fusca.* Macromol. Rapid Commun., **2005,** *26* (17), 1400-1405.

65. Lehmann, C.; Bocola, M.; Streit, W. R.; Martinez, R.; Schwaneberg, U., *Ionic liquid and deep eutectic solvent-activated CelA2 variants generated by directed evolution.* Appl. Microbiol. Biotechnol., **2014,** *98* (12), 5775-85.

66. Shivange, A. V.; Dennig, A.; Schwaneberg, U., *Multi-site saturation by OmniChange yields a pH- and thermally improved phytase.* J. Biotechnol., **2014,** *170*, 68-72.

67. Grognux, J.; Wahler, D.; Nyfeler, E.; Reymond, J. L., *Universal chromogenic substrates for lipases and esterases.* Tetrahedron: Asymmetry, **2004,** *15* (18), 2981-2989.

68. Leroy, E.; Bensel, N.; Reymond, J. L., *A low background high-throughput screening (HTS) fluorescence assay for lipases and esterases using acyloxymethylethers of umbelliferone.* Bioorg. Med. Chem. Lett., **2003,** *13* (13), 2105-8.

69. Schultheiss, E.; Paar, C.; Schwab, H.; Jose, J., *Functional esterase surface display by the autotransporter pathway in Escherichia coli.* J. Mol. Catal. B: Enzym., **2002,** *18* (1-3), 89-97.

70. Hartley, B. S.; Kilby, B. A., *The reaction of p-nitrophenyl esters with chymotrypsin and insulin.* Biochem. J., **1954,** *56* (2), 288-97.

71. Menger, F. M.; Ladika, M., *Origin of rate accelerations in an enzyme model - the para-nitrophenyl ester syndrome.* J. Am. Chem. Soc., **1987,** *109* (10), 3145-3146.

72. Park, J. H.; Meriwether, B. P.; Clodfelder, P.; Cunningham, L. W., *The hydrolysis of p-nitrophenyl acetate catalyzed by 3-phosphoglyceraldehyde dehydrogenase.* J. Biol. Chem., **1961,** *236*, 136-41.

73. Schwaneberg, U.; Schmidt-Dannert, C.; Schmitt, J.; Schmid, R. D., *A continuous spectrophotometric assay for P450 BM-3, a fatty acid hydroxylating enzyme, and its mutant F87A.* Anal. Biochem., **1999,** *269* (2), 359-66.

74. Arnold, F. H.; Moore, J. C., *Optimizing industrial enzymes by directed evolution.* Adv. Biochem. Eng. Biotechnol., **1997,** *58*, 1-14.

75. Spiller, B.; Gershenson, A.; Arnold, F. H.; Stevens, R. C., *A structural view of evolutionary divergence.* Proc. Natl. Acad. Sci. U. S. A., **1999,** *96* (22), 12305-10.

76. Lülsdorf, N.; Vojcic, L.; Hellmuth, H.; Weber, T. T.; Mussmann, N.; Martinez, R.; Schwaneberg, U., *A first continuous 4-aminoantipyrine (4-AAP)-based screening system for directed esterase evolution.* Appl. Microbiol. Biotechnol., **2015,** *99* (12), 5237-46.

77. Griswold, K. E., Directed Enzyme Evolution - Screening and Selection Methods. In *Methods Mol. Biol.*, Arnold, F. H.; Georgiou, G., Eds. Humana Press: **2003**; Vol. 230, 203-211.

78. Rhee, J. K.; Ahn, D. G.; Kim, Y. G.; Oh, J. W., *New thermophilic and thermostable esterase with sequence similarity to the hormone-sensitive lipase family, cloned from a metagenomic library.* Appl Environ Microb, **2005,** *71* (2), 817-25.

79. Plou, F.; Ferrer, M.; Nuero, O.; Calvo, M.; Alcalde, M.; Reyes, F.; Ballesteros, A., *Analysis of Tween 80 as an esterase/ lipase substrate for lipolytic activity assay.* Biotechnol. Tech., **1998,** *12* (3), 183-186.

80. Rao, L.; Zhao, X.; Pan, F.; Li, Y.; Xue, Y.; Ma, Y.; Lu, J. R., *Solution behavior and activity of a halophilic esterase under high salt concentration.* PloS one, **2009,** *4* (9), e6980.

81. Chen, Y. R.; Usui, S.; Queener, S. W.; Yu, C. A., *Purification and properties of ap-nitrobenzyl esterase from Bacillus subtilis.* J Ind Microbiol, **1995,** *15* (1), 10-18.

82. Shi, Y.; Pan, Y.; Li, B.; He, W.; She, Q.; Chen, L., *Molecular cloning of a novel bioH gene from an environmental metagenome encoding a carboxylesterase with exceptional tolerance to organic solvents.* BMC Biotechnol., **2013,** *13*, 13.

83. Schmidt, M.; Henke, E.; Heinze, B.; Kourist, R.; Hidalgo, A.; Bornscheuer, U. T., *A versatile esterase from Bacillus subtilis: cloning, expression, characterization, and its application in biocatalysis.* Biotechnol. J., **2007,** *2* (2), 249-53.

84. Meghji, K.; Ward, O. P.; Araujo, A., *Production, purification, and properties of extracellular carboxyl esterases from Bacillus subtilis NRRL 365.* Appl Environ Microb, **1990,** *56* (12), 3735-40.

85. Jackson, C. J.; Liu, J. W.; Carr, P. D.; Younus, F.; Coppin, C.; Meirelles, T.; Lethier, M.; Pandey, G.; Ollis, D. L.; Russell, R. J.; Weik, M.; Oakeshott, J. G., *Structure and function of an insect alpha-carboxylesterase (alpha esterase 7) associated with insecticide resistance.* Proc. Natl. Acad. Sci. U. S. A., **2013,** *110* (25), 10177-82.

86. Rao, L.; Xue, Y.; Zheng, Y.; Lu, J. R.; Ma, Y., *A novel alkaliphilic bacillus esterase belongs to the 13(th) bacterial lipolytic enzyme family.* PloS one, **2013,** *8* (4), e60645.

87. Xin, L.; Hui-Ying, Y., *Purification and characterization of an extracellular esterase with organic solvent tolerance from a halotolerant isolate, Salimicrobium sp. LY19.* BMC Biotechnol., **2013,** *13*, 108.

88. Oeser, T.; Wei, R.; Baumgarten, T.; Billig, S.; Follner, C.; Zimmermann, W., *High level expression of a hydrophobic poly(ethylene terephthalate)-hydrolyzing carboxylesterase from Thermobifida fusca KW3 in Escherichia coli BL21(DE3).* J. Biotechnol., **2010,** *146* (3), 100-4.

89. Eggert, T.; Pencreac'h, G.; Douchet, I.; Verger, R.; Jaeger, K. E., *A novel extracellular esterase from Bacillus subtilis and its conversion to a monoacylglycerol hydrolase.* Eur. J. Biochem., **2000,** *267* (21), 6459-69.

90. Breeuwer, P.; Drocourt, J. L.; Bunschoten, N.; Zwietering, M. H.; Rombouts, F. M.; Abee, T., *Characterization of uptake and hydrolysis of fluorescein diacetate and carboxyfluorescein diacetate by intracellular esterases in Saccharomyces cerevisiae, which result in accumulation of fluorescent product.* Appl Environ Microb, **1995,** *61* (4), 1614-9.

91. Shao, W.; Wiegel, J., *Purification and characterization of two thermostable acetyl xylan esterases from Thermoanaerobacterium sp. strain JW/SL-YS485.* Appl Environ Microb, **1995,** *61* (2), 729-33.

92. Ikeda, M.; Clark, D. S., *Molecular cloning of extremely thermostable esterase gene from hyperthermophilic archaeon Pyrococcus furiosus in Escherichia coli.* Biotechnol. Bioeng., **1998,** *57* (5), 624-9.

93. Veith, B.; Herzberg, C.; Steckel, S.; Feesche, J.; Maurer, K. H.; Ehrenreich, P.; Baumer, S.; Henne, A.; Liesegang, H.; Merkl, R.; Ehrenreich, A.; Gottschalk, G., *The complete genome sequence of Bacillus licheniformis DSM13, an organism with great industrial potential.* J. Mol. Microbiol. Biotechnol., **2004,** *7* (4), 204-11.

94. Bolivar, F.; Rodriguez, R. L.; Greene, P. J.; Betlach, M. C.; Heyneker, H. L.; Boyer, H. W.; Crosa, J. H.; Falkow, S., *Construction and characterization of new cloning vehicles. II. A multipurpose cloning system.* Gene, **1977,** *2* (2), 95-113.

95. Inoue, H.; Nojima, H.; Okayama, H., *High efficiency transformation of Escherichia coli with plasmids.* Gene, **1990,** *96* (1), 23-8.

96. Bergmans, H. E.; van Die, I. M.; Hoekstra, W. P., *Transformation in Escherichia coli: stages in the process.* J. Bacteriol., **1981,** *146* (2), 564-70.

97. Sambrook, J.; Russell, D. W., *Molecular cloning: a laboratory journal: CSHL.* Press, **2001**.

98. Lacks, S.; Greenberg, B., *A deoxyribonuclease of Diplococcus pneumoniae specific for methylated DNA.* J. Biol. Chem., **1975,** *250* (11), 4060-66.

99. Blanusa, M.; Schenk, A.; Sadeghi, H.; Marienhagen, J.; Schwaneberg, U., *Phosphorothioate-based ligase-independent gene cloning (PLICing): An enzyme-free and sequence-independent cloning method.* Anal. Biochem., **2010,** *406* (2), 141-6.

100. Hanahan, D.; Jessee, J.; Bloom, F. R., *Plasmid transformation of Escherichia coli and other bacteria.* Method Enzymol, **1991,** *204*, 63-113.

101. Wang, W.; Malcolm, B. A., *Two-stage PCR protocol allowing introduction of multiple mutations, deletions and insertions using QuikChange Site-Directed Mutagenesis.* BioTechniques, **1999,** *26* (4), 680-2.

102. Smith, P. K.; Krohn, R. I.; Hermanson, G. T.; Mallia, A. K.; Gartner, F. H.; Provenzano, M. D.; Fujimoto, E. K.; Goeke, N. M.; Olson, B. J.; Klenk, D. C., *Measurement of protein using bicinchoninic acid.* Anal. Biochem., **1985,** *150* (1), 76-85.

103. Laemmli, U. K., *Cleavage of structural proteins during the assembly of the head of bacteriophage T4.* Nature, **1970,** *227* (5259), 680-5.

104. Emerson, E., *The condensation of aminoantipyrine: II A new color test for phenolic compounds.* J. Org. Chem., **1943,** *8*, 417-28.

105. Wong, T. S.; Wu, N.; Roccatano, D.; Zacharias, M.; Schwaneberg, U., *Sensitive assay for laboratory evolution of hydroxylases toward aromatic and heterocyclic compounds.* J. Biomol. Screen., **2005,** *10* (3), 246-52.

106. Krieger, E.; Koraimann, G.; Vriend, G., *Increasing the precision of comparative models with YASARA NOVA--a self-parameterizing force field.* Proteins, **2002,** *47* (3), 393-402.

107. Liu, P.; Ewis, H. E.; Tai, P. C.; Lu, C. D.; Weber, I. T., *Crystal structure of the Geobacillus stearothermophilus carboxylesterase Est55 and its activation of prodrug CPT-11.* J. Mol. Biol., **2007,** *367* (1), 212-23.

108. Schymkowitz, J.; Borg, J.; Stricher, F.; Nys, R.; Rousseau, F.; Serrano, L., *The FoldX web server: an online force field.* Nucleic. Acids Res., **2005,** *33* (Web Server issue), W382-8.

109. Van Durme, J.; Delgado, J.; Stricher, F.; Serrano, L.; Schymkowitz, J.; Rousseau, F., *A graphical interface for the FoldX forcefield.* Bioinformatics, **2011,** *27* (12), 1711-2.

110. Choi, J. H.; Lee, S. Y., *Secretory and extracellular production of recombinant proteins using Escherichia coli.* Appl. Microbiol. Biotechnol., **2004,** *64* (5), 625-35.

111. Lei, S. P.; Lin, H. C.; Wang, S. S.; Callaway, J.; Wilcox, G., *Characterization of the Erwinia carotovora pelB gene and its product pectate lyase.* J. Bacteriol., **1987,** *169* (9), 4379-83.

112. Studier, F. W.; Moffatt, B. A., *Use of bacteriophage T7 RNA polymerase to direct selective high-level expression of cloned genes.* J. Mol. Biol., **1986,** *189* (1), 113-30.

113. Otey, C. R.; Joern, J. M., *High-throughput screen for aromatic hydroxylation.* Methods. Mol. Biol., **2003,** *230*, 141-8.

114. Schwaneberg, U.; Otey, C.; Cirino, P. C.; Farinas, E.; Arnold, F. H., *Cost-effective whole-cell assay for laboratory evolution of hydroxylases in Escherichia coli.* J. Biomol. Screen., **2001,** *6* (2), 111-117.

115. Zhu, L. L.; Tee, K. L.; Roccatano, D.; Sonmez, B.; Ni, Y.; Sun, Z. H.; Schwaneberg, U., *Directed evolution of an antitumor drug (arginine deiminase PpADI) for increased activity at physiological pH.* Chembiochem : a European journal of chemical biology, **2010,** *11* (5), 691-697.

116. Matthews, B. W.; Nicholson, H.; Becktel, W. J., *Enhanced protein thermostability from site-directed mutations that decrease the entropy of unfolding.* Proc. Natl. Acad. Sci. U. S. A., **1987,** *84* (19), 6663-7.

117. MacArthur, M. W.; Thornton, J. M., *Influence of proline residues on protein conformation.* J. Mol. Biol., **1991,** *218* (2), 397-412.

118. Pitzler, C.; Wirtz, G.; Vojcic, L.; Hiltl, S.; Boker, A.; Martinez, R.; Schwaneberg, U., *A fluorescent hydrogel-based flow cytometry high-throughput screening platform for hydrolytic enzymes.* Chem. Biol., **2014,** *21* (12), 1733-42.

119. Tee, K. L.; Schwaneberg, U., *A screening system for the directed evolution of epoxygenases: importance of position 184 in P450 BM3 for stereoselective styrene epoxidation.* Angew. Chem. Int. Ed. Engl., **2006,** *45* (32), 5380-3.

120. Agresti, J. J.; Antipov, E.; Abate, A. R.; Ahn, K.; Rowat, A. C.; Baret, J. C.; Marquez, M.; Klibanov, A. M.; Griffiths, A. D.; Weitz, D. A., *Ultrahigh-throughput screening in drop-based microfluidics for directed evolution.* Proc. Natl. Acad. Sci. U. S. A., **2010,** *107* (9), 4004-9.

121. Taly, V.; Kelly, B. T.; Griffiths, A. D., *Droplets as microreactors for high-throughput biology.* Chembiochem : a European journal of chemical biology, **2007,** *8* (3), 263-72.

122. Lülsdorf, N.; Pitzler, C.; Biggel, M.; Martinez, R.; Vojcic, L.; Schwaneberg, U., *A flow cytometer-based whole cell screening toolbox for directed hydrolase evolution through fluorescent hydrogels.* Chem. Commun. (Camb), **2015,** *51*, 8679-8682.

123. Theberge, A. B.; Courtois, F.; Schaerli, Y.; Fischlechner, M.; Abell, C.; Hollfelder, F.; Huck, W. T., *Microdroplets in microfluidics: an evolving platform for discoveries in chemistry and biology*. Angew. Chem. Int. Ed. Engl., **2010,** *49* (34), 5846-68.

124. Pays, K.; Giermanska-Kahn, J.; Pouligny, B.; Bibette, J.; Leal-Calderon, F., *Double emulsions: how does release occur?* J. Control. Release, **2002,** *79* (1-3), 193-205.

125. van der Graaf, S.; Schroen, C. G. P. H.; Boom, R. M., *Preparation of double emulsions by membrane emulsification - a review*. J. Membr. Sci., **2005,** *251* (1-2), 7-15.

126. Ruff, A. J.; Dennig, A.; Wirtz, G.; Blanusa, M.; Schwaneberg, U., *Flow Cytometer-Based High-Throughput Screening System for Accelerated Directed Evolution of P450 Monooxygenases.* ACS Catal., **2012,** *2* (12), 2724-2728.

127. Kalidasan, K.; Su, Y.; Wu, X.; Yao, S. Q.; Uttamchandani, M., *Fluorescence-activated cell sorting and directed evolution of alpha-N-acetylgalactosaminidases using a quenched activity-based probe (qABP).* Chem. Commun. (Camb), **2013,** *49* (65), 7237-9.

128. Berron, B. J.; Johnson, L. M.; Ba, X.; McCall, J. D.; Alvey, N. J.; Anseth, K. S.; Bowman, C. N., *Glucose oxidase-mediated polymerization as a platform for dual-mode signal amplification and biodetection.* Biotechnol. Bioeng., **2011,** *108* (7), 1521-8.

129. Li, R. H., *Materials for immunoisolated cell transplantation.* Adv. Drug. Deliv. Rev., **1998,** *33* (1-2), 87-109.

130. Uludag, H.; De Vos, P.; Tresco, P. A., *Technology of mammalian cell encapsulation.* Adv. Drug. Deliv. Rev., **2000,** *42* (1-2), 29-64.

131. Elisseeff, J.; McIntosh, W.; Anseth, K.; Riley, S.; Ragan, P.; Langer, R., *Photoencapsulation of chondrocytes in poly(ethylene oxide)-based semi-interpenetrating networks.* J. Biomed. Mater. Res., **2000,** *51* (2), 164-71.

132. Johnson, L. M.; Fairbanks, B. D.; Anseth, K. S.; Bowman, C. N., *Enzyme-mediated redox initiation for hydrogel generation and cellular encapsulation.* Biomacromolecules, **2009,** *10* (11), 3114-21.

133. Arnold, K.; Bordoli, L.; Kopp, J.; Schwede, T., *The SWISS-MODEL workspace: a web-based environment for protein structure homology modelling.* Bioinformatics, **2006,** *22* (2), 195-201.

134. Shivange, A. V.; Serwe, A.; Dennig, A.; Roccatano, D.; Haefner, S.; Schwaneberg, U., *Directed evolution of a highly active Yersinia mollaretii phytase.* Appl. Microbiol. Biotechnol., **2012,** *95* (2), 405-18.

135. Martinez, R.; Jakob, F.; Tu, R.; Siegert, P.; Maurer, K. H.; Schwaneberg, U., *Increasing activity and thermal resistance of Bacillus gibsonii alkaline protease (BgAP) by directed evolution.* Biotechnol. Bioeng., **2013,** *110* (3), 711-20.

136. Eggert, T.; van Pouderoyen, G.; Dijkstra, B. W.; Jaeger, K. E., *Lipolytic enzymes LipA and LipB from Bacillus subtilis differ in regulation of gene expression, biochemical properties, and three-dimensional structure.* FEBS Lett., **2001,** *502* (3), 89-92.

137. Ilmberger, N.; Meske, D.; Juergensen, J.; Schulte, M.; Barthen, P.; Rabausch, U.; Angelov, A.; Mientus, M.; Liebl, W.; Schmitz, R. A.; Streit, W. R., *Metagenomic cellulases highly tolerant towards the presence of ionic liquids - linking thermostability and halotolerance.* Appl. Microbiol. Biotechnol., **2012,** *95* (1), 135-46.

138. Andrady, A. L., *Microplastics in the marine environment.* Mar. Pollut. Bull., **2011,** *62* (8), 1596-605.

139. Staples, C. A.; Peterson, D. R.; Parkerton, T. F.; Adams, W. J., *The environmental fate of phthalate esters: a literature review.* Chemosphere, **1997,** *35* (4), 667-749.

140. Ganji, S. H.; Karigar, C. S.; Pujar, B. G., *Metabolism of dimethylterephthalate by Aspergillus niger.* Biodegradation, **1995,** *6* (1), 61-6.

141. Jackson, M. A.; Labeda, D. P.; Becker, L. A., *Isolation for bacteria and fungi for the hydrolysis of phthalate and terephthalate esters.* J Ind Microbiol, **1996,** *16* (5), 301-304.

142. Niazi, J. H.; Prasad, D. T.; Karegoudar, T. B., *Initial degradation of dimethylphthalate by esterases from Bacillus species.* FEMS Microbiol. Lett., **2001,** *196* (2), 201-5.

143. Barrows, M. E.; Petrocelli, S. R.; Macek, K. J.; Carroll, J., *Bioconcentration of toxic pollutants in fish.* Abstr. Pap. Am. Chem. S., **1978,** *176* (Sep), 125-125.

144. Karegoudar, T. B.; Pujar, B. G., *Metabolism of diethylphthalate by a soil bacterium.* Curr. Microbiol., **1984,** *11* (6), 321-324.

145. Boese, B. L., *Uptake efficiency of the gills of english sole (Parophrys vetulus) for four phthalate-esters.* Can. J. Fish. Aquat. Sci., **1984,** *41* (11), 1713-1718.

146. Eaton, R. W., *Plasmid-encoded phthalate catabolic pathway in Arthrobacter keyseri 12B.* J. Bacteriol., **2001,** *183* (12), 3689-3703.

147. Wofford, H. W.; Wilsey, C. D.; Neff, G. S.; Giam, C. S.; Neff, J. M., *Bioaccumulation and metabolism of phthalate-esters by oysters, brown shrimp, and sheepshead minnows.* Ecotoxicol. Environ. Saf., **1981,** *5* (2), 202-210.

148. Ejlertsson, J.; Svensson, B., *A review of the possible degradation of polyvinyl chloride (PVC) plastics and its components phthalic acid esters and vinyl chloride under anaerobic conditions prevailing in landfills.* Dept. of Water and Environmental Studies, Linkoping University, Sweden, 20 pp., **1995**.

149. Chang, H. K.; Zylstra, G. J., *Novel organization of the genes for phthalate degradation from Burkholderia cepacia DBO1.* J. Bacteriol., **1998,** *180* (24), 6529-37.

150. Nakazawa, T.; Hayashi, E., *Phthalate metabolism in Pseudomonas testosteroni - accumulation of 4,5-dihydroxyphthalate by a mutant strain.* J. Bacteriol., **1977,** *131* (1), 42-48.

151. Bull, C.; Ballou, D. P., *Purification and properties of protocatechuate 3,4-dioxygenase from Pseudomonas putida - a new iron to subunit stoichiometry.* J. Biol. Chem., **1981,** *256* (24), 2673-2680.

152. Aftring, R. P.; Chalker, B. E.; Taylor, B. F., *Degradation of phthalic acids by denitrifying, mixed cultures of bacteria.* Appl Environ Microb, **1981,** *41* (5), 1177-1183.

153. Fischer-Colbrie, G.; Heumann, S.; Liebminger, S.; Almansa, E.; Cavaco-Paulo, A.; Guebitz, G. M., *New enzymes with potential for PET surface modification.* Biocatal Biotransfor, **2004,** *22* (5-6), 341-346.

154. Yoon, M. Y.; Kellis, J.; Poulose, A. J., *Enzymatic modification of polyester.* AATCC Rev., **2002,** *2* (6), 33-36.

155. Figueroa, Y.; Hinks, D.; Montero, G., *A heterogeneous kinetic model for the cutinase-catalyzed hydrolysis of cyclo-tris-ethylene terephthalate.* Biotechnol. Prog., **2006,** *22* (4), 1209-14.

156. Cimecioglu, A. L.; Zeronian, S. H.; Alger, K. W.; Collins, M. J., *Properties of oligomers present in poly(ethylene-terephthalate).* J. Appl. Polym. Sci., **1986,** *32* (4), 4719-4733.

157. Kok, R. G.; Christoffels, V. M.; Vosman, B.; Hellingwerf, K. J., *Growth-phase-dependent expression of the lipolytic system of Acinetobacter calcoaceticus Bd413 - cloning of a gene encoding one of the esterases.* J. Gen. Microbiol., **1993,** *139*, 2329-2342.

158. Marten, E.; Müller, R. J.; Deckwer, W. D., *Studies on the enzymatic hydrolysis of polyesters I. Low molecular mass model esters and aliphatic polyesters.* Polym. Degrad. Stabil., **2003,** *80* (3), 485-501.

159. Silva, C. M.; Carneiro, F.; O'Neill, A.; Fonseca, L. P.; Cabral, J. S. M.; Guebitz, G.; Cavaco-Paulo, A., *Cutinase - a new tool for biomodification of synthetic fibers.* J. Polym. Sci. A. Polym. Chem., **2005,** *43* (11), 2448-2450.

160. Vertommen, M. A. M. E.; Nierstrasz, V. A.; van der Veer, M.; Warmoeskerken, M. M. C. G., *Enzymatic surface modification of poly(ethylene terephthalate).* J. Biotechnol., **2005,** *120* (4), 376-386.

161. Wei, R.; Oeser, T.; Then, J.; Kuhn, N.; Barth, M.; Schmidt, J.; Zimmermann, W., *Functional characterization and structural modeling of synthetic polyester-degrading hydrolases from Thermomonospora curvata.* AMB Express, **2014,** *4*, 44.

162. Sali, A.; Blundell, T. L., *Comparative protein modeling by satisfaction of spatial restraints.* J. Mol. Biol., **1993,** *234* (3), 779-815.

163. Provencher, S. W.; Glockner, J., *Estimation of globular protein secondary structure from circular dichroism.* Biochemistry, **1981,** *20* (1), 33-7.

164. Lide, D. R., *Handbook of Chemistry and Physics*. CRC Press: **2003**; Vol. 84.

165. Jennens, M. L.; Lowe, M. E., *A surface loop covering the active site of human pancreatic lipase influences interfacial activation and lipid binding.* J. Biol. Chem., **1994,** *269* (41), 25470-4.

166. Carriere, F.; Withers-Martinez, C.; van Tilbeurgh, H.; Roussel, A.; Cambillau, C.; Verger, R., *Structure-function relationships of pancreatic lipases.* Fett-Lipid, **1998,** *100* (4-5), 96-102.

VI. Publications

Lülsdorf N., Vojcic L., Hellmuth H., Weber T. T., Mußmann N., Martinez R. and Schwaneberg U. (2015) *A first continuous 4-aminoantipyrine (4-AAP)-based screening system for directed esterase evolution*. Appl. Microbiol. Biotechnol. 99(12), 5237-5246

Lülsdorf N.[*], Pitzler C.[*], Biggel M., Martinez R., Vojcic L. and Schwaneberg U. (2015) *A flow cytometer-based whole cell screening toolbox for directed hydrolase evolution through fluorescent hydrogels*. ChemComm, 51, 8679-8682

[*]shared authorship

VII. Declaration

I hereby declare that all information in this document has been obtained and presented in accordance with academic rules and ethical conduct. I also declare that, as required by these rules and conduct, I have fully cited and referenced all material and results that are not original to this work.

Nina Lülsdorf, Aachen

VIII. *Curriculum vitae*

Personal data

Name:	Nina Lülsdorf
Gender:	Female
Birthday:	26th January, 1988
Nationality:	German

Education

2012 – 2015	**PhD** DWI – Leibniz-Institute for Interactive Materials Thesis: “Protein engineering for polyethylene terephthalate degradation”
2010 – 2012	**Master of Science in Biology** Ruhr - Universität Bochum, Germany Thesis: “Improving heterologous expression of proteins in *E. coli* by fusing solubility tags through phosphorothioate-based ligase-independent gene cloning (PLICing)”
2007 – 2010	**Bachelor of Science in Biology** Rheinisch Westfälische Universität Bonn, Germany Thesis: “Molekulare Charakterisierung von *wurst* und dessen Genpordukt in *Drosophila melanogaster*”
1998 – 2007	**Abitur** Gymnasium zum Altenforst, Troisdorf, Germany

Nina Lülsdorf, Aachen